The Physiology and Biochemistry of Archaeal Ammonia Oxidisers

Chloe Lauren Wright, BSc

A thesis submitted to the School of Biological Sciences in fulfilment of the requirements for the degree of Doctor in Philosophy

December 2021

University of East Anglia

School of Biological Sciences

Norwich, UK

Contents

Abstract

Archaeal and bacterial ammonia oxidisers (AOA and AOB) initiate nitrification by oxidising ammonia (NH_3) to hydroxylamine, catalysed by ammonia monooxygenase (AMO). Archaeal ammonia oxidation was first confirmed 16 years ago with the cultivation of *Nitrosopumilus maritimus* SCM1. Since then, environmental gene surveys have revealed AOA are ubiquitous and often outnumber their bacterial counterparts in many nitrifying environments. Whilst ecological studies have demonstrated that AOA play a significant role in the global N cycle, little is known about the underpinning physiology and biochemistry. Here, culture-dependent research was conducted using phylogenetically distinct AOA isolates to gain insights about AOA energy metabolism. This began with exploring the structure and function of the archaeal AMO enzyme, which is not yet amenable to purification. By characterising the inhibition of archaeal AMOs to specific inhibitors and comparing with other members of the copper-dependent membrane monooxygenase (CuMMO) family, this study provided insights into the structure of the archaeal AMO active site(s) and its potential substrate range. Specifically, archaeal AMO has a narrower hydrocarbon substrate range compared to bacterial AMO and is restricted to oxidising short-chain-length hydrocarbons based on 1-alkynes inhibition profiles. Phenylacetylene inhibited the archaeal and bacterial AMO at different thresholds and by different mechanisms, highlighting structural differences between the two monooxygenases. Further work explored the oxidation and metabolism of methane and methanol by AOA using ^{13}C-tracer experiments. Results suggested that methane and methanol were oxidised and metabolised, but this was dependent on the concentration of ammonia present. Ammonia competes with methane/methanol for the same AMO binding site and provides the only source of reductant for AMO

activity. Subsequently, hydrazine was tested as an external source of reductant for AMO driven oxidations. These findings prompted an exploration into the similarities and differences between the archaeal and bacterial ammonia oxidation pathways, principally the role of nitric oxide (NO).

Declaration

I declare that the work presented in this thesis was conducted by me under the direct supervision of Dr Laura Lehtovirta-Morley, with the exception of those instances where the contribution of others has been specifically acknowledged in Chapters 4 and 5. None of the work presented has been previously submitted for any other degree. The data presented in Chapters 3 have been published (Wright, C.L., *et al.*, 2020. Inhibition of ammonia monooxygenase from ammonia-oxidizing archaea by linear and aromatic alkynes. *Appl Environ Microbiol*, **86**(9), e02388-19).

Acknowledgements

I would like to thank my supervisor, Dr Laura Lehtovirta-Morley, for expert guidance and kind support during my PhD. I would also like to like to acknowledge the support of Prof. Colin Murrell and Dr Andrew Crombie as well all members of Lab 1.32, past and present, for their friendship and encouragement. I would like to thank my family, especially my Mum, my Brother, Liz and Pete for all their love and support. Finally, a very special thank you to Jess, you are absolutely amazing, and I am so proud of you.

List of Figures

List of Tables

Abbreviations

3HP/4HB	3-hydroxypropionate/4-hydroxybutyrate
ADH	alcohol dehydrogenase
ADP	adenosine diphosphate
AMO	ammonia monooxygenase
Amt	ammonium transporter
ANOVA	analysis of variance
AOA	ammonia oxidising archaea
AOB	ammonia oxidising bacteria
ATP	adenosine triphosphate
ATU	allythiourea
CBB	Calvin Benson Bassham cycle
CuMMO	copper-dependent monooxygenase
Da	Dalton
DMSO	dimethylsulfoxide
DNA	deoxyribonucleic acid
DNMS	dilute nitrate mineral salts
EDTA	ethylenediaminetetraacetic acid
EPS	extracellular polymeric substances
FHL	formate hydrogen lyase

GDGT	glycerol dibiphytanyl glycerol tetraether
GDH	glutamate dehydrogenase
GOGAT	glutamine-oxoglutarate aminotransferase
GS-GOGAT	glutamine synthetase-glutamate synthase
h	hour
HAO	hydroxylamine oxidoreductase
HEPES	4-(2-hydroxyethyl) piperazine-1-ethanesulfonic acid
l	litre
IPLs	intact polar lipids
M	molar
MCO	multicopper oxidase
MDH	methanol dehydrogenase
Mep	methylammonium permease
MES	2-(N-morpholino)ethanesulfonic acid
mg	milligram
min	minute
ml	millilitre
mM	millimolar
mol	mole
MOPS	3-(N-morpholino)propane sulfonic acid

N	nitrogen
NAD^+	nicotinamide adenine dinucleotide (oxidised form)
NADH	nicotinamide adenine dinucleotide (reduced form)
$NADP^+$	nicotinamide adenine dinucleotide phosphate (oxidised form)
NADPH	nicotinamide adenine dinucleotide phosphate (reduced form)
ng	nanogram
NirK	nitrite reductase subunit K
NMS	nitrate mineral salts
NOB	nitrite oxidising bacteria
NOO	nitrite oxidoreductase
nycA	nitrosocyanin
OMZ	oxygen minimum zone
PCR	polymerase chain reaction
PEP	phosphoenolpyruvate
PES	polyethersulfone
PIPES	1,4-piperazinediethanesulfonic acid
PPS	pseudo-periplasmic space
PQQ	pyrroloquinoline quinone
pMMO	particulate methane monooxygenase
PTIO	2-Phenyl-4,4,5,5-tetramethylimidazoline-1-oxyl 3-oxide

Rh	rhesus protein
rRNA	ribosomal ribonucleic acid
RT	room temperature
rTCA	reductive tricarboxylic acid cycle
RubisCO	ribulose 1,5-bisphosphate carboxylase-oxygenase
RuMP	ribulose monophosphate
s	seconds
S-layer	cell surface-layer
sMMO	soluble methane monooxygenase
TCA	tricarboxylic acid cycle
TCE	trichloroethylene
V-PDB	Vienna Pee Dee Belemnite
v/v	volume to volume
WWTP	wastewater treatment plant
w/v	weight to volume

1. Introduction

1.1 The global nitrogen cycle

Nitrogen is a major element in the biosphere which is required by all living organisms for the synthesis of essential biomolecules, such as nucleic acids and proteins. Atmospheric dinitrogen gas (N_2) is the largest reservoir of nitrogen (78% (v/v) of the atmosphere). Only nitrogen-fixing bacteria and archaea can utilise this form to fulfil nitrogen requirements for cellular metabolism and growth by reducing dinitrogen to ammonia (NH_3). All other organisms rely on the assimilation of more reactive forms of nitrogen, for instance ammonium (NH_4^+) and nitrate (NO_3^-). Prior to the invention of the Haber-Bosch process (the industrial fixation of N_2 to NH_3), the interchange between inert dinitrogen in the extant atmosphere and the cycling of 'reactive nitrogen' was almost entirely controlled by distinct assemblages of microorganisms that alter the oxidation states from +5 (NO_3^-) to -3 (NH_4^+ and amino-nitrogen) (Falkowski, *et al.*, 2008; Canfield *et al.*, 2010; Bess *et al.*, 2011; Stein and Klotz, 2016; Kuypers *et al.*, 2018). The cycling of nitrogen between different oxidation states has been attributed to six distinct nitrogen-transforming processes: nitrogen fixation, assimilation, ammonification (including dissimilatory nitrate reduction to ammonium (DNRA)), nitrification, denitrification, and anaerobic ammonia oxidation (anammox) (Fig. 1.1). These transformations do not form a continuous, balanced cycle and fluxes in 'reactive nitrogen' frequently occur in the biosphere (Kuypers *et al.*, 2018). Over the last 100 years, the magnitude of these fluxes has been amplified by anthropogenic activity, such as the input of inorganic ammonium-based fertilisers.

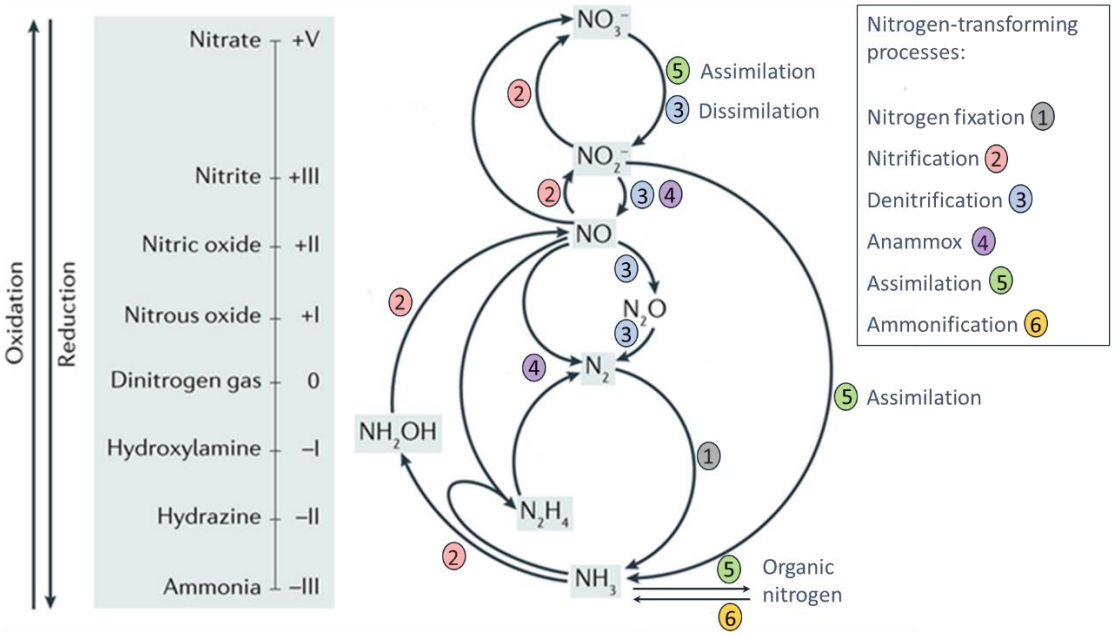

FIG 1.1 The six nitrogen-transforming processes attributed to the biogeochemical nitrogen cycle. Oxidation states range from the most reduced N-species, NH_3, to the most oxidised, NO_3^-. Figure adapted from Kuypers *et al.,* (2018).

1.2 Nitrification

Ammonium is released into the environment through the mineralisation of organic matter as well the use of ammonium-based fertilisers. In terrestrial environments it forms a moderately stable but readily available pool of nitrogen due to its cationic nature and ability to bind to clay particles. Nitrification is a central nitrogen transforming process in nature, linking the most reduced (NH_3) and oxidised (NO_3^-) pools of inorganic nitrogen (Prosser, 1989; Bess *et al.,* 2011). This two-step process begins with the oxidation of ammonia to hydroxylamine (NH_2OH), catalysed by the copper-dependent membrane bound ammonia monooxygenase enzyme (AMO) (Kuypers *et al.,* 2018), which is then oxidised to nitrite (NO_2^-), which is subsequently oxidised to nitrate. These reactions are catalysed by distinct guilds of autotrophic

ammonia and nitrite oxidising microorganisms. In most ecosystems, nitrifying activity is limited by the rate of ammonia oxidation rather than nitrite oxidation (Hink *et al.*, 2017; Herbold *et al.*, 2017).

The invention of the Haber-Bosch process in 1909 has more than quadrupled agricultural productivity and food production and approximately 50% of the world's human population now relies on the use of industrial fertilisers for food security (Erisman *et al.*, 2008; Stein and Klotz, 2016; Kuypers *et al.*, 2018). Currently, the use of inorganic ammonium-based fertilisers and other anthropogenic forms of fixed nitrogen such as urea, by far exceed natural contributions (Klotz and Stein, 2007; Stein and Klotz, 2016). Soil nitrification results in enormous commercial losses of these fertilisers (Prosser and Nicol, 2012) since the ammonia is rapidly oxidised to nitrate, which being anionic, is mobile and prone to leaching. In addition, nitrification initiates a cascade of large-scale environmental impacts including atmospheric and groundwater pollution by nitrous oxide (N_2O) and nitrate, respectively (Canfield *et al.*, 2010; Prosser and Nicol, 2012). Nitrous oxide is a potent greenhouse gas and currently the third largest contributor to global warming, after carbon dioxide (CO_2) and methane (CH_4) (Liu *et al.*, 2017; IPCC, 2018; Nisbet *et al.*, 2021). Additionally, N_2O is projected to be the most dominating ozone-depleting substance emitted in the 21st century (Ravishankara *et al.*, 2009). Ammonia oxidisers emit N_2O enzymatically through hydroxylamine oxidation (a key intermediate of the ammonia oxidation pathway) as well as by abiotic conversions (Prosser *et al.*, 2020). They also contribute indirectly to N_2O emissions by producing oxidised nitrogenous compounds which can be used as substrates by denitrifying organisms (Steiglmeier *et al.*, 2014; Hink *et al.*, 2017). Nitrate leaching causes a suite of environmental problems including the eutrophication of freshwater and marine ecosystems which can lead to oxygen

depletion, algal blooms, loss of biodiversity, acidification, and the establishment of invasive species (Zhu *et al.,* 2018). Conversely, wastewater treatment plants (WWTP) rely on the activities of nitrifiers (in combination with denitrifiers or anammox bacteria) for the removal of nitrogen from industrial and municipal wastewater (Gwak *et al.,* 2019; Ren *et al.,* 2020). Further understanding about the microorganisms and enzymatic pathways that underpin the transformation of ammonia could help mitigate the environmental impacts and improve the efficiency of nitrogen removal in engineered systems (Prosser *et al.,* 2020).

1.3 Ammonia oxidising microorganisms (AOM)

Our understanding of the nitrogen cycle has been drastically revolutionised in the last few decades due to the discovery of novel processes and microbial players. This includes the discovery of anammox bacteria in natural ecosystems (Dalsgaard *et al.,* 2005; Jetten *et al.,* 2005) and most recently the complete ammonia oxidisers (comammox bacteria), which oxidise both ammonia and nitrite within the same cell to produce nitrate (Daims *et al.,* 2015; van Kessel *et al.,* 2015). Perhaps though, the most unanticipated breakthrough was the discovery of aerobic ammonia oxidation within the domain Archaea (Könneke *et al.,* 2005; Francis *et al.,* 2007). For many years after their classification as the third domain of life by Woese and colleagues (1978), Archaea were largely categorised as extremophiles (Nicol *et al.,* 2011) and ammonia oxidation in the environment was attributed to autotrophic ammonia oxidising bacteria (AOB), occasionally supported by heterotrophic nitrifiers (De Boer and Kowalchuk, 2001; Pester *et al.,* 2011). Cultivation-independent techniques have revealed a plethora of microbial diversity, including the presence of 16S ribosomal RNA (rRNA) gene sequences belonging to non-extremophilic archaea (Fuhrman *et al.,* 1992; DeLong 1992). These mesophilic archaea, which are now known to include ammonia

oxidising archaea (AOA), constitute a major fraction of the microbial biomass on Earth (Karner *et al.*, 2001; Offre, *et al.*, 2013).

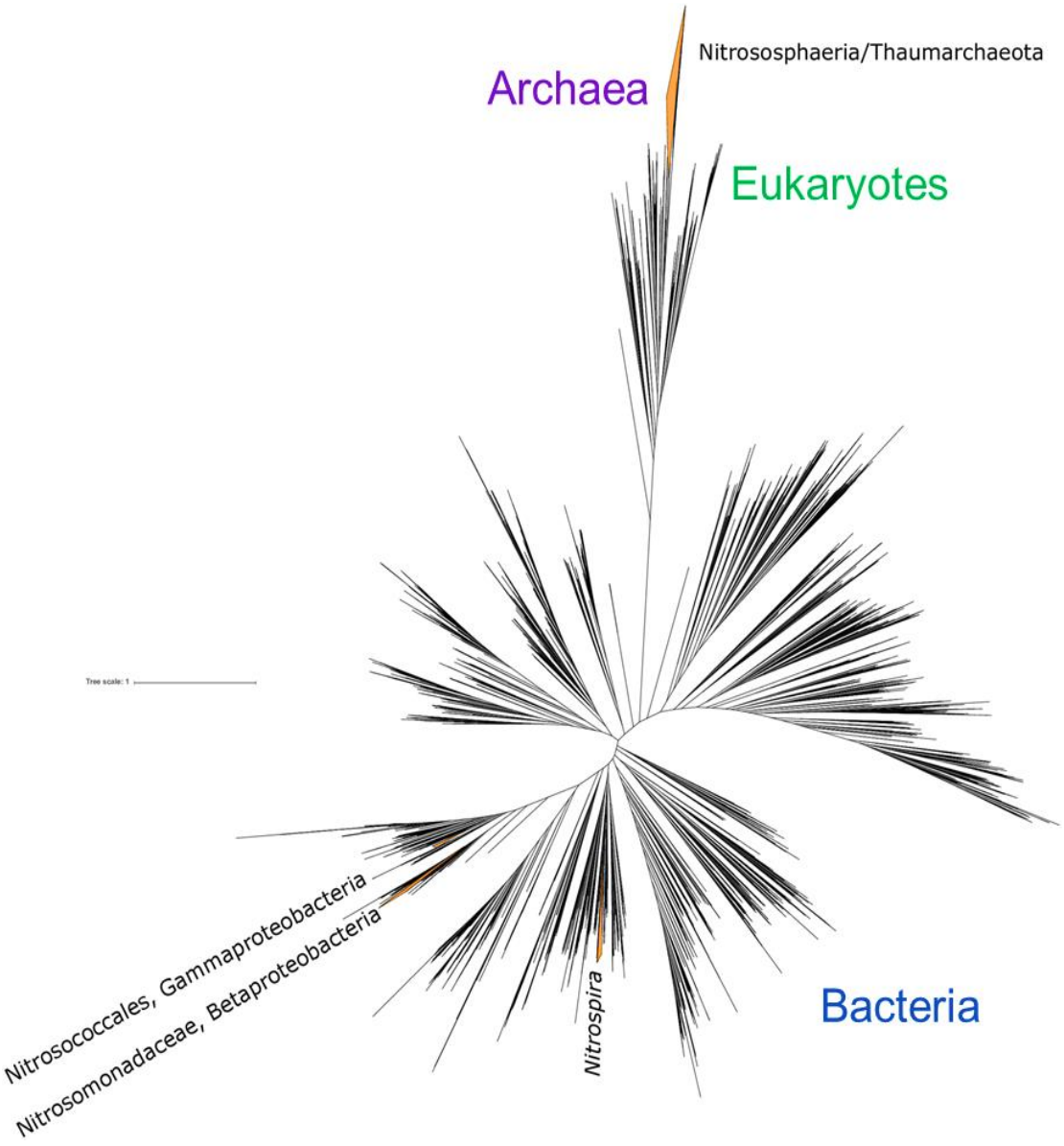

FIG 1.2 Tree of life from Ward *et al.,* (2021), built with concatenated ribosomal proteins. Clades of confirmed ammonia oxidizing organisms are highlighted in orange. The distribution of ammonia oxidation is polyphyletic, spread across one lineage within the Archaea (Nitrososphaeria) and three within the Bacteria (the ammonia oxidising beta- and gammaproteobacteria, and comammox bacteria which belong to the genus *Nitrospira* within the Nitrospirota phylum).

There are now three distinct guilds of ammonia oxidising microorganisms (Fig. 1.2). AOA comprise a diverse group of organisms that belong to the phylum Thaumarchaeota that are spread across one lineage, Nitrososphaeria (Brochier-Armanet *et al.,* 2008; Spang *et al.,* 2010; Alves *et al.,* 2018; Ward *et al.,* 2021). AOB are restricted to two monophyletic lineages within the Proteobacteria. The genera *Nitrosomonas* and *Nitrosospira* are affiliated with the betaproteobacteria sub-class and the genera *Nitrosococcus, Nitrosacidococcus* and *Nitrosoglobus* with the gammaproteobacteria (Head *et al.*, 1993; Purkhold *et al.,* 2000; Hayatsu *et al.,* 2017; Picone *et al.,* 2020). Typically, betaproteobacterial AOB are associated with soil environments and WWTPs, whilst gammaproteobacterial AOB are primarily found in marine environments. Comammox bacteria belong to the genus *Nitrospira* lineage II, which also comprises some nitrite oxidising bacteria (NOB) (Daims *et al.,* 2015; van Kessel *et al.,* 2015; Koch *et al.,* 2018). Comammox *Nitrospira* can further be divided into two monophyletic sister clades designated clades A and B (Daims *et al.,* 2015; van Kessel *et al.,* 2015). Comammox are found in a range of natural and engineered environments but possibly not marine ecosystems (Pjevac *et al.,* 2017; Spasov *et al.,* 2020). Currently, all cultured representatives of comammox *Nitrospira* belong to clade A and have been enriched from artificial ecosystems (Daims *et al.,* 2015; van Kessel *et al.,* 2015). Very recently, the genome of the unclassified Gammaproteobacteria "MBAE14" was found to encode putative AMO genes (Mori *et al.,* 2019). Additionally, distinct archaeal species which clustered within the Thermoplasmatota order, named *Ca.* Angelarcheales, were found to encode divergent CuMMO sequences (Diamond *et al.,* bioRxiv). There may be many more as-of-yet undiscovered ammonia oxidisers.

Much of our understanding about the ecology of ammonia oxidising microorganisms; their diversity, abundance, and distribution, are based on 16S rRNA and *amoA* molecular ecology surveys of natural habitats (for example: Hayatsu *et al.,* 2008; Cao *et al.,*2013; Li *et al.,* 2018). These studies have been crucial for our understanding of the distribution and diversity of ammonia oxidisers, however there is still much to learn regarding their physiology and biochemistry.

1.4 Ammonia oxidising archaea: global players in the nitrogen cycle

The archaeal *amoA*, a homologue of the bacterial *amoA* and the gene encoding the α-subunit of the AMO, was first discovered within genomic fragments derived from uncultivated Crenarchaeaota from the Sargasso Sea (Venter *et al.,* 2004). Subsequent surveys found an abundance of putative archaeal *amoA* genes in both marine and soil environments (Treusch *et al.,* 2005; Francis *et al.,* 2005; Leininger *et al.,* 2006). Archaeal ammonia oxidation was then confirmed with the cultivation and characterisation of *Nitrosopumilus maritimus* SCM1, which was isolated from a marine aquarium (Könneke *et al.,* 2005). This organism shares close genome-wide sequence identity to the mesophilic Crenarchaeota previously found in marine environments and grows autotrophically using bicarbonate and ammonia as its sole carbon and energy source, respectively. The isolation of *N. maritimus* SCM1 combined with the abundance of putative archaeal *amoA* sequences in both aquatic and terrestrial environments suggested AOA play a significant, but previously unrecognized role in the global nitrogen and carbon cycles (Francis *et al.,* 2005).

Following their discovery, molecular studies have demonstrated that AOA are ubiquitous and found in virtually every aquatic and terrestrial habitat including soils, marine and freshwater habitats, marine sponges, geothermal environments, skin and

even spacecraft clean rooms (Francis *et al.,* 2005; Wuchter *et al.,* 2006; Leininger *et al.,* 2006; Hatzenpichler *et al.,* 2008; Moissl-Eichinger, 2011; Lehtovirta-Morley, 2018). Quantitative environmental assessments of archaeal *amoA* and AOA-specific lipids (crenarchaeol) suggest that AOA are some of the most abundant organisms on Earth (Leininger *et al.,* 2006; Pitcher *et al.,* 2011), accounting for up to 40% of all marine bacterioplankton (Karner *et al.,* 2001) and comprising approximately 3% of all prokaryotes in soils, with archaeal *amoA* copy numbers ranging from 7×10^6 to 1×10^8 per gram of dry soil (Leininger *et al.,* 2006). Moreover, AOA often outnumber AOB in many nitrifying environments (by 1 – 2 orders of magnitude in the marine environment, Wuchter *et al.,* (2006)) and can occupy ecological niches inaccessible to AOB such as thermal springs with temperatures up to 86°C, and extremely oligotrophic ecosystems such as deep oceanic sediments (Konneke *et al.,* 2005; Leininger *et al.,* 2006; Hatzenpichler *et al.,* 2008; Zhong *et al.,* 2020).

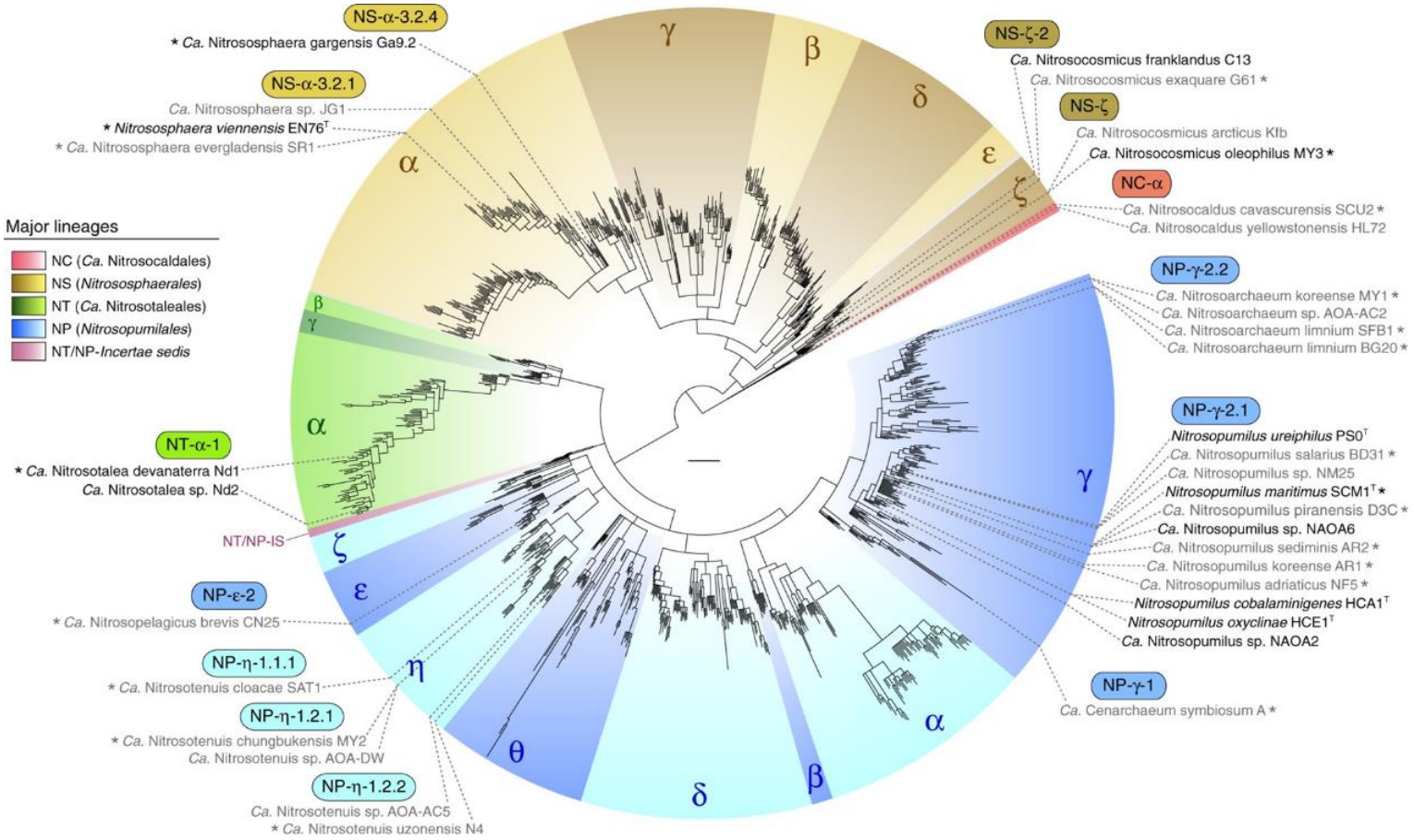

FIG 1.3 Global phylogeny of archaeal *amoA* genes from cultivated and environmental AOA taken from Alves *et al.,* (2018). Asterisks indicate strains with a sequenced genome up until 2018. Order-level lineages are indicated by colour, and major constituent subclades are designated by Greek letters and different shades. Strains in pure or enrichment culture are indicated in black and grey text respectively, and their abbreviated *amoA*-based classification is indicated in coloured boxes. *Insertae sedis* refers to strains that are currently undefined.

Phylogenetic studies and comparative genomics place AOA within the novel phylum Thaumarchaeota (Brochier-Armanet et al., 2008; Spang et al., 2010) although not all archaea of this phylum are ammonia oxidisers (Weber et al., 2015; Alves et al., 2018). To date, four phylogenetic lineages of AOA have been identified, which encompass five main clusters: *Nitrososphaera* and *Nitrosocosmicus* are typically found in neutral pH soils (Pitcher *et al.,* 2010; Tourna *et al.,* 2011; Lehtovirta-Morley *et al.,* 2016b); *Nitrosotalea* is the dominant genus present in acidic soils (Lehtovirta-Morley *et al.,* 2011); *Nitrosocaldus* are thermophilic and prevalent in hot springs (de la Torre *et al.,* 2010; Abby *et al.,* 2018; Daebeler *et al.,* 2018); and *Nitrosopumilus* are associated with the marine environments (Qin *et al.,* 2017). In addition, *Nitrosopumilus* comprises the freshwater genera *Nitrosarchaeum, Nitrosotenuis,* as well as *Nitrosopelagicus,* also affiliated with marine habitats (Fig. 1.3, Gubry-Rangin *et al.,* 2011; Alves *et al.,* 2018; Lehtovirta-Morley, 2018). There is a certain degree of habitat cross-over between AOA clusters, for example *Nitrososphaera* are found in soils with a pH as low as 4.9 and *Nitrosarchaeum* are also present in soils (Gubry-Rangin *et al.,* 2011; Jung *et al.,* 2011; Wang *et al.,* 2014; Alves *et al.,* 2018). Considerable phylogenetic diversity exists within these AOA lineages (Gubry-Rangin *et al.,* 2011), suggesting an intriguing evolutionary history, which has accumulated to allow such breadth of ecological niche expansion (Fig. 1.3).

In-depth studies of isolated AOA strains are paramount in order to understand the underpinning physiology and biochemistry that enabled their diversification, as well as their contribution to nitrification and the associated environmental impacts (Martens-Habbena *et al.,* 2009). Since the isolation of *N. maritimus* SCM1 (Könneke *et al.,* 2005), another 13 AOA have been obtained in pure culture, and many more in enrichment. These include representatives that grow at a pH as low as 4 (*Nitrosotalea*

devanaterra & *Nitrosotalea sinensis*) and at temperatures as high as 74℃ (*Nitrosocaldus islandicus* & *Nitrosocaldus cavascurensis*) (Lehtovirta-Morley *et al.*, 2011; Lehtovirta-Morley *et al.,* 2014; Daebeler *et al.,* 2018; Abby *et al.,* 2018). However, AOA are notoriously difficult to cultivate and comprise a broad diversity of organisms that are greatly underrepresented by the current characterised strains and genomes (Alves *et al.,* 2018).

1.5 Environmental drivers of AOM ecology

Since the discovery of AOA and comammox bacteria, a considerable amount of research has taken place to determine the environmental drivers that influence the ecology of AOM (Prosser & Nicol, 2012). Determining the patterns in their distribution in the environment can be applied to improving agricultural land management to reduce the detrimental environmental impacts associated with nitrification and refine WWTP design for more efficient nitrogen removal. For example, AOB can generate approximately double the amount of N_2O than AOA during ammonia oxidation (Hink *et al.,* 2018), therefore managing soil conditions to favour AOA would theoretically reduce nitrous oxide emissions (Prosser *et al.,* 2020).

The two recurring environmental factors influencing the distribution and activity of AOM are substrate availability and pH (Nicol *et al.,* 2008; Prosser & Nicol, 2012). Other factors that are often associated with the niche occupation of terrestrial ammonia oxidisers include differences in their apparent O_2 and temperature optima, and tolerance to drying and rewetting and sensitivity to nitrification inhibitors (Merbt *et al.,* 2012; Thion & Prosser, 2014; Qin *et al.,* 2016; Palomo *et al.,*2018; Séneca *et al.,* 2020). Ammonia oxidisers within the marine environments show strong segregation by depth, potentially because of dissimilar tolerances to light inhibition

(Merbt *et al.,* 2012). However, O_2, salinity, metal requirements and nutrient fluxes occur throughout the water column and have also been found to influence their distribution (Francis *et al.,* 2005; Mosier *et al.,* 2008; Bayer *et al.,* 2016; Shafiee *et al.,* 2021). Differences in copper (Cu) and iron (Fe) requirements also influences AOM ecology in both aquatic and terrestrial ecosystems (Gwak *et al.,* 2019; Reyes *et al.,* 2020).

1.5.1 Substrate concentration

Ammonia, rather than ammonium, is the growth substrate oxidised by the bacterial AMO (Suzuki *et al.,* 1974), but the preferred substrate (NH_3/NH_4^+) oxidised by the archaeal AMO has not been determined. However, based on amino acid sequence comparisons of the AMO, it is highly likely to also be ammonia (Lehtovirta-Morley *et al.,* 2016a).

Ammonia concentration has been shown to be a strong selector for the abundance, distribution and activity of AOM (Verhamme *et al.,* 2011; Bates *et al..,* 2011). Typically, AOA are the dominant ammonia oxidisers in the open ocean where available nitrogen is extremely low, and the ammonium concentrations typically range from <0.03-1 μM (Könneke *et al.,* 2005; Martens-Habbena *et al.,* 2009). In unfertilised terrestrial environments, low ammonium availability tends to favour ammonia oxidation by AOA and comammox bacteria (Beeckman *et al.,* 2018). Both AOA and comammox tend to have a higher substrate affinity compared to AOB, making them better adapted to oligotrophic environments (Martens-Habbena *et al.,* 2009; Kits *et al.,* 2017; Jung *et al.,* 2021). The application of ammonium-based fertiliser stimulates AOB activity more strongly than AOA, and AOB contribute more to nitrification in agricultural soils (Jia and Conrad, 2009; Sauder *et al.,* 2012; Ouyang *et al.,* 2016).

Correspondingly, the archaeal AMO appears to have a lower maximum rate of ammonia oxidation and is therefore likely to become saturated at high ammonia concentrations (Prosser and Nicol, 2012; Beeckman *et al.*, 2018). Interestingly, ammonia oxidation by AOA appears to be driven by the slow release of organic nitrogen rather than the addition of inorganic nitrogen, suggesting the interactions between mineralisers and AOA could be very significant (Prosser & Nicol, 2012; Thion *et al.*, 2016). This was recently demonstrated in a study by Huang *et al.*, (2021) where AOA, and not AOB and comammox, were found to strongly dominate nitrification activities in agricultural soils with high organic matter content.

Cultivated AOA strains are often more sensitive to ammonia inhibition compared to AOB, which could explain why AOB rather than AOA drive nitrifying activity in heavily fertilised soils (Prosser & Nicol, 2012). Recently however, AOA tolerant to high ammonia concentrations have been cultivated from agricultural soil (*Nitrosocosmicus franklandus*), contaminated sediment (*Nitrosocosmicus oleophilus*) and a municipal WWTP (*Nitrosocosmicus exaquare*), reducing the support for the selective inhibition of archaeal ammonia oxidation at high ammonium concentrations suggesting that AOA also contribute to nitrification rates in relatively eutrophic ecosystems (Lehtovirta-Morley *et al.*, 2016a; Jung *et al.*, 2016; Sauder *et al.*, 2017).

1.5.2 pH

pH was perhaps the most widely accepted environmental driver of niche differentiation between AOA and AOB since the bioavailability of ammonia and metals such as copper are pH-dependent. Ammonia (NH_3) and ammonium (NH_4^+) exist in pH equilibrium with a pK_a of 9.25. Most extant bacterial ammonia oxidisers currently isolated do not function in acidic environments, which is attributed to the

low ammonia availability (Suzuki, 1974). However, approximately 30% of all the world's soils are acidic (pH <5.5) and nitrifying activity is often equal or higher than in neutral pH soils (Lehtovirta-Morley *et al.,* 2011). The isolation of the first obligately acidophilic AOA, *Nitrosotalea devanaterra* Nd1 by Lehtovirta-Morley and colleagues (Lehtovirta-Morley *et al.,* 2011) provided an explanation for nitrification at low pH. Furthermore, thaumarchaeal *amoA* abundance appears to increase relative to AOB with decreasing soil pH (Nicol *et al.,* 2008; Lehtovirta-Morley *et al.,* 2011). The physiological and genomic characterisation *N. devanaterra* Nd1 revealed some potentially unique adaptations for an acidophilic lifestyle including mechanisms of pH homeostasis and a high affinity substrate acquisition system (Lehtovirta-Morley *et al.,* 2016b). Interestingly, many of the core gene families associated with adaptation to low pH are not shared between different *Nitrosotalea* strains and some of these genes appear to have been acquired via horizontal gene transfer (HGT) from other acidophilic microbes (Herbold *et al.,* 2017). Some strains within the genus *Nitrososphaera* are also found in low pH soils (Gubry-Rangin *et al.,* 2011; Wang *et al.,* 2014). Bacterial ammonia oxidisers have also been isolated from acidic environments (De Boer *et al.,* 1991). For example, the gammaproteobacterium "*Ca.* Nitrosoglobus terrae" sp. TAO100 was isolated from acidic agricultural soil and exhibited ammonia oxidising activity at pH 5 (Hayatsu *et al.,* 2017). Survival and growth of AOB at low pH has been attributed to their capacity to hydrolyse urea to produce NH_3 and the ability to form aggregates and biofilms, possibly with NOB which prevents the toxic accumulation of NO_2^- (De Boer *et al.,* 1991; De Boer and Kowalchuk, 2001; Burton & Prosser, 2001). More recently a novel gammaproteobacterium, "*Ca.* Nitrosacidococcus tergens" sp. RJ19, was highly

enriched from a bioreactor and exhibited growth at pH as low as 2.5 (Picone *et al.,* 2021).

1.5.3 Oxygen availability

O_2 plays an important role in nitrification as a substrate for the AMO enzyme and as a terminal electron acceptor for ammonia oxidising microorganisms (Arp *et al.,* 2002). Ecological studies of marine environments suggest that AOA belonging to the *Nitrosopumilaceae* genus, particularly those associated with the marine low ammonia ecotype (LAC-AOA), are extremely successful under low dissolved O_2 conditions, with the highest abundances of archaeal *amoA* and AOA-specific intact polar lipids (IPLs) often detected in oxygen minimum zones (OMZs) and deep ocean sediments (Pitcher *et al.,* 2011; Bouskill *et al.,* 2012; Muck *et al.,* 2019). Bristow *et al.,* (2016) found rates of ammonia oxidation in OMZs were still measurable at <0.01 μM O_2, likely driven exclusively by communities of AOA. The enrichment of AOA from marine sediments was attributed to their ability to outcompete contaminating bacteria at low O_2 (Parks *et al.,* 2010). A low O_2 requirement would give terrestrial AOA a competitive advantage over AOB in environments which frequently and intermittently become hypoxic, due to flooding for instance. Correspondingly, it has been shown that AOA react faster to the presence of O_2 in the fluctuating oxic-anoxic rhizosphere of rice plants compared to AOB (Chen *et al.,* 2008). Comammox bacteria also appear to be adapted to low O_2 availability since they have a preference to form aggregates, creating microaerophilic conditions (Koch *et al.,* 2018). Additionally, comammox are abundant in the oxic-anoxic interface of biofilms that form in WWTPs and have been enriched from bioreactors operating under low dissolved O_2 (Van Kessel *et al.,* 2015; Daims *et al.,* 2015; Camejo *et al.,* 2017; Roots *et al.,* 2019).

1.6 The physiology, metabolism, and cellular architecture of AOA

In the environment, the numerous factors that appear to result in the niche differentiation of ammonia oxidising communities likely act concomitantly, making it difficult to extricate the key environmental drivers from environmental sampling and mesocosm incubations alone. Additionally, soil is an extremely heterogeneous environment. Microenvironments can cause small scale fluxes in pH and nutrient availability and affect local abundances and distributions of ammonia oxidising communities, making it difficult to infer the niche differentiation solely from environmental meta-data. Study of the potential differences in physiology and metabolism between AOA, AOB and comammox is likely to yield more robust explanations for the niche partitioning.

1.6.1 Ammonia oxidation kinetics of AOA, AOB and comammox

Ammonia oxidation kinetics and substrate affinity often reflect the ecological distribution of AOM. Until very recently, AOA were frequently found to have a lower apparent half-saturation constant ($K_{m(app)}$) and higher affinity for NH_3 compared to bacterial ammonia oxidisers (Habbena-Martens *et al.,* 2009; Kits *et al.,* 2017). The first study to investigate whole cell substrate kinetics of an AOA isolate showed that *N. maritimus* SCM1 had the lowest $K_{m(app)}$ for NH_3 of all isolated ammonia oxidisers at that time (3.3 nM), and a substrate threshold of <10 nM. This was far below the optimal threshold of any characterised AOB and closely resembles the nitrifying environments in the oligotrophic open ocean (Martens-Habbena *et al.,* 2009 and 2011). Recently, a study by Jung *et al.,* (2021, Fig. 1.4) found that the acidophilic AOA strains "*Ca.* Nitrosotalea devanaterra" and "*Ca.* Nitrosotalea sinensis" had a $K_{m(app)}$ for NH_3 between ~0.6 and 2.8 nM. It makes perfect sense for these strains to

have an extremely high affinity for ammonia since the acid dissociation constant of ammonium (pK_a = 9.25) limits the availability of ammonia under these conditions. Therefore, a greater substrate affinity gives AOA a competitive advantage in oligotrophic and/or acidic environments. However, some oligotrophic AOB belonging to the *Nitrosomonas* cluster 6a have a similar $K_{m(app)}$ for NH_3 to that of many soil AOA (<4.0 μM), which reduces the support for niche differentiation between AOA and AOB based on their substrate affinity (Sedlacek *et al.*, 2019). Additionally, "*Ca.* Nitrosacidococcus tergens" sp. RJ19 was also found to have a very high affinity for NH_3 ($K_{m(app)}$ = 147 nM, Picone *et al.*, 2021).

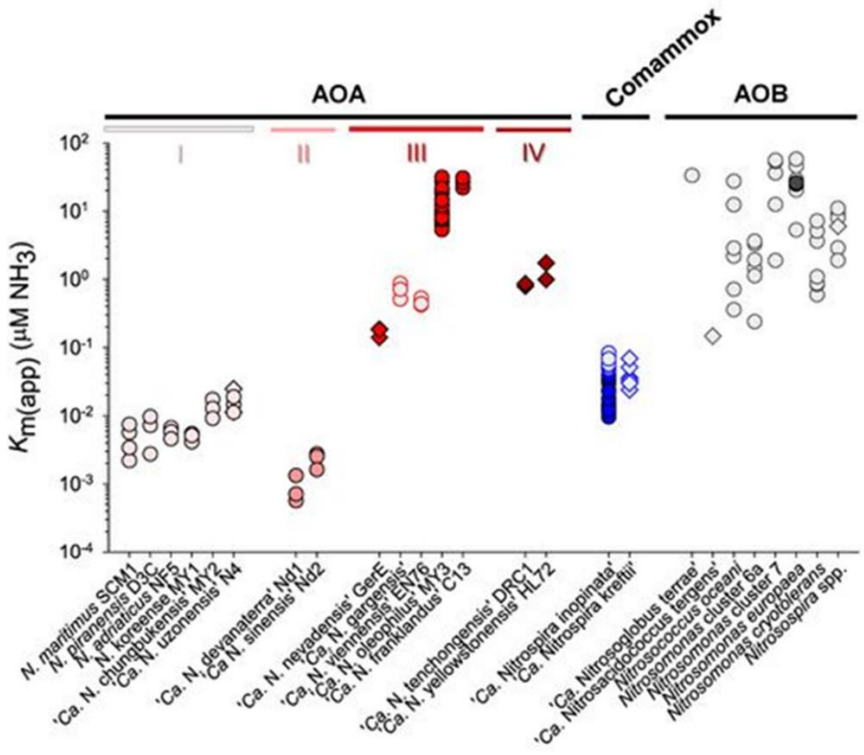

FIG 1.4 The apparent substrate affinity ($K_{m(app)}$) for NH_3 for AOA (red), AOB (blue) and comammox (black) from Jung *et al.,* (2021). The four different gradations of red differentiate the four AOA phylogenetic lineages: **(I)** *Nitrosopumilales*, **(II)** "*Ca*. Nitrosotaleales", **(III)** *Nitrososphaerales*, and **(IV)** "*Ca.* Nitrosocaldales". Measurements were performed with either pure (circles) or enrichment (diamonds) cultures. Multiple symbols per strain represent independent measurements performed in the study by Jung *et al.,* (2021) and/or in the literature.

Comammox bacteria are also very prevalent in low nitrogen environments. Consistent with this, the comammox strain *Nitrospira inopinata*, which was isolated from 1,200m deep oil exploration well, has a very high affinity for ammonia with a $K_{m(app)}$ for NH_3 of 49 nM (Kits *et al.*, 2017). It is currently unknown how substrate affinity affects the competition and/or co-existence between AOA, oligotrophic AOB and comammox in the environment, but the relationship is likely to be very intricate due to the presence of microenvironments.

1.6.2 AOA cell morphology and physiology

Archaeal ammonia oxidisers are often smaller than their bacterial counterparts and isolates affiliated with the *Nitrosopumilus* and *Nitrosotalea* clades are among some of the smallest free-living microorganisms with rod shaped cells <1 μm in length (Könneke *et al.*, 2005; Lehtovirta-Morley *et al.*, 2011). Cell size could influence ammonia oxidation kinetics because of the differences in the surface area-to-volume ratio and therefore small AOA may demonstrate higher substrate affinity (Prosser & Nicol, 2012; Lancaster *et al.*, 2018). However, not all AOA are small and isolates from the *Nitrosocosmicus* and *Nitrososphaera* clades are of a similar cell size and volume (>1 μm) to many AOB but have much lower $K_{m(app)}$ values, therefore differences in substrate acquisition systems and transport affinities are more likely to affect substrate kinetics.

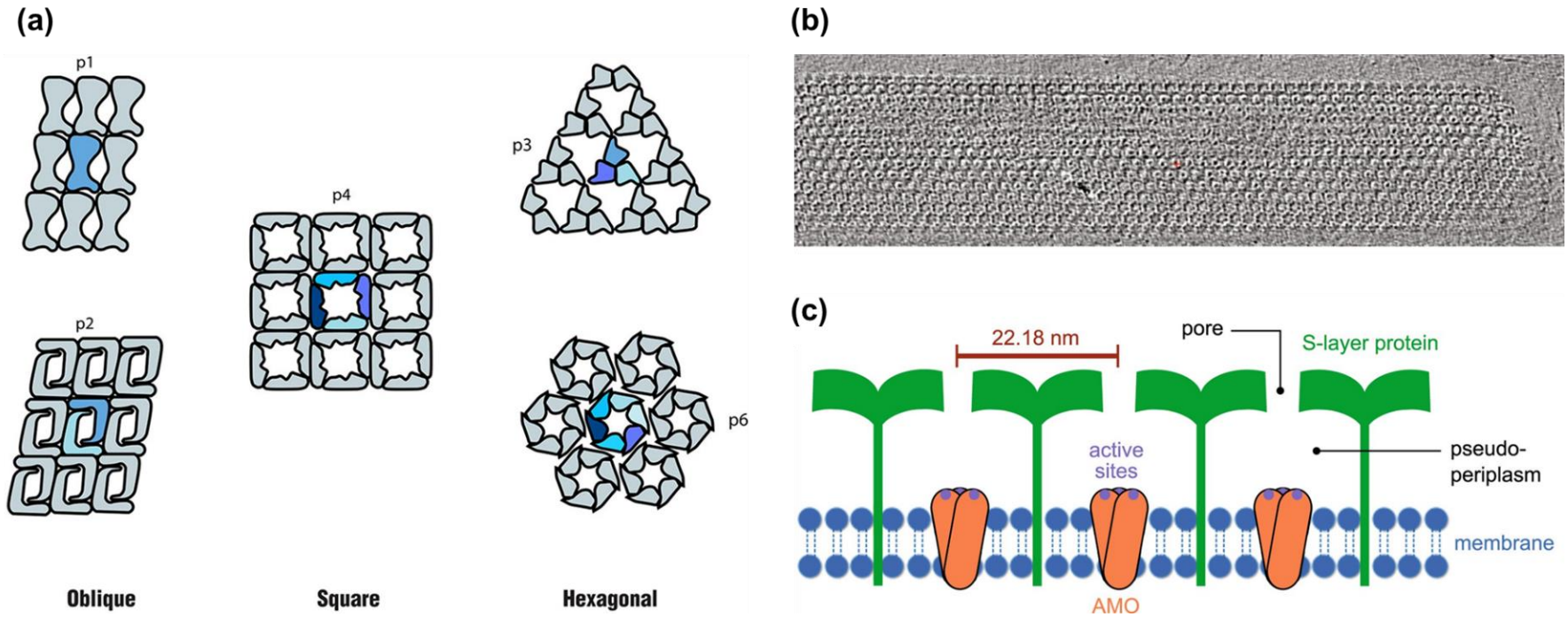

FIG. 1.5 (a) Structure of microbial S-layers from Rodrigues-Oliveira *et al.,* (2017). **(b)** From Li *et al.,* (2018), *N. maritimus* 3-D electron cryotomographic image of cell. Hexagonal pattern of S-layer was visible at magnification of ×22,000. **(c)** The molecular organisation of the S-layer proteins and AMO. S-layer proteins are anchored in the membrane at the N-terminus, forming a canopy to enclose a pseudo-periplasmic space (PPS). Trimers of AMO heterotrimers are anchored in the membrane, with active sites exposed to PPS. Nutrients can pass through the S-layer pores.

Two-dimensional, porous lattices form the outermost cell surface-layer (S-layer) of many archaea and bacteria (Sleytr *et al.,* 1997). S-layers are composed of one, or occasionally two, (glyco) proteins and arranged in lattice structures of either one (p1), two (p2), three (p3), four (p4) or six (p6) proteins, which results in regular spaced pores (Fig. 1.5a, Rodrigues-Oliveira *et al.,* 2017). In AOA these hexagonal structures have been implicated in determining cell shape, protection from osmotic shock and serving as a molecular sieve between the cytoplasmic membrane and the external environment (Fig. 1.5b and c, Steiglmeier *et al.,* 2014a, Li *et al.,* 2018). A recent study by Li *et al.,* (2018) found that the S-layers of AOA are enriched with charged amino acid reactive sites which attract positively charged ammonium ions. Concentrating ammonium at the cell surface would assist growth and activity in low ammonium environments. Interestingly, the genomes of characterised *Nitrosocosmicus* spp. and *Nitrosocaldus* spp. lack the main S-layer protein (encoded by *slp1*), which was previously considered to be the main component of the thaumarchaeal cell wall (Lehtovirta-Morley *et al.,* 2019). Strains associated with these genera typically occupy ecological niches with high ammonium concentrations (*Nitrosocosmicus*), or thermophilic environments *(Nitrosocaldus*) with little competition from other ammonia oxidisers, and therefore may not require the ability to concentrate ammonium at the cell surface (Lu *et al.,* 2020).

The cell membranes of AOA are composed of isoprenoid tetraether lipids, predominantly cyclised glycerol dibiphytanyl glycerol tetraethers (GDGTs). Crenarchaeol and methoxy archaeol are GDGTs that appear unique to *Thaumarchaeota* and can be used as a biomarker for members of this phylum (Elling *et al.,* 2017; Bale *et al.,* 2019) The composition of GDGT-based lipids synthesised by different AOA appears to be shaped by the environmental niches they occupy (Bale *et*

al., 2019; Lehtovirta-Morley *et al.,* 2016a). For example, increasing the cyclisation of cyclopentane rings can increase the packing density and promote energy conservation by reducing membrane permeability (Elling *et al.,* 2014; Lehtovirta-Morley *et al.,* 2016a; Hurley *et al.,* 2016). Dynamic and variable lipid arrangements likely support the activity of AOA at higher temperatures and at lower pH compared to AOB. Fully saturated menaquinones with six isoprenoid units are the major membrane-bound respiratory quinones found in *Thaumarchaeota* (Elling *et al.,* 2016).

AOA lack the intracytoplasmic membranes found within AOB, which could function to increase the surface area available to accommodate maximum amounts of the membrane bound AMO (Fiencke *et al.,* 2006). This could potentially explain why AOB have relatively higher ammonia oxidising activities per cell than AOA, although this has not been tested systematically. *N. viennensis* and *Nitrosoarchaeum koreensis* have additional cytoplasmic structures which may be membrane-bound (Jung *et al.,* 2011; Stieglmeier *et al.,* 2014a). AOA encode various genes related to chemotaxis, cell surface modification and cell adhesion and many possess extracellular polymeric substances (EPS) production pathways (Kerou *et al.,* 2016; Jung *et al.,* 2016). Notably, these include genes from protein families that often feature in the genomes of biofilm forming archaea and bacteria and are essential prerequisites for cell-cell and cell-surface interactions, which leads to the formation of aggregates and the establishment of biofilm. These genes encode various glycol transferases (GTs), proteins belonging to the carbohydrate esterase family 4 (CE4), the E-type oligosaccharyl-transferase (AglB) and the Multidrug/Oligosaccharidyl-lipid/Polysaccharide (MOP) flippase (Kerou *et al.,* 2016). Some AOA synthesise flagella-like appendages, termed archaellum, signifying these strains have the potential to seek favourable environments (Bayer *et al.,* 2016).

1.6.3 AOA respiratory chains and metal requirements

Archaeal and bacterial ammonia oxidisers differ considerably in their respiratory pathways. Heme-based *c*-type cytochromes make up the redox centre of the hydroxylamine oxidoreductase (HAO) enzyme and mediate the majority of electron transfer to the terminal oxidase during ammonia oxidation by AOB (Stahl and de la Torre, 2012; Sedlaeck *et al.*, 2020). In contrast, AOA appear to have an electron transport chain highly enriched in copper-containing metalloproteins (Walker *et al.*, 2010; Reyes *et al.,* 2016a). The ammonia oxidation pathways of AOA and AOB are discussed in detail in Section 1.7. Copper limitation has been shown to be an important constraint on the growth and activity of AOA but not so much for AOB; presumably because copper is required for the maturation of enzymes that serve as electron carriers during ammonia oxidation (Amin *et al.*, 2013; Qin *et al.*, 2017; Gorman-Lewis *et al.*, 2019; Reyes *et al.*, 2020a). Consequently, copper bioavailability is now considered an important factor contributing to niche differentiation between AOA and AOB in the environment. Some organic compounds can form strong complexes with free copper (Cu^{2+}) and many of the organics that were inhibitory to the AOA isolate "*Ca.* Nitrosocosmicus oleophilus" had high metal complexation potential (Jung *et al.*, 2016; Gwak *et al.*, 2019). Subsequently, Gwak *et al.*, (2019) demonstrated that copper supplementation can promote the growth of AOA in the presence of inhibitory organic compounds. Recent studies have shown the copper-limiting thresholds of AOA isolates from terrestrial and non-marine environments appear lower than that of the marine strain *N. maritimus* SCM1, which could be attributed to the presence of more copper transporters and storage proteins in these strains (Amin *et al.*, 2013; Gwak *et al.*, 2019; Reyes *et al.*, 2020a). AOA copper acquisition mechanisms have yet to be fully elucidated but recently Reyes *et al.*, (2020b) demonstrated the copper chelator

and transporter (CopC/D) and multicopper oxidases (MCOs) were highly upregulated by *N. viennensis* under copper limitation. The transcriptional response to copper limitation by *N. maritimus* SCM1 was not the same as *N. viennensis* and it is very conceivable that distinct AOA could differ in their copper acquisition systems and affinities, which may be niche specific.

1.6.4 Ammonium transport and assimilation

Ammonium transport systems in ammonia oxidisers are particularly interesting since ammonia is required for both energy and assimilation, implying there must be reasonably sophisticated regulation of how ammonia/ammonium is partitioned. It is currently unknown if ammonium transport could be coupled to the oxidation too. Uncharged ammonia can cross biological membranes, however in many organisms the uptake of ammonia/ammonium into cells is mediated by a class of ubiquitous membrane proteins which comprise ammonium transporters (Amt), methylammonium permeases (Mep) and rhesus (Rh) proteins (Fig. 1.7, Andrade *et al.*, 2005; Ellerbeck *et al.*, 2007).

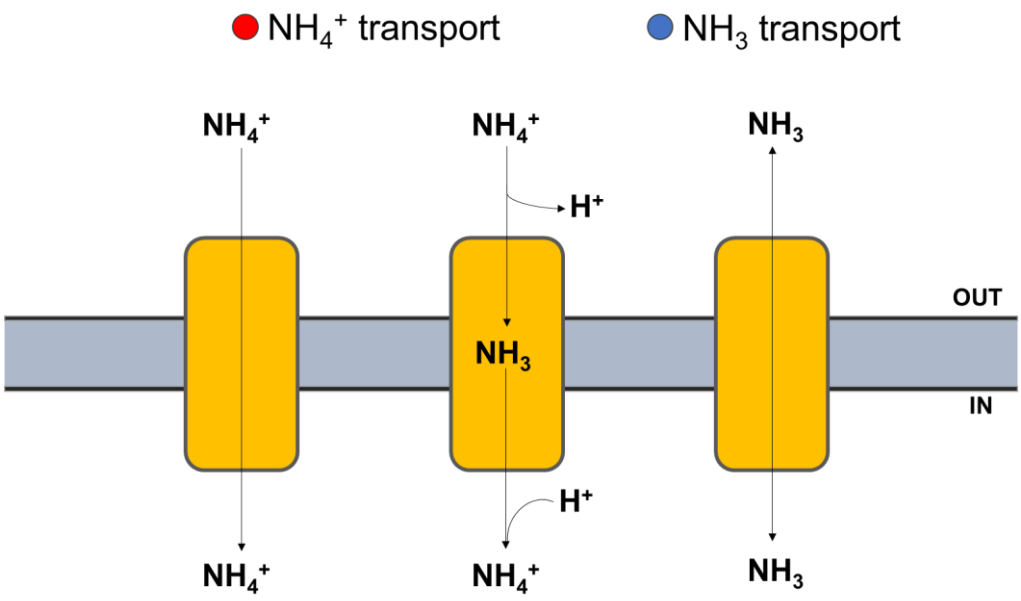

FIG 1.7 Mep/Amt (Red) and Rh (Blue) transporter mechanisms. Mep/Amt transporters are energy-dependent transporters that bind ammonium. Mechanisms include the uniport of NH_4^+ and the deprotonation of NH_4^+ prior to the transport of NH_3 and the co-transport of NH_3 and H^+ (Andrade *et al.,* 2007). Rh proteins are thought to act as NH_3 channels.

Most sequenced AOA encode ≥2 Amt-type transporters whilst approximately half of the available AOB genomes contain Rh proteins. Recent evidence suggests Mep/Amt transporters are energy-dependent electrogenic ammonium transporters whilst Rh-type proteins function as ammonia channels (Fig. 1.7, Wacker *et al.*, 2014; Offre *et al.*, 2014). Some AOB lack transporters and presumably to rely solely on the diffusion of ammonia across the membrane (Andrade *et al.*, 2005; Lehtovirta-Morley *et al.*, 2016b). Ammonia decreases exponentially with decreasing pH through ionization to ammonium and the preference for AOA to transport ammonium may contribute to their greater activity in acidic environments relative to AOB. Sequence and structural dissimilarities indicate AOA Amt transporters are functionally distinct (Offre *et al.*, 2014). Furthermore, the different transcriptional response of Amt transporters to low ammonium and ammonium-replete conditions suggests that many

AOA encode putative high-affinity and low-affinity transporters (Amt2 and Amt1, respectively) (Qin *et al.,* 2018; Santoro *et al.,* 2015; Nakagawa and Stahl, 2013). Notably, all sequenced representatives from the *Nitrosocosmicus* genus only encode the predicted low-affinity Amt, which could reflect their tendency to dominate AOA communities in high ammonium environments (Lehtovirta-Morley *et al.,* 2016b; Jung *et al.,* 2016; Sauder *et al.,* 2017; Alves *et al.,* 2019). Comammox bacteria that belong to clade A encode Rh-type transporters with >70% amino acid similarity to those found in beta-AOB, whilst clade B encode Amt-type transporters (Palomo *et al.,* 2018). Comammox clade B appears adapted to more oligotrophic conditions than clade A, which would be consistent with ammonium transport mechanisms (Liu *et al.,* 2019).

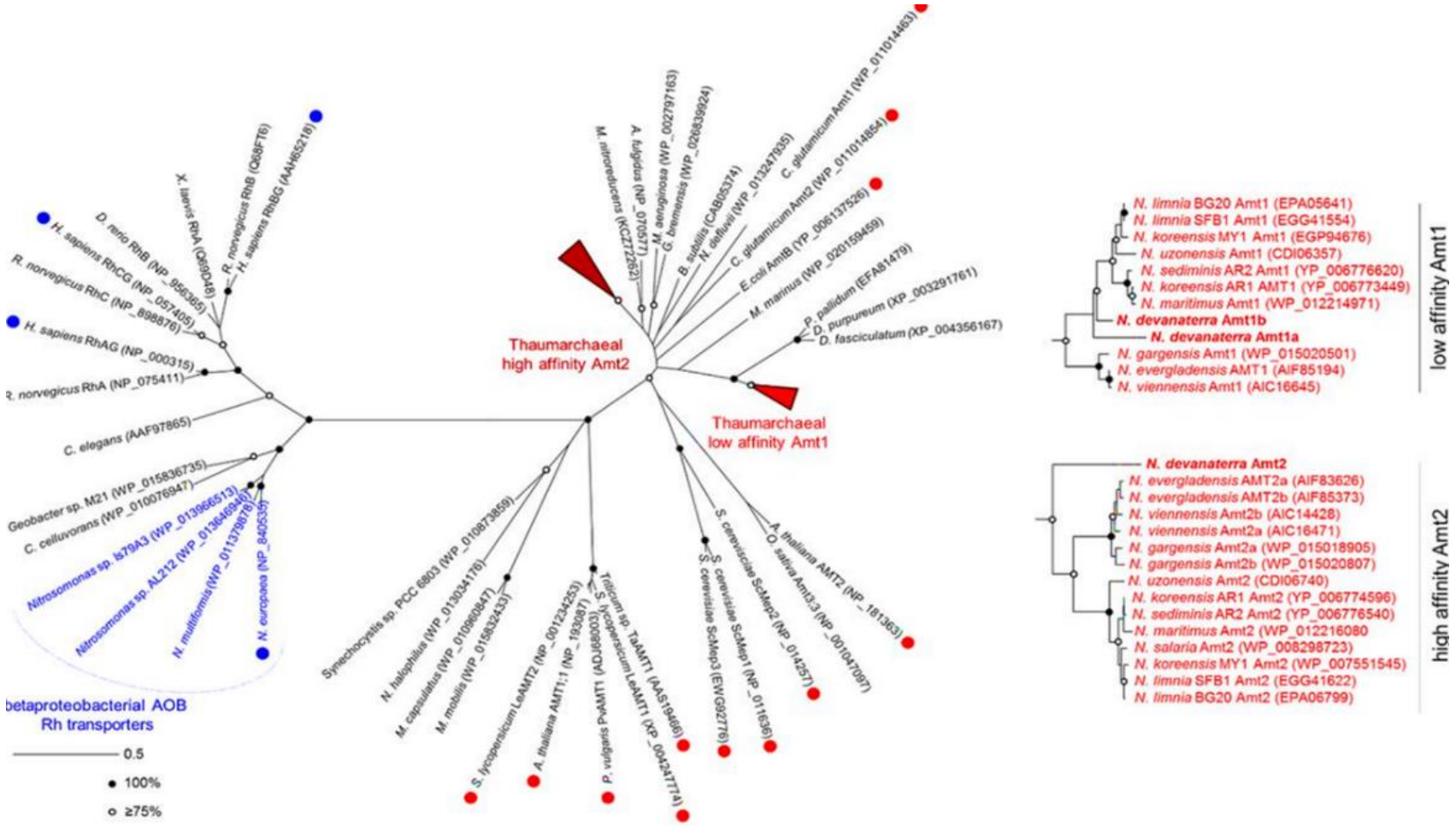

FIG 1.8 The maximum-likelihood phylogeny of Amt/Rh transporters. Red circles represent organisms with validated NH_4^+ transporters and blue NH_3 transporters. Inset shows the phylogeny of AOA 'high affinity' (Amt2) and 'low affinity' (Amt1) Amt transporters. Figure from Lehtovirta-Morley et al., (2016b).

Most sequenced AOA assimilate ammonia via glutamate dehydrogenase (GDH), which catalyses the reversible reductive amination of 2-oxoglutarate to glutamate (Fig. 1.9, Kerou *et al.,* 2016; Alves *et al.,* 2019). This low-affinity pathway requires high concentrations of ammonia to be present within the cell but since no ATP is consumed and less carbon is used per ammonia molecule assimilated, it is favourable under energy and carbon limiting conditions (Helling, 1994; van Heeswijk *et al.,* 2013). Interestingly, *Nitrosocosmicus arcticus* and the closely related *Nitrosocosmicus oleophilus* encodes genes for the glutamine synthetase-glutamate synthase (GS-GOGAT) pathway (Fig. 1.9, Jung *et al.,* 2016; Alves *et al.,* 2019). In this pathway glutamate is converted to glutamine by the ATP-dependent glutamine synthetase. glutamine-oxoglutarate aminotransferase (GOGAT) catalyses the NADPH-dependent formation of two glutamate molecules from glutamine and 2-oxoglutarate. This low affinity, energy consuming pathway for ammonia assimilation functions well at high ammonia concentrations, and when the cell is not energy or carbon limited (Helling, 1994; van Heeswijk *et al.,* 2013).

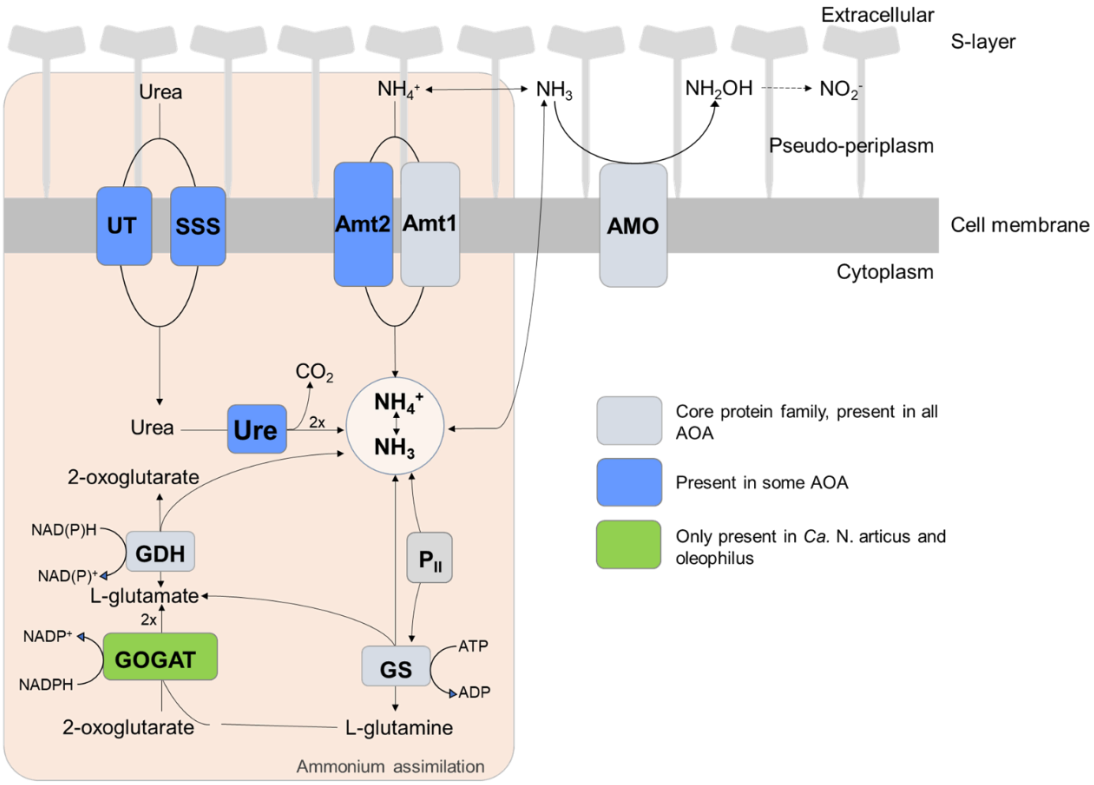

FIG 1.9 Ammonia assimilation pathways adapted from Alves *et al.,* (2019). The glutamine synthetase (GS)/glutamate dehydrogenase (GDH) pathway is found in all sequenced AOA. The glutamine synthetase-glutamate synthase (GS-GOGAT) pathway is only present in "*Ca.* Nitrosocosmicus articus" and "*Ca.* Nitrosocosmicus oleophilus".

Members of the P_{II} superfamily of signal transduction proteins play a vital role in regulating nitrogen metabolism (Forchhammer, 2008), and they are abundant in nearly all analysed AOA genomes with relatively conserved genetic linkage to Amt transporters (Kerou *et al.*, 2016; Lehtovirta-Morley *et al.*, 2016a). Sequence analysis indicates AOA homologues belong to the glnK/B subfamily of P_{II} proteins. GlnK and GlnB directly interact with Amt transporters and GS respectively, to regulate ammonium influx into the cell and GS activity in response to extracellular and intracellular nitrogen concentrations (Fig. 1.9). Other central molecules, such as pyruvate, have also been implicated in P_{II}-mediated regulation (Arcondeguy *et al.*, 2001).

1.6.5 Carbon fixation pathways

Thaumarchaea fix inorganic carbon using a modified version of the 3-hydroxypropionate/4-hydroxybutyrate (3HP/4HB) pathway (Fig. 1.10). The 3HP/4HB cycle begins with one acetyl-CoA and two bicarbonate molecules being converted via 3-hydroxypropionate to succinyl-CoA. Succinyl-CoA is then converted via 4-hydroxybutyrate to two molecules of acetyl-CoA, one of which serves as a carbon precursor. Other carbon precursors include pyruvate, phosphoenolpyruvate (PEP), oxaloacetate and 2-oxoglutarate, which are all generated from succinyl-CoA (Konneke *et al.,* 2014). The Thaumarchaea-specific variant of the 3HP/4HB pathway is the most energy-efficient aerobic carbon fixation pathway currently described (Konneke *et al.,* 2014). The efficiency of the cycle has been attributed to unique adaptations which includes: the use of ADP- rather than AMP-producing enzymes (reducing the number of high energy bonds required per one turn of the cycle), bifunctional enzymes that catalyse multiple reactions (reducing the cost of protein synthesis) and the oxygen tolerance of the key enzyme 4-hydroxybutyryl-CoA dehydratase (lowers enzyme maintenance and turnover costs) (Konneke *et al.,* 2014). An economical carbon fixation pathway is advantageous in energy-limited environments. AOB use the energy demanding Calvin-Benson-Bassham cycle to fix CO_2 and comammox bacteria fix inorganic carbon using a reductive tricarboxylic acid (rTCA) cycle which could be advantageous under microaerophilic conditions (Palomo *et al.,* 2017; Koch *et al.,* 2018).

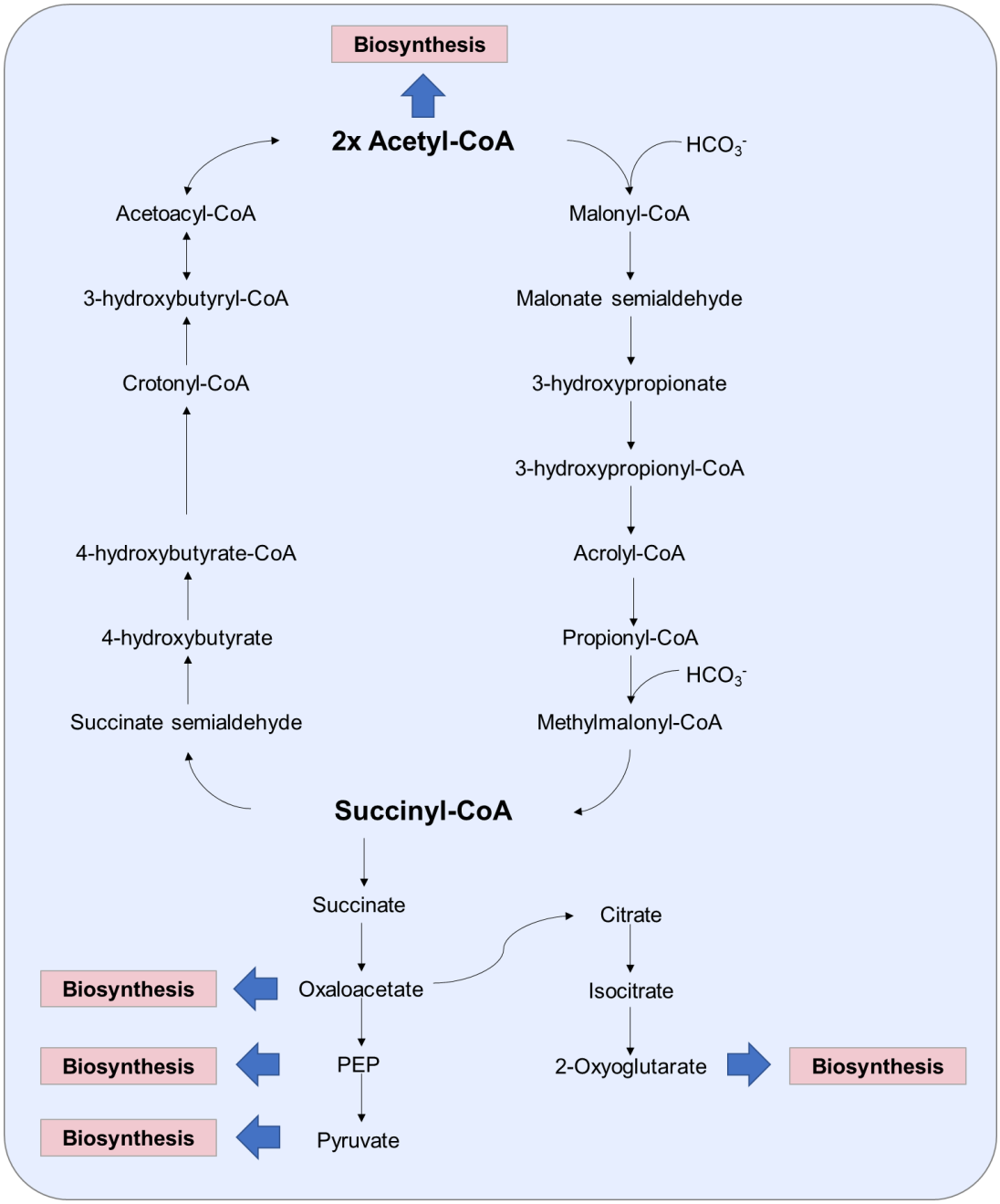

Fig. 1.10 The Thaumarchaeal 3-hydroxypropionate/4-hydroxybutyrate (3HP/4HB) carbon fixation pathway (Adapted from Alves *et al.,* 2019). One acetyl-CoA and two bicarbonate (HCO_3^-) moleculaes are converted to succinyl-CoA via 3-hydroxypropionate. Succinyl-CoA is converted via 4-hydroxybutyrate to two molecules of acetyl-CoA, one of which serves as a carbon precursor. Additional carbon precursors formed from succinyl-CoA include oxaloacetate, phosphoenolpyruvate (PEP), pyruvate and 2-oxoglutarate.

1.6.6 The genetic potential for metabolic flexibility

Many nitrogen-transforming microorganisms demonstrate remarkable metabolic flexibility, for example some NOB can derive energy for growth from formate, hydrogen and sulfide (Kuypers *et al.,* 2018; Koch *et al.,* 2018). Most AOA currently isolated or in enrichment demonstrate tight coupling between rates of ammonia oxidation and growth, even though the oxidation of ammonia provides very little energy for growth and cell maintenance. Intriguingly, recent characterisation of "*Ca.* Nitrosocosmicus arcticus" revealed that it was capable of growth uncoupled from ammonia oxidation, suggesting this strain has alternative or supplementing energy metabolism(s) (Alves *et al.,* 2019). Often AOA genomes encode genes that suggest a metabolism not solely reliant on ammonia oxidation, including transport systems and metabolic pathways, all of which offer hypotheses for future experimental exploration.

Many AOA have the genomic repertoire to carry out mixotrophic growth. Early studies of carbon metabolism in marine archaea indicated both autotrophic and heterotrophic modes of carbon assimilation occur (Ouverney & Fuhrman, 2000; Ingalls *et al.*, 2006; Nicol & Schleper, 2006). Recently Muck *et al.,* (2019) highlighted the high abundance of marine AOA in the lower water column which does not correlate with the low nitrification rates at these depths. The absence of *in-situ* bicarbonate incorporation and assimilation by AOA present in WWTPs also questions their strictly chemolithoautotrophic lifestyle (Sauder *et al.,* 2017; Mussman *et al.,* 2011). Potentially, the growth of these AOA communities could be stimulated by organic carbon present in biofilms. In fact, many AOA genomes harbour a complete or partially complete tricarboxylic acid (TCA) cycle as well as transporters for the uptake of intermediates (Spang *et al.,* 2012; Walker *et al.,* 2010; Hallam *et al.,* 2006). The incorporation of metabolic intermediates directly into the TCA cycle could

provide reducing power or precursors for biomolecule synthesis (Sauder *et al.,* 2017; Spang *et al.,* 2012).

Ammonia oxidisers often differ in their responses to organic compounds. For instance, the AOB *N. europaea* is stimulated by fructose and pyruvate but other AOB are not (Hommes *et al.,* 2003). Likewise, organic compounds stimulate the growth of some AOA strains whilst inhibit others, potentially due to their high copper complexation potential or ability to alleviate the toxic effect of organic acids a low pH (Gwak *et al.,* 2019; Lehtovirta-Morley *et al.,* 2014). Curiously, catalase-negative AOA appear to be stimulated by α-keto acids; however, this is attributed to the alleviation of oxidative stress, and catalase-positive strains are either unaffected or inhibited by α-keto acids (Kim *et al.,* 2016). The genome of "*Ca.* Nitrosocosmicus exaquare" encodes putative genes related to one-carbon (C_1) metabolism including methanol oxidation to formaldehyde and formate oxidation to CO_2 (Sauder *et al.,* 2017). All characterised AOA encode all the necessary genes to perform gluconeogenesis, however it is unknown if they carry out glycolysis (Jung *et al.,* 2016). The genomes of some *Nitrosocosmicus* strains encode putative periplasmic or membrane-bound pyrroloquinoline quinone (PQQ)-dependent dehydrogenases, which oxidise sugars/alcohol by simultaneously reducing electron acceptors, potentially contributing reducing equivalents to the respiratory chain (Alves *et al.,* 2019). Interestingly, PQQ-dependent dehydrogenases were among the most highly expresses genes by the newly discovered heterotrophic marine thaumarchaea (HMT), and therefore are very likely to be important for energy metabolism since these *Thaumarchaeota* lack the ability to oxidise ammonia (Alyward and Santoro, 2020).

Many AOA can use urea or cyanate as the sole source of energy and reductant as both are enzymatically converted to ammonium (Tourna *et al.,* 2011; Palatinszky

et al., 2015). Growth on urea or cyanate is not pH-dependent and therefore would be advantageous in acidic and/or low ammonium environments (Burton and Prosser, 2001; Lu *et al.,* 2012). The hydrolysis of urea is thought to support the growth of AOB such as *Nitrosoglobus* at low pH (Burton and Prosser, 2001; Hatysu *et al.,* 2017). Curiously, the oxidation of urea-derived N by marine AOA does not appear to be directly related to either pH or ammonium concentrations (Tolar *et al.,* 2016). Urea uptake is mediated by specific urea transporters (UTs) and solute/sodium symporters (SSS) where it is then hydrolysed intracellularly by a urease (Fig. 1.10). Comammox also have the genetic inventory for urea hydrolysis including a putative high-affinity uptake system, which could be an adaptation to low or fluctuating urea concentrations (Camejo *et al.,* 2017; Palomo *et al.,* 2017). *Nitrososphaera gargensis* is currently the only sequenced AOA that encodes a known cyanase which catalyses conversion cyanate to ammonium and CO_2 (Palatinszky *et al.,* 2015). Remarkably though, *N. maritimus* lacks a canonical cyanase but also appears to oxidise cyanate to nitrite (Kitzinger *et al.,* 2019). Genes possibly encoding enzymes belonging to a novel class of nitrilases or cyanide hydratases have been found in the genomes of AOA from the *Nitrosocaldus, Nitrosotenuis* and *Nitrosopumilus* genera (Walker *et al.,* 2010; Mosier *et al.,* 2012; Bayer *et al.,* 2016; Daebeler *et al.,* 2018). Nitrilases catalyse the conversion of nitriles to the corresponding acid and cyanide hydratases covert hydrogen cyanide (HCN) to formamide, both can produce ammonia (Luo *et al.,* 2021; Daebeler *et al.,* 2018). AOA deep seafloor sediments proteolysis and deamination to regenerate ammonia (Vuillemin *et al.,* 2019). All potentially advantageous when ammonia is limiting.

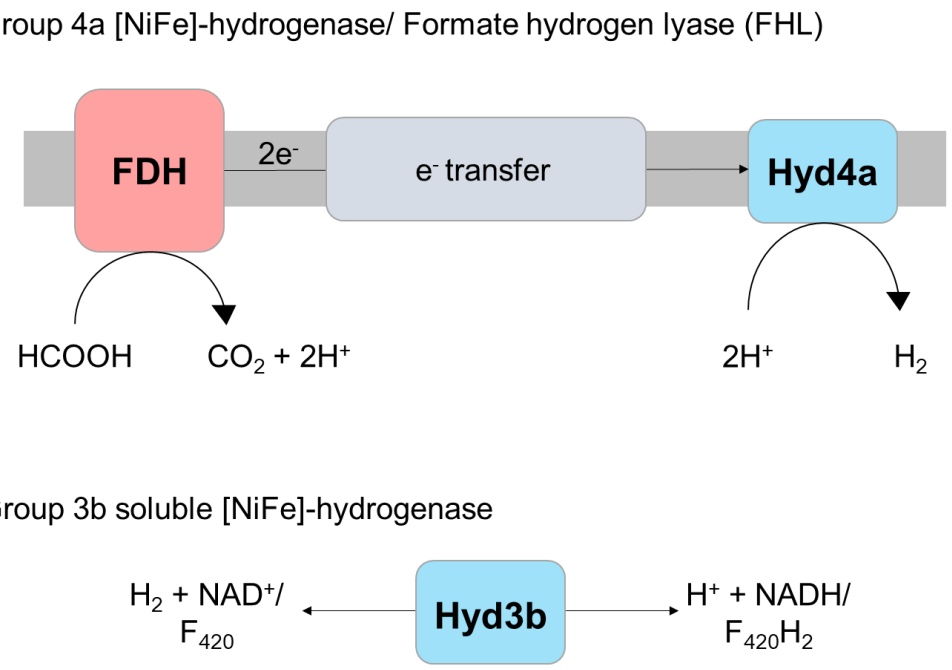

FIG 1.11 A The membrane associated Group 4a [NiFe]-hydrogenase/formate hydrogen lyase (FHL) which comprises of a formate dehydrogenase (FDH) and a [NiFe]-hydrogenase (Hyd4a), adapted from Enthaler *et al.,* (2010). Formate (HCOOH), generated from a biosynthetic pathway or imported into the cell is converted to CO_2 and $2H^+$, generating 2 e^-. The 2 e^- enter a membrane-bound electron transfer chain and delivered to a [NiFe]H_2ase which reduces $2H^+$ to generate H_2. **B** The Group 3b soluble [NiFe]-hydrogenase (Hyd3b) where oxidised F_{420} is predicted to be a substrate for Hyd3b. Adapted from Abby *et al.,* (2018).

The genomes of "*Ca.* Nitrosocaldus cavascurensis" and "*Ca.* Nitrosocaldus islandicus" both contain a full set of genes encoding for the four subunits of a soluble type NAD(P)-3b [NiFe]-hydrogenase (Abby *et al.,* 2018; Daebeler *et al.,* 2018). This group of hydrogenases can couple oxidation of H_2 to reduction of NAD(P) to provide reducing equivalents for biosynthesis (Abby *et al.,* 2018; Greening *et al.,* 2016). Interestingly, "*Ca.* Nitrosocaldus cavascurensis" 3b-[NiFe]-hydrogenase contained coenzyme F_{420}-reducing hydrogenase subunits. AOA can synthesise this cofactor and encode several F_{420}-dependent oxidoreductases with a yet unknown function. Abby and colleagues (2018) speculate that oxidised F_{420} could be a potential substrate for the 3b-[NiFe]-hydrogenase. The genomes of other AOA contain genes encoding a

Group 4a [NiFe]-hydrogenase or formate hydrogen lyase (FHL). The majority of Group 4a [NiFe]-hydrogenases have a respiratory function (Greening et al., 2016). Subunits associate into complexes, comprising of primary dehydrogenases and terminal hydrogenases, and conserve energy during electron transfer as proton or sodium motive force (Fig. 1.11A). FHL does not normally operate under standard conditions but are expressed under certain physiological conditions. In *E. coli*, during mixed-acid fermentation, the membrane-bound FHL complex disproportionates formate to CO_2 with the concomitant reduction of protons to H_2. (McDowall et al., 2014). Considering the function of the FHL in *E. coli*, the putative FHL encoded by AOA could generate proton-motive force and maintain redox homeostasis in the absence of O_2 (Berney et al. 2014). This type of metabolic flexibility would be advantageous to an ammonia oxidiser in an environment with fluctuating O_2 or ammonium concentrations (potentially due to changes in pH). Interestingly, hydrogenases appear to be mainly absent in the genomes of AOB, apart from in two representatives from the *Nitrosomonas* cluster 6a and *Nitrosopira multiformis* (Sadlacek *et al.*, 2019; Norton et al., 2008).

1.7 The enzymology of ammonia oxidation

AOA, AOB and comammox initiate the ammonia oxidation pathway with the oxidation of ammonia to hydroxylamine using conserved membrane associated AMO enzymes (Stein, 2019; Vajrala *et al.*, 2012). The oxidation of ammonia to hydroxylamine occurs with a concomitant reduction of one molecule of oxygen to water. Whilst the oxidation of ammonia generates two electrons, four electrons are required to reduce one molecule of oxygen, therefore and additional two electrons must be supplied to AMO from downstream reactions (Arp *et al.*, 2002). The AMO is the only enzyme of the pathway which is shared by all three major groups of ammonia

oxidisers (Lehtovirta-Morley, 2018). Thereafter, the downstream enzymology differs considerably between archaeal and bacterial ammonia oxidisers (Vajrala *et al.,* 2012; Martens-Habbena *et al.,* 2015; Caranto & Lancaster, 2017). Comparative genomics indicates that the ammonia oxidation genomic repertoire of comammox bacteria is very similar to that of AOB (Daims et al, 2015).

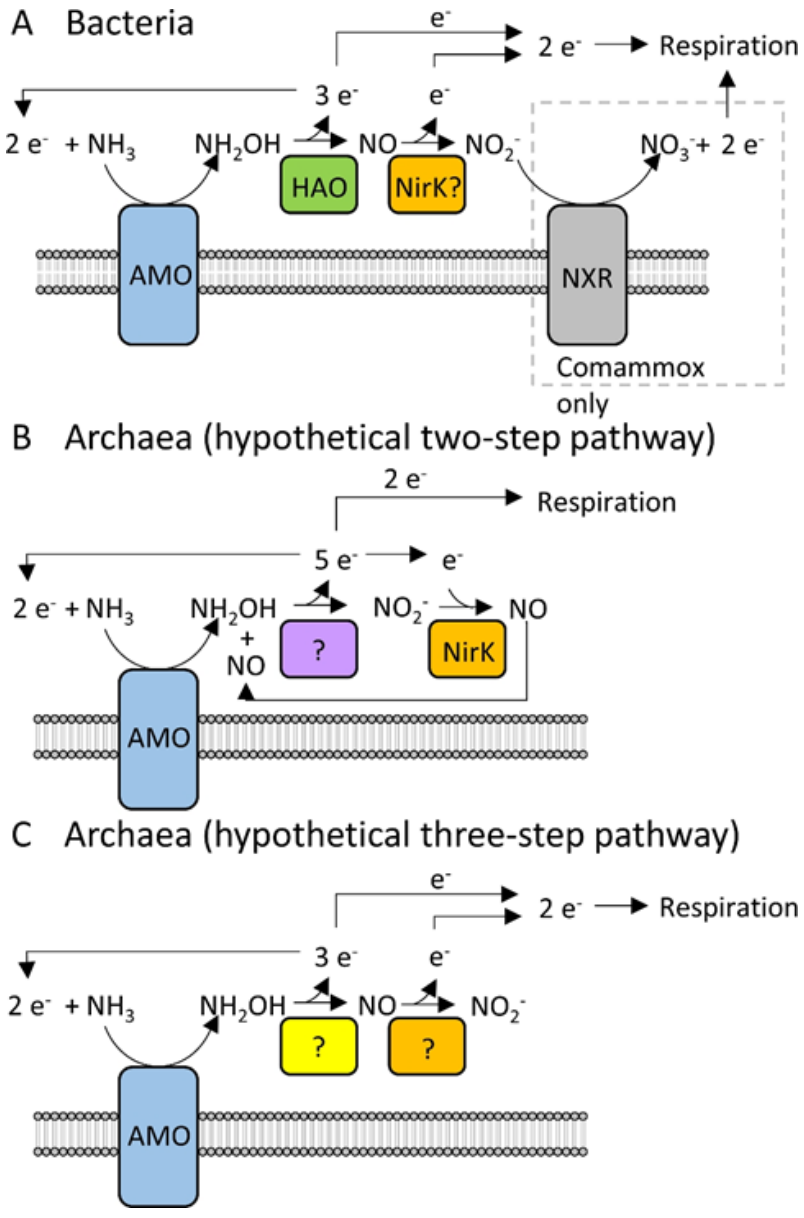

FIG 1.12 A The bacterial ammonia oxidation pathway proposed by Caranto and Lancaster (2017). **B** The hypothetical two-step pathway for ammonia oxidation by AOA. NO is a co-reactant for the unknown hydroxylamine oxidising enzyme/enzyme complex (Kozlowski *et al.,* 2016). **C** The three-step pathway for ammonia oxidation by AOA (Lehtovirta-Morley, 2018; Lancaster *et al.,* 2018; Carini *et al.,* 2018). Figures from Lehtovirta-Morley (2018).

1.7.1 Ammonia oxidation by AOB

In AOB, the subsequent oxidation of hydroxylamine releases four electrons, two enter the electron transport chain to generate ATP and reducing equivalents and two are transferred to the AMO as reducing equivalents (Whittaker *et al.,* 2000; Arp *et al.,* 2002; Gonzalez-Cabaleiro *et al.,* 2019; Prosser *et al.,* 2020). The oxidation of hydroxylamine is catalysed by a heme-enriched hydroxylamine dehydrogenase (HAO) enzyme. Previously, the ammonia oxidation pathway in AOB was considered to be a two-step process, beginning with the oxidation of ammonia to hydroxylamine, followed by the dehydrogenation of hydroxylamine to nitrite. Caranto and Lancaster, (2017) have recently shown that nitric oxide (NO), and not nitrite is the most likely product of hydroxylamine oxidation. Hydroxylamine oxidation to NO would generate three electrons and the fourth electron would be generated by the oxidation of NO to nitrite. The enzyme catalysing NO to nitrite has not yet been identified. Caranto and Lancaster (2017) suggested that copper-dependent nitrite reductase (NirK) could catalyse NO to nitrite. Previously, NirK was thought to be involved in denitrification of nitrite to NO in AOB, but in this scenario, NirK would function in reverse. On the other hand, *nirK* is not present in all AOB genomes and the expression does not appear tightly linked to ammonia oxidation (Stein, 2019). Additionally, the growth of *N. europaea* appeared to be unaffected by the deletion of *nirK* (Kozlowski *et al.,* 2014). Another potential candidate is the red copper protein nitrosocyanin, encoded by *ncyA*, which is unique to AOB and co-ordinately expressed with other ammonia oxidation genes (Zorz *et al.,* 2018). Nevertheless, *ncyA* is absent in the genomes of some oligotrophic AOB strains and is not found in comammox bacteria (Stein, 2019; Bollmann *et al.,* 2013; Sedlacek *et al.,* 2019).

1.7.2 Ammonia oxidation by AOA

The biochemistry of ammonia oxidation in archaea is even more intangible compared to AOB. No homologues of HAO genes have been identified in the genomes of AOA and the system of electron carriers linking hydroxylamine oxidation to the terminal oxidase is currently unknown. Potential hydroxylamine oxidising enzymes include a periplasmic multicopper oxidase (MCO1) (Walker *et al.,* 2010; Kerou *et al.,* 2016), although MCO1 are absent from the core genome of *Nitrosotalea* (Herbold *et al.,* 2017). Several studies have demonstrated that NO is both produced and consumed by AOA during the oxidation of hydroxylamine (Steiglmeier *et al.,* 2014b; Martens-Habbena *et al.,* 2015) and that ammonia oxidation by AOA is much more sensitive to inhibition by PTIO (2-phenyl-4,4,5,5-tetramethylimidazoline-1-oxyl-3-oxide), a scavenger of free NO, compared to AOB (Yan *et al.,* 2012; Shen *et al.,* 2013; Sauder, Ross and Neufield, 2016; Lehtovirta-Morley, 2018). This suggests that the archaeal ammonia oxidation pathway is different to the bacterial pathway and the production and consumption of NO is tightly coupled in AOB, whilst the energy metabolism of AOA requires free NO. A study by Steiglmeier *et al.,* (2014b) found the isotopic signature of N_2O, which is produced by *N. viennensis* during hydroxylamine oxidation, indicated that one nitrogen originated from ammonium and the other came from nitrite. Subsequently, the same group proposed a model two-step ammonia oxidation pathway in which a novel copper containing HAO accepts both hydroxylamine and NO as co-substrates, resulting in a five-electron oxidation to form two molecules of nitrite. In this model, NirK catalyses the reduction of one molecule of nitrite to NO, which is required for the previous reaction (Kozlowski *et al.,* 2016). The function of *nirK* homologues in AOA has not been confirmed however they are amongst some of the most abundant transcripts detected in many transcriptome and

meta-transcriptome datasets, indicating an important role in AOA energy metabolism (Kerou *et al.,* 2016; Carini *et al.,* 2018). Furthermore, *nirK* expression by *N. maritimus* significantly decreases under ammonia starvation (Qin *et al.,* 2017). However, the marine sponge symbiont *Cenarchaeam symbiosum* and representatives from the *Nitrosocaldus* genus do not encode *nirK* (Hallam *et al.,* 2006; Abby *et al.,* 2018; Daebaler *et al.,* 2018). It should also be noted that hydroxylamine and nitrous acid can react abiotically to form N_2O, which would still yield one nitrogen sourced from ammonium and the other from nitrite, respectively, which is in agreement with the isotopic signature of N_2O from *N. viennensis* (Steiglmeier *et al.,* 2014b; Lehtovirta-Morley, 2018).

An alternative model is that AOA could use a three-step pathway, whereby ammonia is oxidised to hydroxylamine and subsequently to NO and nitrite, as suggested for AOB (Lehtovirta-Morley, 2018; Lancaster *et al.*, 2018). In this scenario, the rate of hydroxylamine oxidation exceeds that of NO oxidation, and the presence of free NO is required to induce NO oxidising activity, which could account for the increased sensitivity of AOA to NO-scavengers compared to AOB. NirK could catalyse the conversion of NO to nitrite, as suggested for AOB, but this would not resolve the fact that NO in AOA without *nirK* homologues also appears to be an obligate intermediate. Recently, a purple cupredoxin was isolated from *N. maritimus* with the capability *in vitro* of oxidising NO to nitrite, however, NO oxidising activity *in vivo* has yet to be investigated (Hosseinzadeh *et al.,* 2016).

1.8 The structure and function of AMO

The AMO is a copper-dependent multimeric transmembrane enzyme belonging to the CuMMO superfamily which comprises of ammonia, methane and

alkane monooxygenases. Difficulties in purifying active AMO has limited the amount of structural data available and many predictions about the structure of AMO are based on homology to the better-characterised particulate methane monooxygenase (pMMO) from methanotrophs (Holmes *et al*, 1995; Lawton *et al.*, 2014).

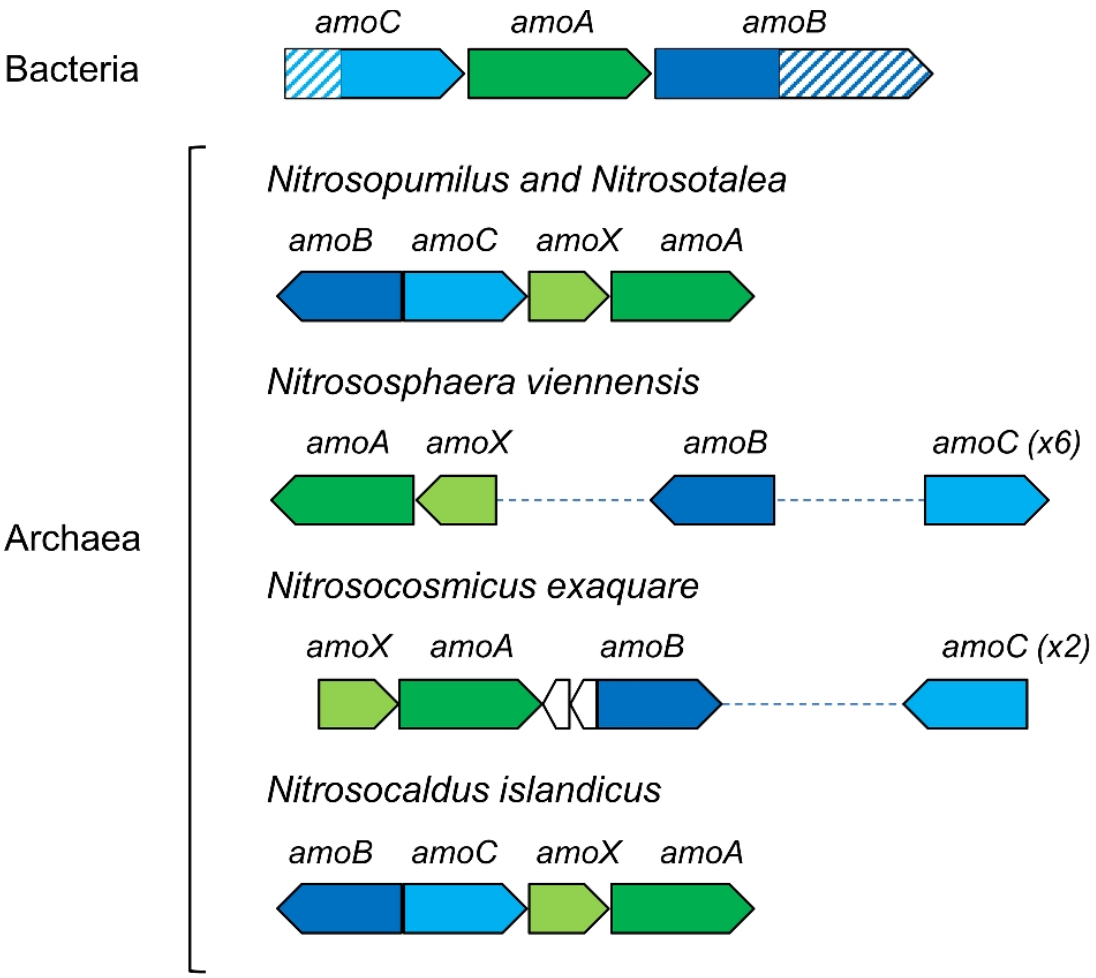

FIG 1.13 Organisation of the AMO gene clusters in bacteria and archaea. The N-terminus of AmoC and C-terminus of AmoB are truncated in archaea (indicated by stripes in bacteria) (Figure from Lehtovirta-Morley, 2018).

The AMO is predicted to exist as a heterotrimeric complex composed of three subunits; AmoA, AmoB and AmoC (Tolar *et al.*, 2017). In AOB, the AMO is encoded by an *amoCAB* operon. Often there are additional copies of *amoC* present (Khadka *et al.*, 2019). The archaeal AMO is very divergent from bacterial AMO (other CuMMOs)

and includes a fourth subunit, *amoX*, found adjacent to *amoA* in all sequenced AOA genomes (Lehtovirta-Morley, 2018; Lancaster *et al.*, 2018). Unlike bacteria, archaea do not use operons or produce polycistronic transcript (Lehtovirta-Morley, 2018). In some AOA, the AMO subunits are located together in an *amoAXCB* arrangement, but this is not always the case. The archaeal *amoB* and *amoC* are truncated compared to bacterial AMO and pMMO (Lehtovirta-Morley, 2018). In addition, some AOA harbour multiple copies of *amoA*, *amoB* and *amoC*. In AOB, a monocistronic variant of *amoC* has been implicated in stress response, acting to repair or stabilise the AMO holoenzyme during ammonia starvation and heat stress (Berube and Stahl, 2012). The additional copies of archaeal *amoC* could also be involved stress response since the transcription of *amoC* by *N. maritimus* persisted, relative to *amoA* and *amoB*, during energy starvation (Qin *et al.*, 2017). AmoX is predicted to consist of three transmembrane helices but its function is currently unknown (Tolar *et al.*, 2017).

The location and nature of the AMO active site has not been identified. Analysis of the AmoA and AmoC protein structure favours an extracellular active site (outwards facing) (Lehtovirta-Morley *et al.*, 2016), which would be logical considering the toxicity of hydroxylamine. Substrates and inhibitors of the AMO are largely non-polar, suggesting the active site is hydrophobic, which is consistent with ammonia rather than ammonium as the native substrate (Lancaster *et al.*, 2018). All ammonia oxidisers are inhibited by the copper chelator allylthiourea (ATU), albeit at different thresholds, which confirms the AMO is copper-dependent (Hatzenpichler *et al.*, 2008; Taylor *et al.*, 2010; Shen *et al.*, 2013; Lehtovirta-Morley *et al.*, 2013). Interestingly, linear terminal alkynes differentially inhibit bacterial and archaeal AMOs. For example, ammonia oxidation by the AOB *N. europaea* and *N. multiformis* is strongly and irreversibly inhibited by 1-octyne. In comparison, AOA are

considerably less sensitive to 1-octyne inhibition and in *N. viennensis* the inhibition was shown to be fully reversible (Taylor *et al.,* 2013; Taylor *et al.,* 2015). Differences in the sensitivity to inhibitors could indicate variances in the AMO binding and catalytic site(s) between AOA and AOB (Taylor *et al.,* 2015).

Typically, CuMMO have broad substrate ranges. Both the bacterial AMO and pMMO can co-oxidise a range of hydrocarbons, aromatic compounds and sulphides (Further discussed in Chapters 3 and 4). It has been suggested that the downstream metabolism defines the functional role of microbes containing CuMMO (Pester *et al.*, 2011). For example, the bacterial ammonia oxidisers *Nitrosococcus oceani* and *N. europaea* can oxidise methane but lack necessary downstream enzymes to gain energy from methane oxidation (Hyman & Wood, 1983). Likewise, several methanotrophs have been shown to co-oxidise ammonia however this does not support growth (Dalton, 1977; Nyerges & Stein, 2009). AMO- and pMMO-expressing microbes have received interest for their potential use in bioremediation due to their capability to co-oxidize persistent organic pollutants such as halogenated alkanes and alkenes and chlorinated hydrocarbons (Sayavedra-Soto *et al.,* 2010; Semrau, 2011). Little is known about alternative substrates co-oxidised by the archaeal AMO. Recently, it was shown that *N. gargensis* was capable of co-metabolising two tertiary amines, mianserin and ranitidine (pharmaceutical drugs), with the initial oxidative reaction possibly carried out by AMO (Men *et al.,* 2016). It is interesting to consider the global significance of the co-oxidation of substrates such as methane by the archaeal AMO, given their abundance and distribution in the environment. In addition, investigating alternative substrate reactions and products could advance our understanding of the structure of archaeal AMO, particularly regarding the location and structure of the active site(s).

1.9 Thesis objectives

(1) Active AMO is difficult to purify, and its structure and function are largely unexplored in archaea. The project aimed to characterise the substrate range of the archaeal AMO by studying the inhibition of the AMO from "*Ca.* Nitrosocosmicus franklandus" and "*Ca.* Nitrosotalea sinensis" to specific alkyne inhibitors and comparing with inhibition of other members of the copper-dependent membrane monooxygenase family, namely the bacterial AMO from *N. europaea* and the pMMO from *M. capsulatus.* Additionally, insights regarding the structure of the archaeal AMO and the active site(s) were investigated using whole cell inhibition kinetics.

(2) Members of the CuMMO family typically co-oxidise a range of substrates (detailed in Section 1.8). The primary aims were to firstly, characterise the inhibition of the AMO from "*Ca.* Nitrosocosmicus franklandus" by methane and methanol using whole cell inhibition kinetics. Secondly, ^{13}C-methane tracer experiments were used to explore methane oxidation and metabolism.

(3) The AMO from *N. europaea* can oxidise alternative substates in the absence of ammonia, using an external source of reductant such as hydrazine. Hydrazine was therefore tested as an external source of reductant for alternative substrate oxidations by "*Ca.* Nitrosocosmicus franklandus".

(4) The archaeal ammonia oxidation pathway is poorly understood. Two putative pathways have been put forward (described in Section 1.7.2, Fig. 1.12). Previous studies suggest that free-NO (i.e able to be scavenged) is important for AOA energy metabolism in AOA but not in AOB. Consequently, NO features prominently in the two hypothetical pathways, but with very different roles. Therefore, the effect of NO-

scavenger, PTIO, on both NH_3 and hydroxylamine oxidation by "*Ca.* Nitrosocosmicus franklandus" and *N. europaea* was assessed to provide insights into the role of NO in AOA.

2. Materials and methods

2.1 Materials

Analytical grade chemicals were obtained from Sigma-Aldrich (St Louis, MO, USA), Fisher Scientific (Loughborough, UK), Melford (Ipswich, UK) and Formedium (Hunstanton, UK). Gases were obtained from Sigma-Aldrich, Apollo Scientific Ltd (Stockport, UK) and BOC (Manchester UK). Custom oligonucleotide primers were obtained from Invitrogen (Paisley, UK).

2.2 Growth media and maintenance of microorganisms

All glassware used for media preparation and cultivation was acid washed in 10% nitric acid and rinsed with ddH_2O to remove contaminants. All media components were prepared with ddH_2O water and sterilised by autoclaving at 15 psi for 15 minutes at 121°C. Heat sensitive components were sterilised using 0.2 μm pore size disposable Minisart syringe filters (Sigma Aldrich/Sartorius, Germany).

2.2.1 Growth of ammonia oxidising archaea

"*Ca.* Nitrosocosmicus franklandus" and *Nitrososphaera viennensis* EN76 were routinely grown at 37°C and "*Ca.* Nitrosotalea sinensis" at 30°C, in 200 - 800 ml volumes in 1 litre Duran bottles (Fisher Scientific). All AOA strains were cultivated statically in the dark and transferred (0.1-10% inoculum) to fresh medium when 1 mM NH_4^+ had been oxidised by both "*Ca.* Nitrosocosmicus franklandus" and *N. viennensis* EN76 and 0.1 mM NH_4^+ by "*Ca.* Nitrosotalea sinensis". The purity of AOA cultures was routinely screened by plating onto solid R2A media (1.5 % w/v) and by phase contrast microscopy.

Media stock solutions:

Fresh water medium (FWM) (Tourna *et al.*, 2011) contained per litre:

NaCl	1.0 g
$MgCl_2 \cdot 6H_2O$	0.4 g
$CaCl_2 \cdot 2H_2O$	0.1 g
KH_2PO_4	0.2 g
KCl	0.5 g

The solution was sterilised by autoclaving and stored at room temperature.

Modified non-chelated trace solution (Könneke *et al.*, 2005) contained per litre:

HCl (12.5 M)	8.0 mL
H_3BO_3	30.0 mg
$MnCl_2 \cdot 4H_2O$	100.0 mg
$CoCl_2 \cdot 6H_2O$	190.0 mg
$NiCl_2 \cdot 6H_2O$	24.0 mg
$CuCl_2 \cdot 2H_2O$	2.0 mg
$ZnSO_4 \cdot 7H_2O$	144.0 mg
$Na_2MoO_4 \cdot 2H_2O$	36.0 mg

The solution was sterilised by autoclaving and stored at 4°C.

Vitamin solution (pH 7.0) contained per litre:

Biotin	0.02 g
Folic acid	0.02 g
Pyridoxine HCl	0.10 g
Thiamine HCl	0.05 g
Riboflavin	0.05 g
Nicotinic acid	0.05 g
$_{DL}$-Pantothenic acid	0.05 g
$_{P}$-Aminobenzoic acid	0.05 g
Choline Chloride	2.00 g
Vitamin B_{12}	0.01 g

The pH of the solution was adjusted with 10 M KOH to 7.0, filter sterilised and stored at 4°C for a maximum of 6 months.

4-(2-hydroxyethyl)-1-piperazineethanesulfonic acid (HEPES) buffer (1 M HEPES, 0.6 M NaOH, pH 7.5):

HEPES	119.0 g
NaOH	12.0 g

NaOH was dissolved in 300 ml of water. HEPES was slowly added to the solution whilst stirring continuously. The pH was adjusted to 7.5 with 10 M NaOH or 12.5 M HCl and the final volume was 500 ml. The buffer was sterilised by autoclaving and stored at 4°C.

2-(N-morpholino) ethanesulfonic acid (MES) buffer (0.5 M, pH 5.3) was prepared by dissolving 53.3 g MES hydrate in 400 ml water. The pH was adjusted to 5.3 with 12.5 M HCl and solution was sterilised by autoclaving.

Phenol red solution was prepared by dissolving 0.05 g phenol red in 100 ml water. The solution was filter-sterilised and stored at 4°C.

"*Ca.* Nitrosocosmicus franklandus" C13 was cultivated in FWM supplemented with sterile stocks of the following (per litre): 1 ml modified non-chelated trace solution, 1 ml FeNaEDTA (7.5 mM), 2 mM $NaHCO_3$, 5 mM NH_4Cl, 10 or 20 ml HEPES buffer (pH 7.5), 1 ml vitamin solution and 1 ml phenol red solution as pH indicator.

***Nitrososphaera viennensis* EN76** was cultivated in FWM supplemented with sterile stocks of the following (per litre): 1 ml modified non-chelated trace elements, 1 ml FeNaEDTA (7.5 mM), 2 mM $NaHCO_3$, 2.5 mM NH_4Cl, 20 ml HEPES buffer (pH 7.5), 1 ml vitamin solution, 0.1 mM pyruvate, 50 mg kanamycin and 1 ml phenol red solution.

"*Ca.* Nitrosotalea sinensis" Nd2 was cultivated in FWM supplemented with sterile stocks of the following (per litre): 1 ml modified non-chelated trace elements, 1 ml FeNaEDTA solution (7.5 mM), 4 mM $NaHCO_3$, 0.5 mM NH_4Cl, 2.5 mM MES buffer (pH 5.3). The pH of the medium was adjusted to 5.3 with 1.25 M HCl.

2.2.2 Growth of *Nitrosomonas europaea* ATCC19718:

N. europaea ATCC19718 was obtained from the University of Aberdeen Culture Collection and cultivated in 100 - 200 ml volumes, in 500 ml conical flasks, with shaking (160 rpm) and in the dark at 30°C. *N. europaea* was routinely grown in a modified Skinner and Walker (1961) medium (pH 7.5). The purity of cultures was

screened by phase-contrast microscopy using a Zeiss Axioskop 50 microscope, 130 VS Type B (Carl Zeiss Ltd, Cambridge, UK) at ×1,000 magnification.

Modified Skinner and Walker (1961) medium

Mineral salt solution contained per litre:

$(NH_4)_2SO_4$	0.235 g
KH_2PO_4	0.200 g
$CaCl_2 \cdot 2H_2O$	0.040 g
$MgSO_4 \cdot 7H_2O$	0.040 g

The solution was sterilised by autoclaving and stored at room temperature (RT).

The mineral salt solution was supplemented with sterile stocks of the following (per litre): 1 ml FeNa-EDTA, 10 mM HEPES buffer (1 M HEPES, 0.6 M NaOH, pH 7.5) and 8 ml 5% (w/v) Na_2CO_3 (anhydrous).

2.2.3 Growth of *Methylococcus capsulatus* (Bath)

M. capsulatus strain Bath (Whittenbury *et al.,* 1970) was cultivated in 50 ml volumes in 250 mL Quickfit conical flasks sealed with autoclaved SubaSeals, shaking (180 rpm) at 37°C. *M. capsulatus* was grown in nitrate mineral salts (NMS) medium, supplemented with 20 μM copper to promote pMMO expression (Stanley *et al.,* 1983) and under an atmosphere of 40% methane (95%:5% mix of CH_4:CO_2) in air. Growth was determined by measuring optical density at 540 nm (OD_{540}) on a UV-1800 spectrophotometer (Shimadzu, Milton Keynes, UK) and the purity of cultures was routinely screen by phase-contrast microscopy as described earlier.

NMS medium (modified from Whittenbury *et al.*, 1970)

Required stock solutions:

NMS salts contained per litre:

KNO_3	1.0 g
$MgSO_4 \cdot 7H_2O$	1.0 g
$CaCl_2 \cdot 2H_2O$	0.2 g

The solution was sterilised by autoclaving and stored at RT.

Sodium molybdate solution contained per litre:

Na_2MoO_4	0.26 g

The solution was sterilised by autoclaving and stored at RT.

Trace elements contained per litre:

$FeSO_4 \cdot 7H_2O$	500.0 mg
$ZnSO_4 \cdot 7H_2O$	400.0 mg
H_3BO_3	15.0 mg
$CoCl_2 \cdot 6H_2O$	50.0 mg
EDTA di-sodium salt	250.0 mg
$MnCl_2 \cdot 4H_2O$	20.0 mg
$NiCl_2 \cdot 6H_2O$	10.0 mg

The trace element components were dissolved the order described above, sterilised by autoclaving and stored in the dark at RT.

Sodium phosphate buffer (pH 6.8) contained per litre:

$Na_2HPO_4 \cdot 12H_2O$	71.6 g
KH_2PO_4	26.0 g

The pH was adjusted to 6.8, sterilised by autoclaving and stored at RT.

The complete medium consisted of the NMS salt solution supplemented with sterile stocks of the following (per litre): 1 ml trace elements solution, 1 ml FeNa-EDTA (7.5 mM), 1 ml sodium molybdate solution and 10 ml sodium phosphate buffer (pH 6.8).

To confirm that *M. capsulatus* cells were only expressing pMMO and not soluble MMO (sMMO), the naphthalene assay, which is specific for sMMO activity, was used (Brusseau *et al.*, 1990) with sMMO-expressing *Methylocella silvestris* cells as positive controls. *M. silvestris* cultures were grown and maintained according to Dunfield *et al.*, (2003).

2.2.3.1 Naphthalene assay (Brusseau *et al.*, 1990)

A qualitative naphthalene assay was used to detect naphthalene oxidising activity. Approximately 1 ml of active cells at OD_{540} was incubated with a few crystals of naphthalene for 30 min at 30°C. Freshly prepared tetrazotized *o*-dianisidine (40 µl of 10 mg ml^{-1}) was added and the immediate development of purple colour was evidence of naphthalene oxidation.

2.3 Cell harvesting

AOA and *N. europaea* cells were routinely harvested by filtration onto 45 mm diameter PES membrane filters (0.22 μm pore size) (PALL, Port Washington, NY). "*Ca.* Nitrosocosmicus franklandus" and *N. viennensis* cells were washed with 10 mM HEPES (pH 7.5)-buffered FWM, with no added NH_4Cl, to remove residual NH_4^+ and NO_2^-. Cells were then resuspended by reverse filtration into 10 mM HEPES (pH 7.5)-buffered FWM without NH_4Cl to the desired cell concentration. "*Ca.* Nitrosotalea sinensis" cells were washed and resuspended in 2.5 mM MES (pH 5.3)-buffered FWM. *N. europaea* cells were washed and resuspended in 50 mM sodium phosphate buffer (pH 7.8) containing 2 mM $MgCl_2$ (Hyman and Wood, 1983). *M. capsulatus* was cultivated to an OD_{540} of 0.8 and cells were collected by centrifugation **(**14,000 × *g*, 10 min, 20°C), washed twice and resuspended in 10 mM 1,4-piperazinediethanesulfonic acid (PIPES) buffer (pH 7.0). All concentrated cell suspensions were maintained in the dark, at their respective growth temperatures and used within 3 h of harvesting.

2.4 Cell counts and protein quantification

2.4.1 Cell counts

Total cell concentration was determined microscopically in 1 ml samples. Cells were fixed by the addition of 5% formaldehyde (final concentration; v/v) and stored at 4°C until enumeration. For enumeration, fixed cells were stained with 30 μl of 200 μg ml^{-1} DAPI and incubated at RT for 5 min in the dark. The stained cells were filtered onto a Cyclopore 0.22-μm pore-sized black polycarbonate filter (Sigma-Aldrich) using a vacuum in a standard filtration set-up. Dried filters were mounted onto glass slides with antifadent (Citifluor AF2, Citifluor Ltd, Leicester, UK) and a

cover slip. Cells were counted under immersion oil using a Zeiss Axioskop 50 microscope, 130 VS Type B (Carl Zeiss Ltd, Cambridge, UK) at ×1,000 magnification. Cells were diluted to yield 10-200 cells per view and were counted for at least five fields of view.

2.4.2 Protein quantification

"*Ca.* Nitrosocosmicus franklandus" cells were harvested from stationary phase cultures and resuspended in 1 ml FWM salt solution. Protein concentration was determined colorimetrically using the Pierce bicinchoninic acid (BCA) Protein Assay Kit (Thermo Scientific) using the 'Enhanced Test Tube Protocol' according to the manufacturer's instructions. Cells (100 µl) were lysed by adding 10 µl SDS (10% w/v) and 17.5 µl NaOH (1.6 M) and boiling for 10 min. Samples were neutralised by the addition of HCl (1.2 M) prior to protein determination.

For *N. europaea,* a total cellular protein concentration of 120 fg cell^{-1}, reported by Martens-Habbena *et al.,* (2009), was used to normalise activity and growth rates.

2.5 Nutrient measurements

2.5.1 Nitrite measurements

Ammonia oxidisers demonstrate stoichiometric conversion of NH_3 to NO_2^- under aerobic conditions. Therefore, NO_2^- production was used to estimate NH_3 oxidation rates. NO_2^- production by AOMs also correlates with increasing cell densities and was used to estimate the growth of AOA and *N. europaea* cultures (Tourna *et al.,* 2011). NO_2^- was measured colorimetrically in 96-well flat bottom clear microtiter plates by diazotising and coupling with Griess reagent (Shinn, 1941). Firstly, 20 µl of sulphanilamide solution (5 g L^{-1} in 2.4 M HCl) was added to 100 µl of sample or standard, followed by the addition of 20 µl N-(1-naphthl)ethylenediamine

dihydrochloride solution (3 g L^{-1} in 0.12 M HCl). Standards were performed in duplicate and prepared using KNO_2 ranging from 1.6 to 50 μM. The absorbance was recorded at 540 nm wavelength using a VersaMax platereader (Molecular Devices, CA, US).

2.5.2 Ammonium measurements

Ammonium (NH_4^+) was determined colorimetrically using a modified indophenol method (Berthelot method). A working reagent was prepared by mixing 1:1 v/v ratio of sodium salicylate solution (27.6 g L^{-1} sodium salicylate and 0.9 g L^{-1} sodium nitroprusside in 0.5 M NaOH) and sodium hypochlorite solution (3% v/v sodium hypochlorite in 1 M NaOH). In 96-well flat bottom clear microtiter plates, 100 μl of working reagent was added to 100 μl of sample/standard. Standards were performed in duplicate and prepared using NH_4Cl ranging from 10 to 250 μM. The absorbance was recorded at 660 nm wavelength using a VersaMax platereader (Molecular Devices, CA, US). The optimal incubation time was approximately 20 min, and samples and standards were measured simultaneously.

2.6 "*Ca.* Nitrosocosmicus franklandus" and *N. europaea* growth assays

Growth curves were carried out in 120 ml acid washed glass vials containing 50 ml of growth medium. Vials were sealed with grey butyl rubber stoppers that had been autoclaved twice to remove contaminants and crimped with aluminium rings. The media was inoculated with 1-2% inoculum from late exponential phase cultures (~1 and 5 mM NO_2^- accumulated by "*Ca.* Nitrosocosmicus franklandus" and *N. europaea,* respectively). NO_2^- was monitored every 1-2 days and cell counts were carried out from time zero (T_0) and endpoint samples, unless otherwise stated. Treatments were performed in triplicate vials. To calculate growth rates (*k*), the natural

logarithm of NO_2^- production was plotted against time and a straight line fitted to the exponential phase. The NO_2^- concentration at first time point (t_1) and last time point (t_2) of the exponential phase (the linear phase) were taken. *k* was calculated using the following formula (Eq. 1):

$$k = \frac{\ln[NO_2^-](t_2) - \ln[NO_2^-](t_1)}{(t_2 - t_1)} \quad (1)$$

2.7 Oxygen electrode

A Clark-type Oxygen Electrode (Rank Brothers Ltd, Cambridge, UK) was used to measure substrate-induced O_2 consumption by whole cells. The instrument comprised of a 3 ml reaction chamber which could be sealed with a stopper containing an injection port and enclosed by a circulating water bath (Churchill Co. Ltd, Perivale, UK) to maintain the temperature. Ammonia oxidising microorganisms (AOM) were harvested as described in Section 2.3 and resuspended to final cell concentrations of $10^8 – 10^{10}$ cells ml^{-1} for "*Ca.* Nitrosocosmicus franklandus" and *N. viennensis* and 10^7 - 10^8 cells ml^{-1} for *N. europaea*. The instrument was set to 0.6 mV and calibrated by the comparison of 3 ml O_2-saturated cell resuspension buffer with that of O_2-depleted buffer, achieved by the addition of approximately 0.05 g sodium dithionate. For cell measurements, 3 ml fully oxygenated cell suspension (achieved by stirring cell suspensions for 5 min) was added to the chamber and capped with the chamber stopper. Following the establishment of an endogenous rate for 2 – 5 min, substrate was added (0.01 – 2.0 mM) using a Hamilton syringe through the injection port and induced rates were measured for 2 – 10 min. Substrate induced O_2 uptake rates were calculated by subtracting the endogenous rate from the substrate induced rate.

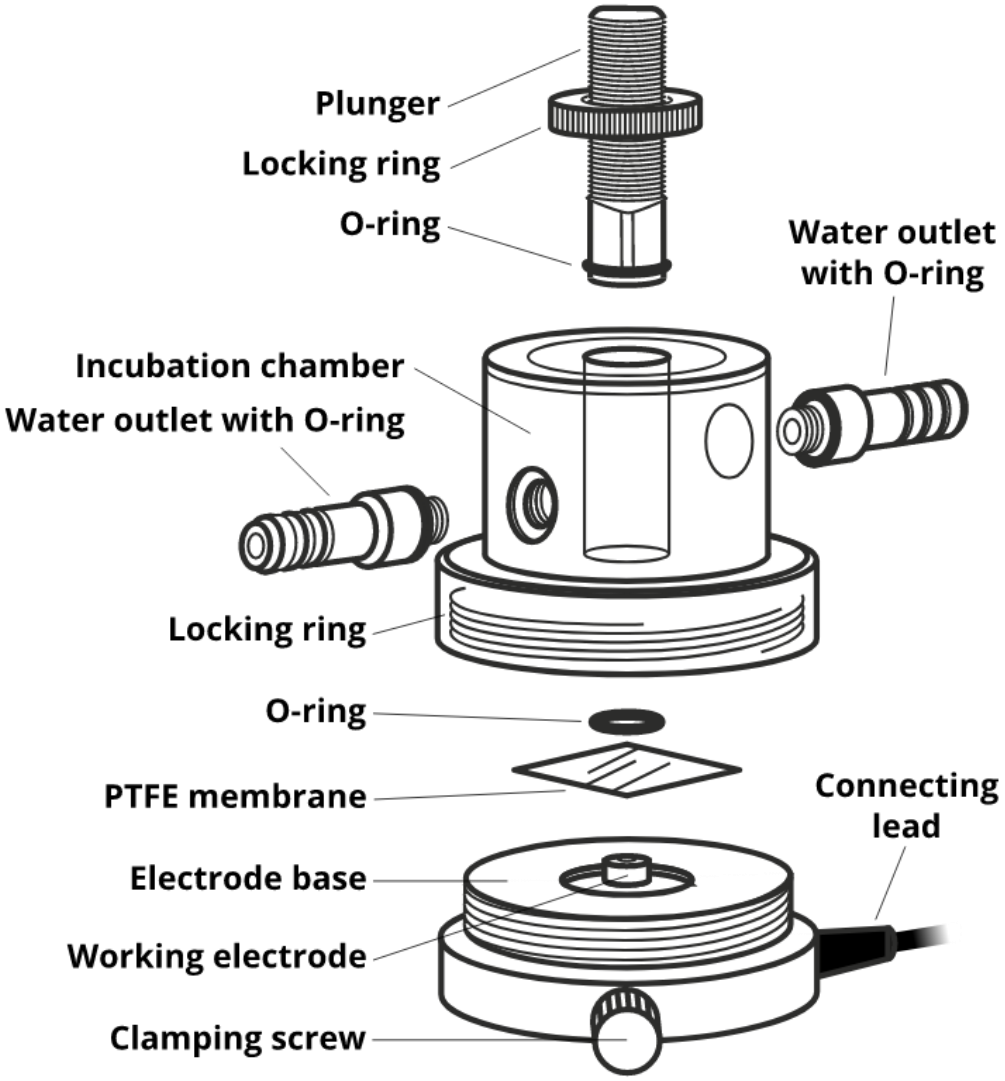

FIG 2.1 Schematic of the dissolved O_2 electrode. The chamber base contains the central platinum electrode and the surrounding silver/silver chloride reference electrode. Conduction between these electrodes is by 3M potassium chloride with a semi-permeable membrane used to separate the sample. Figure from Rank Brothers Limited, Cambridge, UK (www.rankbrothers.co.uk)

2.8 Ammonia oxidation kinetics

Kinetic characteristics of ammonia oxidation by whole cells was estimated using total inorganic ammonium (NH_3 plus NH_4^+), referred to as NH_4^+, or O_2 as the substrate. Cells were harvested from mid-exponential phase cultures (~0.8 and 3 mM

NO_2^- accumulated by "*Ca.* Nitrosocosmicus franklandus" and *N. europaea,* respectively) and resuspended as described in Section 2.3. Concentrated cells were rested for ~1 h at their respective growth temperatures and without NH_3 to allow for endogenous respiration to cease. Rates of NH_4^+-dependent NO_2^- production or NH_4^+-dependent O_2 uptake was plotted against the substrate concentration. Single trace O_2 uptake measurements were performed as described in Section 2.5. For multiple-trace O_2 uptake measurements, discrete slopes of O_2 uptake were measured for 2 min for each individual injection of NH_4^+. The injections resulted in different starting concentrations of NH_4^+ in the chamber and therefore, the total concentration of NH_4^+ in the reaction chamber at the start of each trace was calculated from O_2 uptake rates according to the ratio of NH_4^+ oxidation to O_2 uptake of 1:1.5. O_2 affinity was determined by adding a saturating concentration of NH_4^+ to the chamber and tracking O_2 consumption as O_2 was depleted.

2.8.1 Calculations of kinetic constants

NH_4^+-dependent NO_2^- production or substrate-dependent O_2 uptake was plotted against the substrate concentration. Kinetics followed Michaelis-Menten-type saturation, where the velocity (v) of the reactions was hyperbolically related to the total substrate concentration ([S] (Eq. 2):

$$\mathrm{v} = \frac{\mathrm{V_{max}}\cdot[\mathrm{S}]}{(\mathrm{K_m} + [\mathrm{S}])} \qquad (2)$$

Hyperbolic regression analysis was used to estimate apparent half-saturation constants [$K_{m(app)}$] and apparent maximum velocities [$V_{max(app)}$] using the Hyper32 kinetics package. NH_3 concentrations were calculated based on the pH of the experiment and the respective stoichiometric dissociation constants of NH_3 and NH_4^+ using the Henderson-Hasselbalch equation. Lineweaver-Burk plots were used to

visually analyse the characteristics of ammonia oxidation in the presence of reversible inhibitors. The inhibitory constant [$K_{i(app)}$] was calculated using according to methods outlined in 'Understanding Enzymes' by Palmer (1995). These methods are described in detail in Chapter 4, Section 4.2.3.2.

2.9 Sensitivity of whole cells to alkyne inhibition

Ammonia and methane oxidisers were cultivated to mid-exponential phase and cells were harvested as described in Sections 2.2 and 2.3. "*Ca.* Nitrosocosmicus franklandus" and "*Ca.* Nitrosotalea sinensis" cells were concentrated to approximately 2×10^7 and 3×10^7 cells ml^{-1} by harvesting 1.6 L of culture into 200 ml and 100 ml of buffered FWM salts, respectively. *N. europaea* cells were concentrated 2-fold into 200 ml of 50 mM sodium phosphate buffer (pH 7.7) containing 2 mM $MgCl_2$ to $\sim 3 \times 10^7$ cells ml^{-1}. *M. capsulatus* cells were concentrated 2-fold into 50 ml 10 mM PIPES buffer (pH 7) to $\sim 2 \times 10^8$ cells ml^{-1}. Cells were incubated for 1 h at their respective growth temperatures. Aliquots of 5 ml "*Ca*. Nitrosocosmicus franklandus," *N. europaea,* and *M. capsulatus* and 4 ml "*Ca*. Nitrosotalea sinensis" cell suspension were added to acid-washed 23-ml glass vials, which were then sealed with autoclaved grey butyl rubber stoppers and aluminium crimp caps. Cells were incubated with inhibitors for 30 min to allow for the gas-liquid phase partitioning prior to the addition of NH_4Cl or $(NH_4)_2SO_4$ (reflecting the growth medium) to initiate NH_3-oxidizing activity. Vials were incubated in a water bath at the respective growth temperatures of the microorganisms. *M. capsulatus* was incubated with shaking (150 rpm). AMO and pMMO activity was determined by assaying NO_2^- production from NH_3 oxidation. NO_2^- was sampled using a Hamilton syringe every 15 min for 1-2 h and quantified as described in Section 2.5.1. All treatments were carried out in triplicate, and experiments were performed at least three times with similar results.

2.9.1 C_2 – C_8 linear 1-alkynes

C_2 to C_8 linear 1-alkynes were added to the headspace as vapour using a gas-tight syringe to achieve a 10 μM aqueous concentration (C_{aq}), calculated using the Henry's Law Coefficients obtained from Sander (2015). To initiate NH_3 oxidation by "*Ca*. Nitrosocosmicus franklandus," *N. europaea*, and "*Ca*. Nitrosotalea sinensis," NH_4^+ was added to a concentration of 1 mM by injection through the septum. For *M. capsulatus* (Bath), sodium formate was added first, as a source of reductant, immediately followed by NH_4^+, both at a final concentration of 20 mM.

2.9.2 Phenylacetylene

Phenylacetylene was dissolved in 100% dimethyl sulfoxide (DMSO) to achieve various stock solutions. A final volume of 5 μl stock solution was added to cell suspensions, resulting in 0.1% (vol/vol) DMSO plus the desired concentration of phenylacetylene. Control treatments contained 0.1% (vol/vol) DMSO without phenylacetylene. Phenylacetylene was added to achieve final concentrations ranging from 2.5 to 20 μM for "*Ca*. Nitrosocosmicus franklandus" and 0.5 to 10 μM for *N. europaea*. To initiate ammonia oxidation, NH_4^+ was added at final concentrations of 0.5 mM and 5 mM to "*Ca*. Nitrosocosmicus franklandus" and *N. europaea*, respectively. NO_2^- production was measured for 60 min.

2.10 Characteristics of alkyne inhibition

2.10.1 Kinetic relationship between NH_4^+ and alkyne inhibition

To determine NH_3 oxidation kinetics in the presence of phenylacetylene, "*Ca*. Nitrosocosmicus franklandus" and *N. europaea* cells were harvested as described in Sections 2.2 and 2.3 to final concentrations of 1×10^7 and 8×10^6 cells ml^{-1} respectively. "*Ca*. Nitrosocosmicus franklandus" cell suspensions were preincubated

with phenylacetylene (0, 4, or 8 μM) or acetylene (0 or 3 μM) for 30 min before the addition of various concentrations of NH_4^+ (0.005 to 1 mM). *N. europaea* cell suspensions were preincubated with phenylacetylene (0, 0.2, or 0.4 μM) before the addition of 0.05 to 10 mM NH_4^+. NO_2^- production was measured at 15 min intervals for 1 h**.** The rate of NO_2^- production was plotted against NH_4^+ concentration and kinetic parameters determined as described in Section 2.8.1. Additional kinetic assays were carried out to test the effect of 0.1% (v/v) DMSO on NH_3 oxidation kinetics by "*Ca*. Nitrosocosmicus franklandus" and *N. europaea*.

2.10.2 Inhibition of hydroxylamine oxidation by phenylacetylene and 1-octyne

"*Ca*. Nitrosocosmicus franklandus" cell suspensions *(*2×10^7 cells ml^{-1}) were preincubated with 0 (control) or 100 μM phenylacetylene. Hydroxylamine was added at a final concentration of 200 μM, and hydroxylamine-dependent NO_2^- production was measured at 15 min intervals for 60 min.

2.10.3 Inactivation of AMO by phenylacetylene and 1-octyne and protein synthesis-dependent recovery

"*Ca*. Nitrosocosmicus franklandus" was cultivated to mid-exponential phase and 3,200 ml was harvested and concentrated into 70 ml of 10 mM HEPES (pH 7.5)-buffered FWM salts. Aliquots of 5 ml cell suspension were added to glass vials and sealed with butyl rubber seals. Phenylacetylene (100 μM) and 1-octyne (200 μM) were added from DMSO stock solutions (described in Section 2.9.2), and acetylene (20 μM) was added from a 1% (v/v in air) gaseous stock. Both control and acetylene treatments also contained 0.1% (v/v) DMSO. The addition of NH_4^+ (1 mM) initiated NH_3-oxidizing activity and vials were incubated at 37°C overnight (16 h). NO_2^- production was monitored for 1 h to assess baseline activity. To remove the alkynes and test AMO

recovery, samples were pooled into 50-ml Falcon tubes, and the cells were washed three times in 10 mM HEPES (pH 7.5)-buffered FWM salts) by centrifugation (12,000 × *g* for 10 min at 5°C). The pellet was resuspended in 700 µl FWM salts. Aliquots (200 µl) of cell suspension were added to 4.8 ml 10 mM HEPES (pH 7.5)-buffered FWM salts plus 1 mM NH_4^+, resulting in a final cell concentration of ~1.3×10^7 cells/ml. Vials were incubated in a water bath (37°C, static), and NO_2^- production was measured over 24 h.

2.11 Inhibition of NH_3 oxidation by "*Ca.* Nitrosocosmicus franklandus" by methane

2.11.1 NO_2^- production in the presence of CH_4 during growth

NO_2^- production during the growth of "*Ca.* Nitrosocosmicus franklandus" in the presence of CH_4 was carried out as described in Section 2.6. CH_4 (99%, BOC) was added to the headspace using a gas tight syringe at concentrations ranging from 2 – 50% (v/v in air). To prevent over-pressurisation, the equivalent amount of headspace was removed prior to CH_4 additions. To control for the subsequent reduction of O_2 concentrations in headspace, 50% N_2 (v/v in air) treatments were also included. NO_2^- accumulation was measured every 72 h for 16 days.

Subsequent growth assays investigated if CH_4 inhibited the growth of "*Ca.* Nitrosocosmicus franklandus" by competing with NH_3 for the same oxidation site. Cells were harvested from 3.2 litres of late-exponential phase culture into 25 ml of 10 mM HEPES-buffered (pH 7.5) FWM salts. Aliquots of 49 ml of "*Ca.* Nitrosocosmicus franklandus" media without added NH_4^+ was added to 120 ml glass vials. The medium was supplemented with different concentrations of NH_4Cl, ranging from 1 – 40 mM, in triplicates. The vials were sealed with grey butyl rubber stoppers and aluminium

crimp caps. CH_4 (99%) was injected into the headspace at 20% (v/v in air) using a gas tight syringe after the equivalent amount of headspace was removed. The control treatments, with no added CH_4, contained 20% N_2 (v/v) in air) instead and was to account for reduction in headspace O_2 concentrations. The concentrated cells (1 ml) were used to inoculate the vials using a needle and syringe. NO_2^- concentration during growth was sampled every 24 h for 5 days. Samples for cells counts were withdrawn at T_0 and at the end of the assay.

2.11.2 Rates of NO_2^- production by whole cells in the presence of CH_4

Cells were harvested and resuspended to 1×10^8 cells ml^{-1} in 20 ml 10mM HEPES-buffered FWM salts. Aliquots of 4 ml 10 mM HEPES-buffered FWM salts plus either 1 mM NH_4Cl or 0.2 mM hydroxylamine were added to 23 ml glass vials and sealed with grey butyl rubber stoppers. CH_4 (99%) was added to the headspace using a gas-tight syringe at concentrations ranging from 10 – 50% (v/v in air), in triplicates. The equivalent amount of air was removed from the headspace before CH_4 was added and 50% N_2 (v/v in air) treatments were included. Vials were incubated at 37°C, with shaking (160 rpm) for 1 h to allow for the CH_4 to equilibrate between the gas and liquid phase. To initiate ammonia/hydroxylamine oxidation, 1 ml of concentrated cells was added to the vials with a needle and syringe. The vials were incubated in a water bath (37°C, 160 rpm), and NO_2^- production was sampled every 15 min for 1 h.

2.11.3 Kinetic relationship between NH_4^+ and CH_4

To investigate NH_3 oxidation kinetics in the presence of CH_4, mid-exponentially grown cells were harvested and resuspended to a cell concentration of ~1×10^7 cells ml^{-1}. Cells were incubated for ~ 1 h at 37°C in the dark to allow

endogenous respiration to cease. Aliquots of 4 mL 10mM HEPES-buffered (pH7.5) FWM salts were added to 23 mL glass vials. NH_4Cl was then added at concentrations ranging from 0.01 – 6 mM, in triplicates. Vials were crimp sealed with butyl rubber stoppers and aluminium crimp caps. CH_4 (99%) was added to the headspace (0, 2.5, 5 or 10% v/v in air). The vials were incubated at 37°C, shaking for 1 h to allow CH_4 to equilibrate between the gas and liquid phase. NH_3 oxidation was initiated by the addition of 1 ml concentrated cell suspension using a needle and syringe. Vials were incubated in a water bath (37°C, 160 rpm), and NO_2^- production was measured every 15 min for 1 h. The initial rate of NO_2^- production was plotted against NH_4^+ concentration and kinetic parameters were determined as described in Section 2.8.1.

2.12 Methane oxidation by "*Ca.* Nitrosocosmicus franklandus"

2.12.1 Incubations with ^{13}C-labelled compounds

Activity assays were designed to establish if (1) the AMO from "*Ca.* Nitrosocosmicus franklandus" oxidised CH_4 and (2) if the product of CH_4 oxidation was further metabolised by the cells to produce CO_2. Cells were harvested from 2.4 litres of mid-exponential phase culture into 60 ml 10 mM HEPES (pH 7.5)-buffered FWM salts and incubated for 1 h. Aliquots of 3 ml concentrated cell suspension (~10^8 cells ml^{-1}) was added to 23 ml acid-washed glass vials which were then sealed with grey butyl stoppers and aluminium rings. Treatments consisted of 20 and 50% (v/v) in air) $^{13}CH_4$, 20% $^{13}CH_4$ plus 20 µM (C_{aq}) C_2H_2, 500 µM $^{13}CH_3OH$ and 500 µM $^{13}CH_3OH$ plus 20 µM (C_{aq}) C_2H_2 in the presence of 1 mM NH_4Cl. The control treatment contained no labelled substrates. Cells were pre-incubated with the labelled compounds and acetylene (C_2H_2) for 1 h to allow for the gas-liquid phase partitioning prior to the addition of NH_4Cl. NH_3-dependent NO_2^- production was monitored over 24 h and cell suspensions were spiked twice more with an additional 1 mM NH_4Cl

once 1 mM NO_2^- had been produced. This was routinely found to be after 4 and 8 h from the start of the assay. Acetylene (20 µM) was added to fully inhibit AMO activity. An additional treatment of 20% $^{13}CH_4$ in the presence of 40 mM NH_4^+ was also included. All treatments were carried out in triplicate. After 24 h, the headspace was sampled to determine the stable isotope ratios of carbon ($\delta^{13}C$) in CO_2.

Growth assays were used to determine if carbon from CH_4 oxidation was incorporated into biomass. Cells were harvested from 3.2 litres of mid-exponential phase culture and resuspended in 20 ml 10 mM HEPES-buffered (pH 7.5) FWM salts. Cells were incubated at 37°C for 1 h before 1 ml was inoculated aseptically into 49 ml of "*Ca.* Nitrosocosmicus franklandus" medium containing 0.4 mM sodium bicarbonate (at a reduced concentration to prevent dilution of ^{13}C) and no NH_4^+ in 120 ml acid washed glass vials. The vials were sealed with grey butyl stoppers and aluminium crimp caps. ^{13}C-labelled compounds were then added aseptically to the vials using a gas tight syringe fitted with a 0.2 µm pore sized Minisart syringe filter (Sigma Aldrich/Sartorius, Germany). Treatments included 20% $^{13}CH_4$ (vol/vol in air), 0.14% $^{13}CO_2$ (vol/vol in air) and no added ^{13}C-labelled compounds supplemented with either 1 or 40 mM NH_4Cl. Cell counts were made from time 0 and endpoint samples and NO_2^- production was measured every two days. The treatments containing 1 mM NH_4Cl were spiked with additional 1 mM NH_4Cl once 1 mM NO_2^- had been produced to maintain CH_4 inhibition of NH_3 oxidation by AMO. After 3 mM NO_2^- had been produced, the headspace was sampled and the cells were harvested to determine the $\delta^{13}C$ values of CO_2 and the biomass, respectively.

2.12.2 Sampling ^{13}C-enriched headspace and biomass

For growth assays, 15 ml of headspace was extracted using a gas-tight needle and syringe fitted with a luer lock and immediately injected into 12 ml pre-evacuated

exetainers (Labco Ltd, Lampeter, Wales). The cells were then collected from each vial by centrifugation (12,000 x g, 40 min) in 50 ml falcon tubes (10 ml at a time). The pellets were freeze-dried in preparation for isotope analysis. To sample headspace of activity assay vials (23 ml vials), 15 ml of dH_2O acidified with phosphoric acid (pH 2-3) was injected into the vials with a needle and syringe to release dissolved CO_2 and over-pressurise vials. Subsequently, 15 ml of headspace was extracted using a gas-tight needle and syringe fitted with a luer lock and injected into 12 ml pre-evacuated exetainers (Labco Ltd, Lampeter, Wales).

2.12.3 Analytical methods

The $\delta^{13}C$ of CO_2 was measured using GasBench - isotope ratio mass spectrometry (IRMS) at the Stable Isotope Facility, UC Davis, California (https://stableisotopefacility.ucdavis.edu). Headspace samples were analysed using a Thermo Scientific GasBench system interfaced to a Thermo Scientific Delta V Plus isotope ratio mass spectrometer (Thermo Scientific, Bremen, Germany). CO_2 was sampled by a six-port rotary valve (Valco, Houston TX) using helium as the carrier gas. CO_2 was separated from N_2O and other residual gases by a Poroplot Q GC column (25m x 0.32mm ID, 45°C, 2.5 mL/min). A pure reference gas (CO_2) was used to calculate provisional delta (δ) values of the sample peak. Final $\delta^{13}C$ values were corrected using laboratory reference materials and expressed in parts per thousand (‰) relative to the international standard Vienna Pee Dee Belemnite (V-PDB), where *R* is the molar ratio of $^{12}C/^{13}C$:

$$\delta^{13}C(‰) = 1000[\left(\frac{R_{sample}}{R_{standard}}\right) - 1] \quad (3)$$

Isotopic analysis of biomass was performed by elemental analyser-IRMS (EA-IRMS). A minimum of 0.2 mg freeze-dried cell material was weighed into tin capsules (manufacturer) and sealed. Samples were analysed at the University of East Anglia Stable Isotope Facility, Norwich, UK on a Finnigan Delta plus XP IRMS (Thermo Scientific) connected via a Conflo IV to Flash HT (Thermo Scientific), using helium as the carrier gas. CO_2 was used as the reference gas and the instrument was calibrated against laboratory reference materials (collagen and casein). Final $\delta^{13}C$ values were reported in ‰ relative to the V-PDB standard.

2.13 Preparation of the NO-donor PROLI-NONOate

1-(hydroxy-NNO-azoxy)-L-proline disodium salt (PROLI-NONOate) dissociates to form L-proline and nitric oxide (NO) with a half-life of 1.8 s at 37°C in 0.1 M phosphate buffer (pH 7.4). A stock solution of 100 mM PROLI-NONOate was prepared in 0.01 M NaOH to prevent dissociation and added to "*Ca.* Nitrosocosmicus franklandus" cell suspension (pH 7.3) a final concentration of 1 mM.

2.14 Statistics

Linear 1-alkyne data were plotted as average activity as a fraction of the control treatments (no inhibitor). To analyse inhibition kinetics, the initial rates of NO_2^- production were plotted against NH_4^+ concentration. A non-linear regression was used to estimate the $K_{m(app)}$ and $V_{max(app)}$ for NH_4^+ using the Hyper32 kinetics package. Significant differences between treatments were identified by one-way ANOVA with Dunnett (2-sided) post-hoc test or by student *t*-test (IBM SPSS version 25).

2.15 Ammonia (NH_3) versus ammonium (NH_4^+)

Ammonia (NH_3) and the protonated form, ammonium (NH_4^+) exist in pH equilibrium with a pKa of 9.25. The two forms are used interchangeably throughout

this thesis. Previous studies have suggested that ammonia is the substrate oxidised by the bacterial AMO (Suzuki *et al.,* 1970), but the preferred substrate oxidised by the archaeal AMO has not been determined. However, it is highly likely to also be NH_3 based on archaeal and bacterial AMO sequence comparisons (Lehtovirta-Morley, 2018). At the pH of the systems used here, the majority of the NH_3 would be protonated. Therefore, calculations of kinetic parameters presented in this study are based on total reduced inorganic nitrogen (NH_3 + NH_4^+) as the substrate.

3. Inhibition of ammonia monooxygenase from ammonia oxidising archaea by linear and aromatic alkynes

3.1 Introduction

So far, the AMO has eluded purification attempts which limits the amount of structural data available for this important N-transforming enzyme. Many predictions about the structure of AMO are based on the homology to the pMMO (Lawson *et al.,* 2104; Holmes *et al.,* 1995; Lieberman and Rosenzweig, 2005; Walker *et al.,* 2010). However, the pMMO itself has proven challenging to fully characterise and the nature and location of the site of O_2 activation and methane oxidation remains uncertain (Lieberman and Rosenzweig, 2005; Chan and Yu, 2008; Cao *et al.,* 2018; Lu *et al.,* 2019; Ross *et al.,* 2019; Ro *et al.,* 2019, see Chapter 1.8). Members of the CuMMO superfamily typically have a broad range of co-oxidation substrates. The pMMO can co-oxidise NH_3, (Dalton, 1977; O'Neill and Wilkinson, 1977; Nyerges and Stein, 2009) as well as some 1-alkanes (C_2-C_5) and alkenes (C_2-C_4), but none of these oxidation substrates can support growth (Burrows *et al.,* 1984; Bedard and Knowles, 1989; Miyaji *et al.,* 2011). The bacterial AMO has a broader substrate range than the pMMO and is capable of co-oxidising CH_4 (Hyman and Wood, 1983), linear 1-alkanes (C_2-C_8) and alkenes (C_2-C_5) (Hyman *et al.,*1988), halogenated hydrocarbons (Rasche *et al.,* 1991; Keener and Arp, 1993), aromatic compounds (Keener and Arp, 1994) and sulfides (Hyman *et al.,* 1990; Juliette *et al.,* 1993) to yield hydroxylated products. Currently, very little is known about the substrate range of the archaeal AMO.

Insights regarding the structure and biochemistry of the AMO have come from whole cell studies investigating its interaction with both reversible and irreversible inhibitors. Acetylene is a well characterised inhibitor of both the AMO and pMMO

(Hynes and Knowles, 1982; Prior and Dalton, 1985; Hyman and Wood, 1985). With *N. europaea*, acetylene acts as a suicide substrate and cells require *de novo* protein synthesis of new AMO to re-establish NH_3 oxidising activity (Hyman and Arp, 1992). Incubations with ^{14}[C]-acetylene resulted in the covalent radiolabelling of *N. europaea* AMO, enabling identification of the genes coding for AMO (Hyman and Wood, 1985; McTavish *et al.*, 1993). A subsequent study found that the ketene product of acetylene activation bound covalently to a histidine residue (H191) on the AmoA subunit of *N. europaea*, a residue thought to be in the proximity of the AMO active site (Gilch *et al.*, 2009). While acetylene is also an irreversible inhibitor of the archaeal AMO, the AMO from archaea lack the histidine residue responsible for binding in *N. europaea*, suggesting that the product of acetylene oxidation must bind at a different position on the enzyme. AMO from *N. europaea* is also irreversibly inhibited by other terminal and sub-terminal alkynes including C_3-C_{10} 1-alkynes (Hyman *et al.*, 1988), 3-hexyne (Keener *et al.*, 1998) and 1,7-octadiyne (Bennett *et al.*, 2016).

Previously, Taylor *et al.*, (2013; 2015) demonstrated that, in whole cells, aliphatic *n*-alkynes (C_2-C_9) differentially inhibited bacterial and archaeal AMOs, with the AOA being less sensitive to $\geq C_5$ 1-alkynes. 1-octyne (C_8) is now used in environmental and mesocosm studies to distinguish between the contributions of AOA and AOB to soil nitrification (Lu *et al.*, 2015; Taylor *et al.*, 2017; Giguere *et al.*,2017; Hink *et al.*,2017). A field study by Im *et al.*, (2011) found that the abundance of archaeal *amoA* genes decreased when the soil was treated with the aromatic alkyne phenylacetylene, although the effects of phenylacetylene on pure cultures of AOA were not investigated. Phenylacetylene was shown to be a strong inhibitor of the AMO from *N. europaea* (Hyman and Wood, 1985), with complete inhibition at <1 µM (Lontoh *et al.*, 2000). The AMO from *N. europaea* is capable of oxidising aromatic

compounds including the analogue of phenylacetylene, ethylbenzene (Keener and Arp, 1994; Vannelli and Hooper, 1995). Notably, the oxidation of aromatic hydrocarbons by the pMMO has not been observed (Colby *et al.*,1977; Burrows *et al.*, 1984; Hyman *et al.*, 1988; Prior and Dalton, 1985).

The first aim of this study was to undertake a comprehensive assessment of the inhibition of archaeal AMO activity by C_2-C_8 linear 1-alkynes using two previously unstudied terrestrial AOA strains from distinct thaumarchaeal lineages, "*Candidatus* Nitrosocosmicus franklandus" C13 and "*Candidatus* Nitrosotalea sinensis" Nd2. 1-alkyne inhibition profiles of *N. europaea* AMO and the pMMO from the obligate methanotroph *Methylococcus capsulatus* (Bath) were also investigated for comparison, and to provide insights about the potential substrate range oxidised by the archaeal AMO, respectively. Next, phenylacetylene inhibition of NH_3 oxidation by "*Ca.* Nitrosocosmicus franklandus" and *N. europaea* cells were assessed. The kinetic mechanism of inhibition of intact cells of "*Ca.* Nitrosocosmicus franklandus" and *N. europaea* by phenylacetylene and acetylene was then investigated to explore differences in the structure and biochemistry of the archaeal and bacterial AMO.

3.2 Oxidation of NH_3 by *M. capsulatus*

For consistency and to provide a direct comparison with the AMO, the inhibition of NH_3-oxidising activity by the pMMO from *M. capsulatus* was investigated. NH_3 is a co-metabolic substrate of the pMMO from *M. capsulatus* and is oxidised to hydroxylamine, which is further oxidised to produce NO_2^- (Dalton, 1977; Campbell *et al.*, 2011). The expression of pMMO, rather than soluble methane monooxygenase (sMMO), was promoted by the addition of copper (20 μM) during the cultivation of *M. capsulatus* and pMMO activity in harvested cells was confirmed

using the naphthalene assay which is specific for sMMO activity, with sMMO-expressing *Methylocella silvestris* (Crombie and Murrell, 2014) cells as positive controls (Brusseau *et al.*, 1990). Sodium formate (20 mM) was added to *M. capsulatus* cell suspensions as an external source of reductant which facilitated pMMO activity in the absence of CH_4. NO_2^- production from NH_4^+ (20 mM) by the pMMO from *M. capsulatus* is shown in Fig. 3.1. The rate of NO_2^- production began to decrease after 30 min of incubation, likely due to the toxic build-up of NO_2^- and hydroxylamine during the assay.

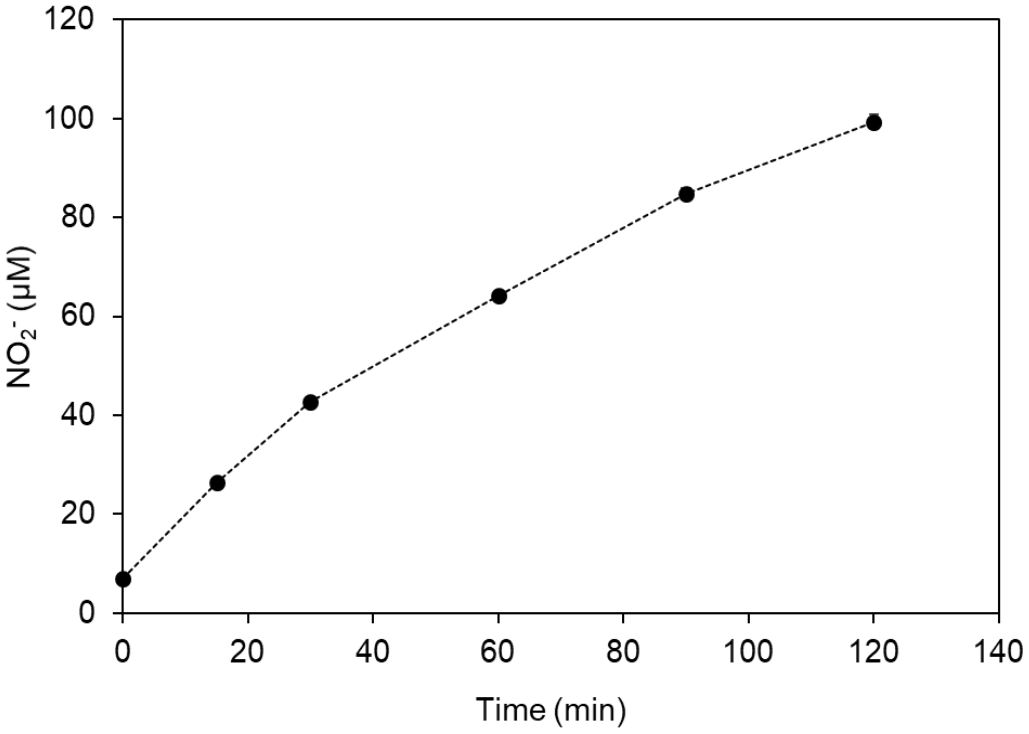

FIG 3.1 NO_2^- production by *M. capsulatus* in response to the addition of 20 mM NH_4Cl and in the presence of 20 mM sodium formate as a source of external reductant. Error bars representing SE are not visible (n = 3).

3.3 Sensitivity of "Ca. Nitrosocosmicus franklandus", "Ca. Nitrosotalea sinensis", *N. europaea* and pMMO-expressing *M. capsulatus* (Bath) to C_2 to C_8 1-alkynes

The sensitivity of NH_3-oxidising activity by intact "*Ca.* Nitrosocosmicus franklandus" and "*Ca.* Nitrosotalea sinensis" cells to 10 μM $C_{(aq)}$ C_2-C_8 1-alkynes was compared with *N. europaea* and pMMO-expressing *M. capsulatus* (Fig. 3.2). The concentration of alkyne was chosen to allow comparison of the 1-alkyne inhibition profiles with that of previously tested AOA isolates by Taylor *et al.*, (2013; 2015). NH_3-dependent NO_2^- production by both "*Ca.* Nitrosocosmicus franklandus" and "*Ca.* Nitrosotalea sinensis" was inhibited by C_2-C_5 1-alkynes ($p < 0.001$) but not by C_7 and C_8 (Fig. 3.2 A and B). "*Ca.* Nitrosotalea sinensis" was strongly inhibited by C_4 and C_5 alkynes (degree of inhibition 54% ± 5% and 70% ± 1%, respectively, compared with controls), however, these alkynes effected only partial inhibition of NH_3 oxidation by "*Ca.* Nitrosocosmicus franklandus" (24% ± 2% and 14% ± 1%, respectively), highlighting differences in the sensitivity of the two AOA strains to the shorter chain-length 1-alkynes. Additionally, C_6 had a significant inhibitory effect on "*Ca.* Nitrosotalea sinensis" ($p = 0.004$) but not on "*Ca.* Nitrosocosmicus franklandus" ($p =$ 0.47

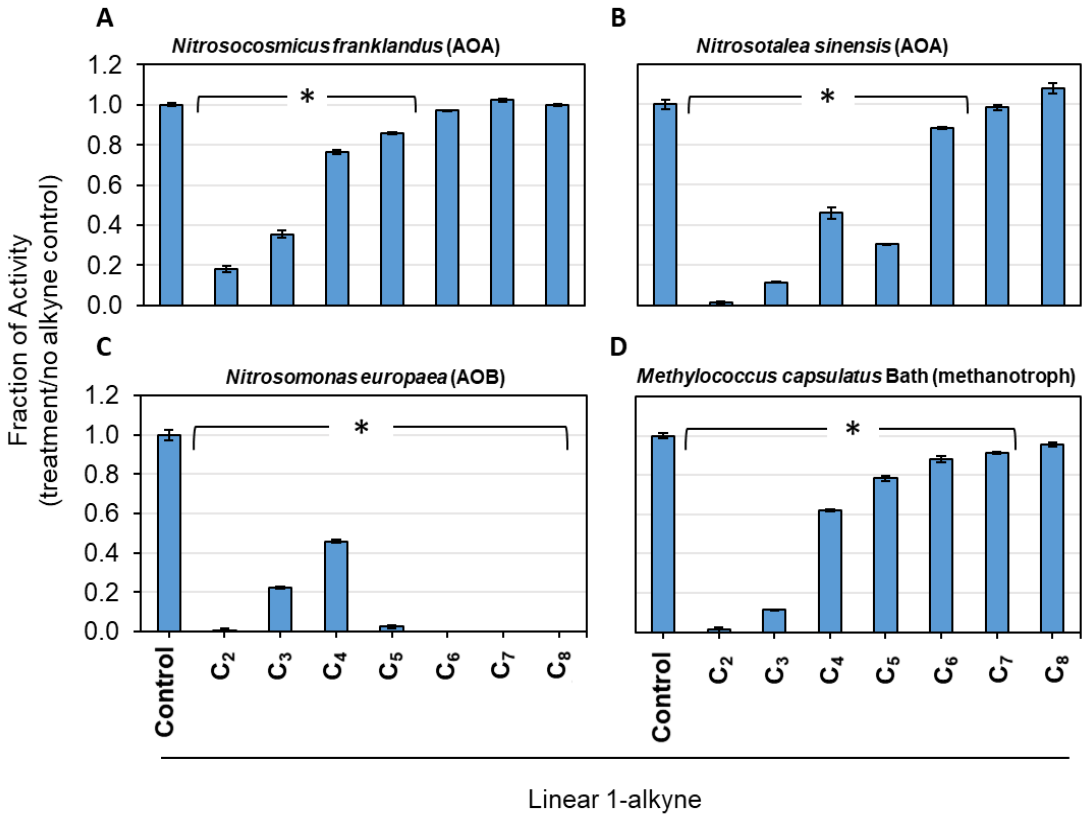

FIG 3.2 Inhibition of NO_2^- production by "*Ca.* Nitrosocosmicus franklandus" (A), "*Ca.* Nitrosotalea sinensis" (B), *N. europaea* (C) and *M. capsulatus* (D) in response to 10 µM (C_{aq}) C_2- C_8 1-alkynes. *N. europaea* was incubated with 2 mM NH_4^+, "*Ca.* Nitrosocosmicus franklandus" and "*Ca.* Nitrosotalea sinensis" with 1 mM NH_4^+ and *M. capsulatus* with 20 mM NH_4^+. Error bars represent standard error (SE) of the mean (n = 3). * Indicates 1-alkyne treatments that significantly inhibited NO_2^- production relative to the control treatment (p < 0.01).

NO_2^- production by *N. europaea* was strongly inhibited by all 1-alkynes tested (C_2-C_8), which corroborates with previous studies (Hyman *et al.*,1988; Taylor *et al.*, 2013). 1-pentyne resulted in 98% ± 1% inhibition and AMO activity was completely inhibited by C_6-C_8 1-alkynes (Fig. 3.2 C). In the presence of C_3 and C_4 1-alkynes, inhibition decreased to 78% ± 1% and 54% ± 1%, respectively. pMMO-expressing *M. capsulatus* cells oxidised NH_3 to NO_2^- and NO_2^- production was significantly inhibited by C_2-C_7 1-alkynes ($p \leq 0.001$), but C_6 and C_7 1-alkynes resulted in only approximately 10% inhibition compared with the control (Fig. 3.2 D).

Notably, "*Ca.* Nitrosotalea sinensis", *N. europaea* and *M. capsulatus* were very sensitive to 10 µM acetylene (C_2) with NO_2^- production inhibited by >95 %, however, "*Ca.* Nitrosocosmicus franklandus" appeared less sensitive to acetylene (degree of inhibition, 82% ± 3%).

3.4 Inhibition of NO_2^- production by "*Ca.* Nitrosocosmicus franklandus" and *N. europaea* in response to phenylacetylene

Given the contrasting responses of ammonia oxidising archaea and bacteria to linear 1-alkynes, AMO activity in the presence of the aromatic alkyne phenylacetylene was examined in "*Ca.* Nitrosocosmicus franklandus" and *N. europaea* cells (Fig. 3.3).

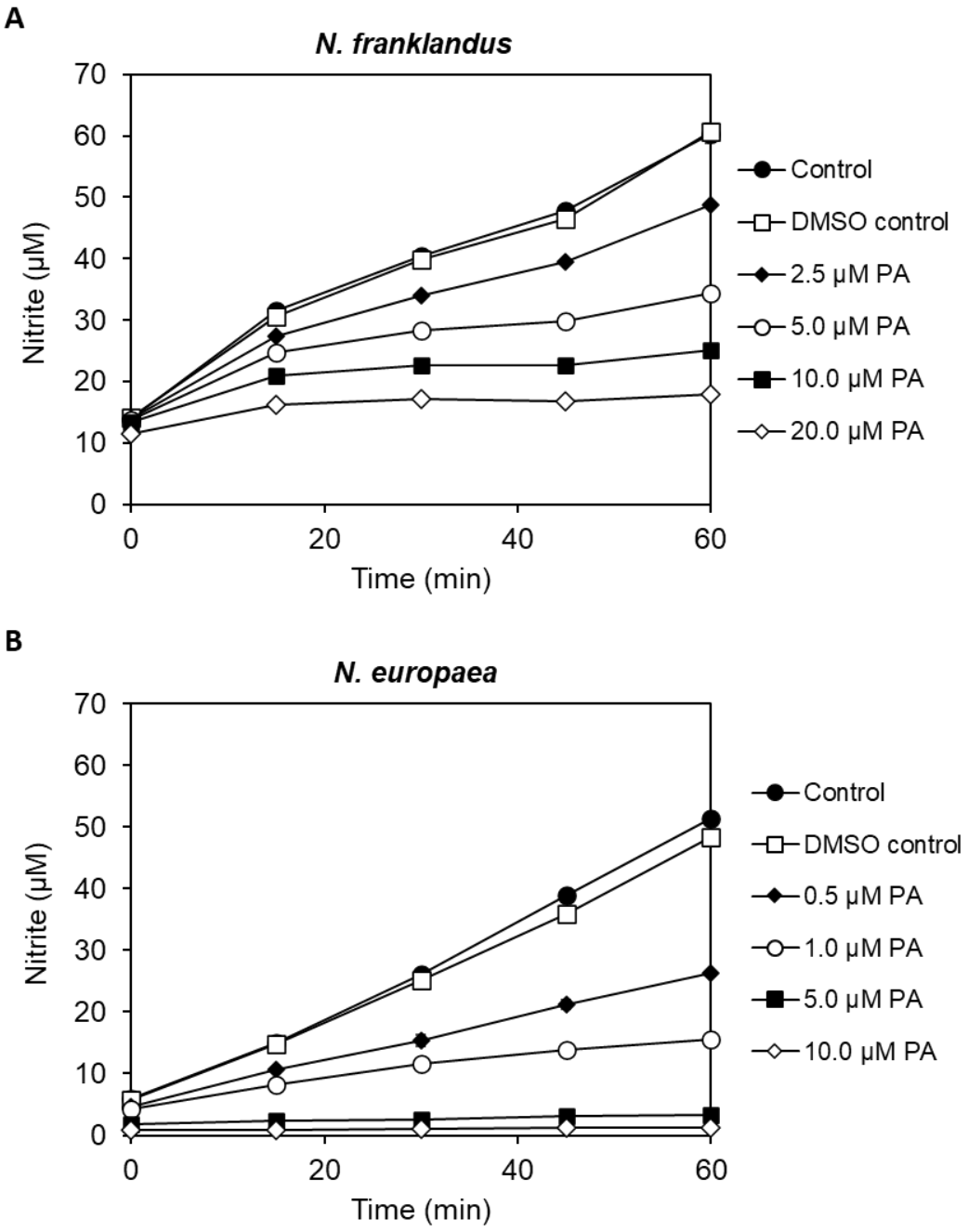

FIG 3.3 NO_2^- production by "*Ca.* Nitrosocosmicus franklandus" (A) and *N. europaea* (B) in response to different concentrations of phenylacetylene (PA) dissolved in DMSO. Error bars representing SE are included but are usually smaller than markers (n = 3).

After 1-hour of incubation, the rate of NH_3-dependent NO_2^- production by "*Ca.* Nitrosocosmicus franklandus" was inhibited by 55.4% ± 1.4% in the presence of 5 μM phenylacetylene compared to the DMSO control. Incubations in the presence of 10 and 20 μM phenylacetylene increased the inhibition to 74.7% ± 0.5% and 86.0% ± 0.4%, respectively (Fig. 3.3A). NO_2^- production by *N. europaea* was inhibited by 52.5% ± 1.7% in the presence of 0.5 μM phenylacetylene and, unlike the results of Lontoh *et al.,* (2000), who demonstrated full inhibition of AMO activity at 0.6 μM phenylacetylene, there was still partial NH_3-oxidising activity in the presence of 1 μM (75.1% ± 1.6% inhibition on the rate of NO_2^- production) (Fig. 3.3B). Together, the results show that "*Ca.* Nitrosocosmicus franklandus" is approximately 10 × less sensitive to phenylacetylene inhibition compared to *N. europaea.* Both "*Ca.* Nitrosocosmicus franklandus" and *N. europaea* cells treated with 0.1 % DMSO, in which the phenylacetylene was dissolved, produced NO_2^- at a similar rate to the untreated controls**.**

3.5 Kinetic analysis of phenylacetylene inhibition of NH_4^+-dependent NO_2^- production by "*Ca.* Nitrosocosmicus franklandus" and *N. europaea*

Evidence from a study by Suzuki *et al.,* (1974) suggests that NH_3, rather than ammonium (NH_4^+), is the growth substrate oxidised by the bacterial AMO, but the preferred substrate (NH_3/NH_4^+) oxidised by the archaeal AMO has not been determined. However, it is highly likely to also be NH_3 based on archaeal and bacterial AMO protein sequence comparisons and the fact that inhibitors tend to be non-polar (Lancaster *et al.,* 2018; Lehtovirta-Morley *et al.,* 2016a, discussed in more detail in Chapter 1, Section 1.8). At the pH of the systems used in this current study, the majority of the NH_3 (pKa of 9.25) would be protonated. Therefore, the calculations of

kinetic parameters presented below are based on total reduced inorganic nitrogen (NH_3 + NH_4^+) as the substrate.

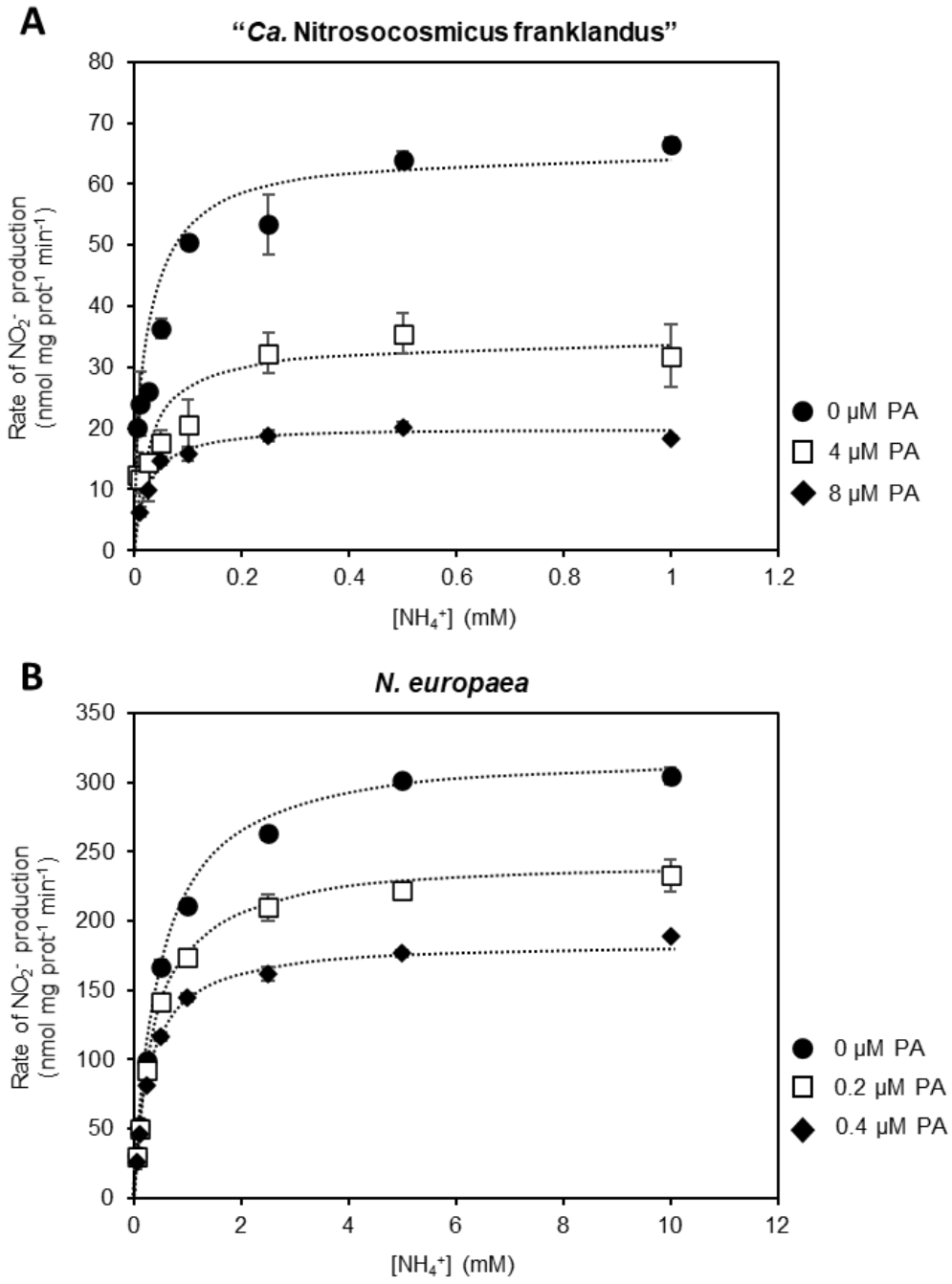

FIG 3.4 Michaelis-Menten hyperbolic plot showing the initial rate of NO_2^- production by "*Ca.* Nitrosocosmicus franklandus" (A) and *N. europaea* (B) to phenylacetylene (PA) dissolved in DMSO as a function of NH_4^+ concentration. The x-axis is the substrate (NH_4^+) concentration, and the y-axis is the initial rate of NO_2^- production. Inhibition was not overcome by increasing concentration of NH_4^+, indicating that phenylacetylene and NH_3 do not compete for the same binding site. Error bars represent SE (n = 3).

To investigate the mode of inhibition of phenylacetylene on AMO, the initial reaction velocity of NO_2^- production by "*Ca.* Nitrosocosmicus franklandus" and *N. europaea* were determined over a range of substrate (total NH_4^+) concentrations. The concentrations of phenylacetylene used in the kinetic analysis were chosen to achieve partial inhibition of NO_2^- production (Fig. 3.3). NH_3-dependent kinetics of initial NO_2^- production followed Michaelis-Menten-type saturation kinetics for both "*Ca.* Nitrosocosmicus franklandus" and *N. europaea* (Fig. 3.4 A & B), where the velocity (v) of the AMO-catalysed reactions was hyperbolically related to total NH_4^+ concentration ([S]) (Eq. 1):

$$v = \frac{V_{max}.[S]}{(K_m + [S])} \quad (1)$$

Apparent half-saturation constants for total NH_4^+ ($K_{m(app)}$) and maximum velocities ($V_{max(app)}$) in the presence/absence of phenylacetylene were calculated using hyperbolic regression analysis. The hyperbolic plots show that increasing the NH_4^+ concentration did not alleviate the inhibitory effect of phenylacetylene on NO_2^- production in "*Ca.* Nitrosocosmicus franklandus" or *N. europaea* (Fig. 3.4 A & B). This suggests that phenylacetylene is not a simple competitive inhibitor of either the archaeal or the bacterial AMO with respect to NH_3 oxidation. Interestingly, the mechanism of inhibition by phenylacetylene appears to be different between "*Ca.* Nitrosocosmicus franklandus" and *N. europaea*. With "*Ca.* Nitrosocosmicus franklandus", the presence of 4 and 8 µM phenylacetylene the $V_{max(app)}$ of NO_2^- production decreased from 64.1 ± 2.6 nmol mg $prot^{-1}$ min^{-1} to 33.8 ± 2.2 and 20.1 ± 0.5 nmol mg $prot^{-1}$ min^{-1} respectively (Table 3.1). There was no significant change in the $K_{m(app)}$ for cells inhibited by phenylacetylene compared to the control (p = 0.503 and p = 0.526, for 4 and 8 µM phenylacetylene, respectively), indicating that

phenylacetylene and NH_3 do not compete for the same binding site. Inhibition of *N. europaea* by 0.2 and 0.4 µM phenylacetylene reduced both the $K_{m(app)}$ and the $V_{max(app)}$ by approximately 30 and 40%, respectively (Table 3.1). This is indicative of uncompetitive inhibition and suggests that phenylacetylene binds to the AMO subsequent to NH_3 binding and at a different binding site, and it is the binding of NH_3 that induces the conformational change that enables phenylacetylene to bind.

Table 3.1 Kinetics of NH_3-dependent NO_2^- production by "*Ca.* Nitrosocosmicus franklandus" and *N. europaea* in the presence of phenylacetylene. SE of three replicates are in parentheses (n=3). For 0 µM phenylacetylene, SE is from two independent experiments (n=6).

Strain	Phenylacetylene (µM)	$K_{m(app)}$ (µM)	$V_{max(app)}$ (nmol mg prot^{-1} min^{-1})
"*Ca.* Nitrosocosmicus franklandus"	0	26.7 (4.7)	64.1 (2.6)
	4	30.3 (8.3)	33.8 (2.2)
	8	22.9 (3.2)	20.1 (0.5)
N. europaea	0	1041.0 (39.2)	324.4 (3.7)
	0.2	750.2 (34.8)	240.7 (2.7)
	0.4	636.9 (27.6)	188.7 (2.0)

3.6 Kinetic analysis of acetylene inhibition of NH_4^+-dependent NO_2^- production by "Ca. Nitrosocosmicus franklandus"

Previously, acetylene was shown to be a competitive inhibitor of NH_3 oxidation by the archaeal AMO from *Nitrososphaera viennensis* (Taylor *et al.*, 2015). To examine if acetylene interacts competitively with "*Ca.* Nitrosocosmicus franklandus" AMO, the kinetic response of NH_3-dependent NO_2^- production by "*Ca.* Nitrosocosmicus franklandus" to 3 µM acetylene was tested using the same

experimental design used to investigate phenylacetylene inhibition. In contrast to phenylacetylene, increasing the total NH_4^+ availability reduced acetylene inhibition, demonstrating that acetylene and NH_3 compete for the same AMO binding site (Fig. 3.5). Additionally, the $K_{m(app)}$ increased dramatically from 18.5 ± 2.9 µM to 691.3 ± 158.1 µM NH_4^+ in the presence of 3 µM acetylene, but there was no change in the $V_{max(app)}$ (Table 3.2), also demonstrating that acetylene interacts with the NH_3-binding site and decreases the affinity of the AMO for NH_3.

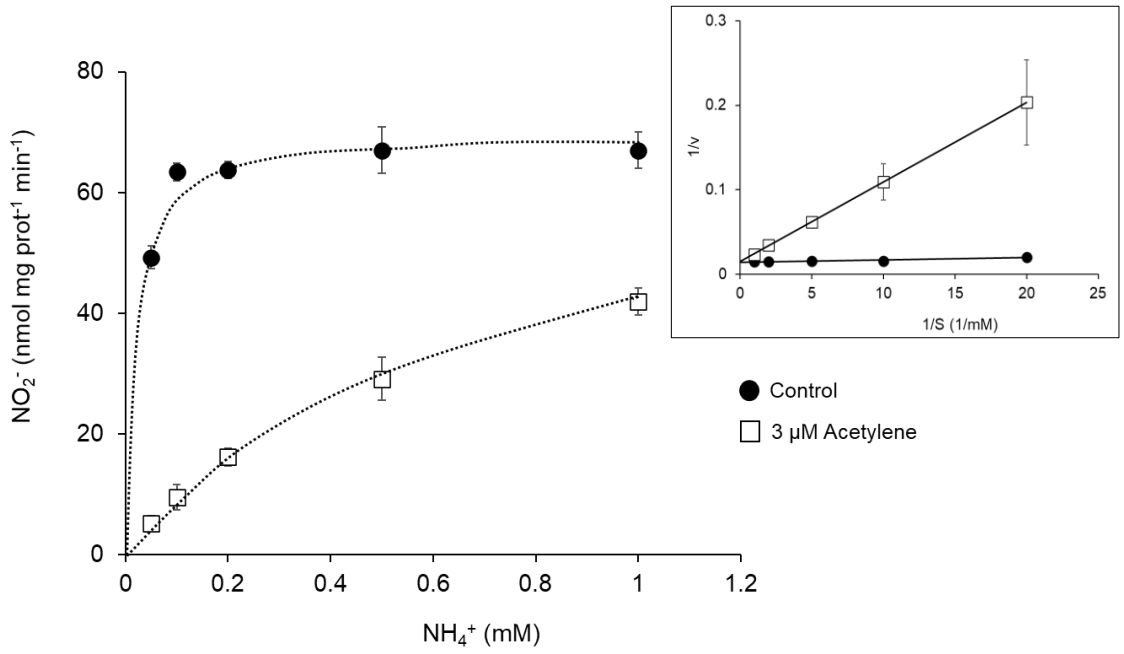

FIG 3.5 Michaelis-Menten hyperbolic plot showing the initial rate of NO_2^- production by *N. franklandus* with acetylene (3 µM) as a function of total NH_3/NH_4^+ concentration. The x-axis shows NH_4^+ substrate concentrations (S, mM) and the y-axis shows initial rate of NO_2^- production (v, nmol mg protein^{-1} min^{-1}). Increasing the concentration of NH_4^+ reduced the rate of inhibition, indicating acetylene was a non-competitive inhibitor. The inset shows the data as a Lineweaver-Burk plot. Error bars represent SE (n = 3).

Table 3.2 Kinetics of NH_3-dependent NO_2^- production by "*Ca.* Nitrosocosmicus franklandus" in the presence of acetylene and 0.1% (v/v) DMSO. SE of three replicates are in parentheses (n=3).

Acetylene (μM)	$K_{m(app)}$ (μM)	$V_{max(app)}$ (nmol mg $prot^{-1}$ min^{-1})
0	18.5 (2.9)	69.6 (1.6)
3	691.3 (158.1)	69.4 (11.7)

3.7 The effect of DMSO on kinetic parameters

Phenylacetylene was dissolved in 100% DMSO and all cell suspensions used in both the phenylacetylene and acetylene experiments contained 0. 1% (v/v) DMSO. Therefore, the addition of 0.1% (v/v) DMSO on NH_3 oxidation kinetics was tested separately. DMSO had no effect on kinetics parameters for NH_3 oxidation by "*Ca.* Nitrosocosmicus franklandus". For *N. europaea*, the presence of 0.1% (v/v) DMSO reduced both the $K_{m(app)}$ and $V_{max(app)}$ by ~10% (Table 3.3).

Table 3.3 Kinetics of NH_3-dependent NO_2^- production by "*Ca.* Nitrosocosmicus franklandus" and *N. europaea* in the presence of 0.1% DMSO. SE of three replicates are in parentheses (n=3).

Strain	Treatment	$K_{m(app)}$ (μM)	$V_{max(app)}$ (nmol NO_2^- mg protein min^{-1})
"*Ca.* Nitrosocosmicus franklandus"	Control	21.1 (3.14)	69.8 (2.6)
	0.1% DMSO	20.1 (1.8)	69.6 (1.5)
N. europaea	Control	1075.0 (53.4)	375.3 (4.4)
	0.1% DMSO	949.6 (37.5)	329.2 (3.3)

3.8 The effect of phenylacetylene on hydroxylamine oxidation by "*Ca.* Nitrosocosmicus franklandus"

Hydroxylamine is the product of NH_3 oxidation by both the archaeal and bacterial AMO and is subsequently oxidised to other intermediates in the NO_2^- production pathway (Vajrala *et al.*, 2013; Caranto and Lancaster, 2017). In order to verify that the reduction in the rate of NO_2^- production by "*Ca.* Nitrosocosmicus franklandus" was due to inhibition of NH_3 oxidation, rather than the effects of downstream enzymatic reactions, hydroxylamine oxidation by "*Ca.* Nitrosocosmicus franklandus" in the presence of phenylacetylene was investigated. NO_2^- production by "*Ca.* Nitrosocosmicus franklandus" was unaffected by 100 µM phenylacetylene relative to the DMSO control treatment, demonstrating that phenylacetylene is likely to be a specific inhibitor of the "*Ca.* Nitrosocosmicus franklandus" AMO (Fig. 3.6). Hydroxylamine-dependent NO_2^- production proceeded rapidly but ceased after 30 minutes when approximately 27 µM NO_2^- had accumulated. A similar response was previously observed for the marine AOA *Nitrosopumilus maritimus* SCM1 (Vajrala *et al.*,2013). This phenomenon is further discussed in Chapter 5, but it could be due to abiotic reactions or an unknown detoxification mechanism.

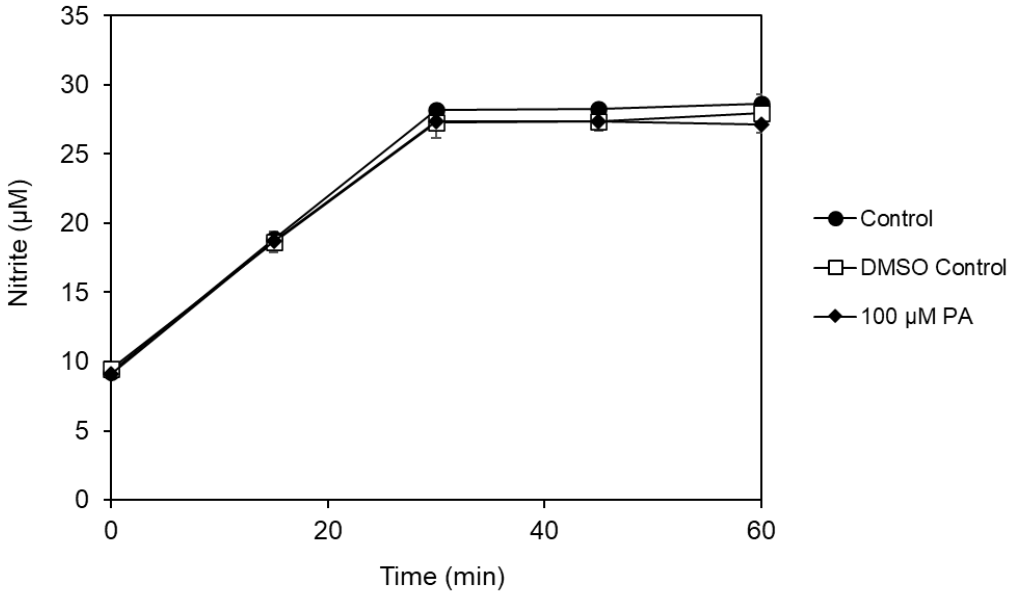

FIG 3.6 NO_2^- production from hydroxylamine oxidation by "*Ca.* Nitrosocosmicus franklandus" in the presence or absence of 100 µM phenylacetylene (PA) dissolved in DMSO. Error bars represent SE (n = 3).

3.9 Recovery of AMO activity by "*Ca.* Nitrosocosmicus franklandus" following phenylacetylene inhibition

In order to establish whether phenylacetylene is a reversible or irreversible inhibitor of AMO of "*Ca.* Nitrosocosmicus franklandus", the recovery of NH_3-oxidising activity after exposure to phenylacetylene was investigated. Previous work has shown that to restore NH_3 oxidising activity following inhibition by an irreversible inhibitor, for example acetylene, the cells need to synthesize new AMO enzyme, which results in a lag phase before activity resumes (Hyman and Arp, 1992). "*Ca.* Nitrosocosmicus franklandus" cells were inhibited overnight by 100 µM phenylacetylene in the presence of 1 mM NH_4^+. Since Taylor *et al.*, (2015) demonstrated that the inhibition by 1-octyne was reversible in the AOA strain *N. viennensis*, in contrast to the irreversible action of acetylene, treatments with both 1-octyne and acetylene were included as controls. To ensure that the inability of cells to

respond to substrate addition (NH_4^+) was not due to the effects of starvation, controls incubated for a similar amount of time without either inhibitor or NH_4^+ were included (starved cells). After the removal of the inhibitors by washing, cells were resuspended in NH_4^+-replete medium. NO_2^- production, the proxy for NH_3 oxidation, by "*Ca.* Nitrosocosmicus franklandus" recovered immediately following removal of 1-octyne. Cells inhibited by either acetylene or phenylacetylene had a 3 to 5-hour lag time before NO_2^- production commenced, suggesting that cells required *de novo* synthesis of new AMO in order to oxidise NH_3 (Fig. 3.7). The starved cells recovered at the same rate as the control (data not shown).

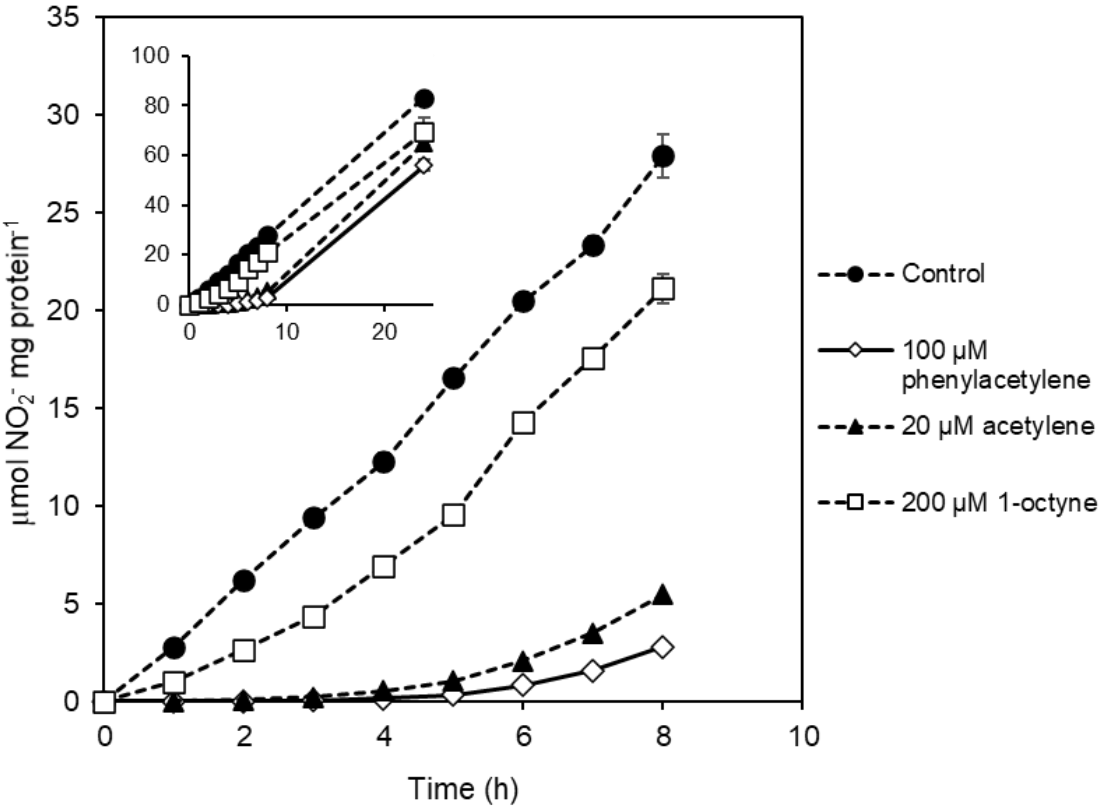

FIG 3.7 Time course recovery of NO_2^- production by "*Ca.* Nitrosocosmicus franklandus" following overnight inhibition of NH_3 oxidation by phenylacetylene (100 µM), acetylene (20 µM) and 1-octyne (200 µM). Error bars represent SE (n = 3).

3.10 Discussion

3.10.1 The inhibition of AMO and pMMO by linear alkynes

Linear terminal alkynes have previously been shown to differentially inhibit archaeal and bacterial AMO activity (Taylor *et al.,*2013; Taylor *et al.,* 2015). In agreement with this, NH_3-dependent NO_2^- production by the AOA strains "*Ca.* Nitrosocosmicus franklandus" and "*Ca.* Nitrosotalea sinensis" was considerably less sensitive to inhibition by longer-chain-length 1-alkynes ($\geq C_6$) compared to *N. europaea* (Fig. 3.2). The linear 1-alkyne inhibition profile therefore appears be conserved across AOA lineages with the overall trend of increased sensitivity to short-chain alkynes and reduced sensitivity to longer-chain-length alkynes. This could indicate that, unlike the AMO from *N. europaea,* the binding cavity of the archaeal AMO cannot orientate and activate larger linear hydrocarbons such as 1-octyne, potentially due to steric hindrance caused by the bulkiness of these substrates or inhibitors. Interestingly, inhibition of the AMO from "*Ca.* Nitrosocosmicus franklandus" by 1-octyne, when used at 200 μM, was reversible and recovery of NH_3-oxidising activity began immediately after removal of the inhibitor (Fig. 3.7). Similarly, Taylor *et al.,* (2015) showed the inhibition of AMO from *N. viennensis* by 1-octyne was also reversible.

In contrast with AOA, NH_3 oxidation by *N. europaea* was fully or partially inhibited by all C_2-C_8 1-alkynes, with complete inhibition occurring in the presence of the longer-chain-length alkynes ($\geq C_6$). This is consistent with previous results published by Hyman *et al.,* (1988) and Taylor *et al.,* (2013) who found that long-chain-length 1-alkynes inhibited AMO of *N. europaea* more effectively than short-chain 1-alkynes. Additionally, it was observed by Hyman *et al.,* (1988) that the effectiveness of *n*-alkynes as inhibitors of AMO from *N. europaea* inversely reflects the oxidation

rate of *n*-alkanes of increasing chain length. For example, 1-octyne inactivates *N. europaea* AMO more rapidly and effectively than shorter-chain-length 1-alkynes, however, the corresponding alkane, 1-octane, is oxidised more slowly and yields less product compared to short-chain alkanes. This could be due to the reactivity of the triple carbon bond present in 1-octyne.

The pMMO from the methanotrophs *M. capsulatus* and *Methylosinus trichosporium* have a narrower hydrocarbon substrate range compared to the AMO of *N. europaea* but is capable of oxidising short-chain *n*-alkanes ($\leq C_5$) and alkenes ($\leq C_3$) to their respective alcohols and epoxides (Burrows *et al.*, 1984; Bédard and Knowles, 1989). The specific site where hydrocarbon oxidation takes place within the pMMO is unclear. Intriguingly, a hydrophobic cavity identified in proximity to the predicted tricopper site in the PmoA from *M. capsulatus* was shown to be of sufficient size to accommodate hydrocarbons of up to five carbons in length (Chan and Yu, 2008; Ng *et al.*, 2008; Culpepper and Rosenzweig, 2012). Correspondingly, here we found that C_2-C_5 alkynes inhibited the NH_3-oxidising activity of pMMO from *M. capsulatus* by more than 20%, reflecting the predicted size of this pMMO binding cavity (Fig. 3.2D). The inhibition of the pMMO by longer-chain alkynes (C_6-C_8) has not previously been tested and we found that NH_3 oxidation by *M. capsulatus* was marginally inhibited by C_6 and C_7 alkynes, indicating that the pMMO can interact with longer-chain-length hydrocarbons than those already known to be substrates.

The effectiveness of C_2-C_8 linear 1-alkynes as inhibitors of NH_3 oxidation by the AOA strains used in this study and in previous studies (Taylor *et al.*, 2013; Taylor *et al.*, 2015) indicates that the archaeal AMO has a narrower hydrocarbon substrate range compared to the AMO of *N. europaea*. Furthermore, in terms of the 1-alkyne inhibition profile, the AMO of "*Ca.* Nitrosocosmicus franklandus" and "*Ca.*

Nitrosotalea sinensis" AOA more closely resembles the pMMO from *M. capsulatus* than the AMO of *N. europaea* (Fig. 3.2). It could therefore be anticipated that the archaeal AMO oxidises a similar range of linear *n*-alkanes and alkenes to that oxidised by the pMMO from *M. capulatus*.

Based on the diversity of archaeal AMO sequences (Alves *et al.,* 2018), it is very likely that variation exists between the structure and stereoselectivity of the AMO active site from different AOA strains. Taylor *et al.,* (2013 and 2015) observed differences in the sensitivity of *N. maritimus, N. viennensis* and *Nitrososphaera gargensis* to inhibition by 1-hexyne (C_6) and 1-heptyne (C_7). In this study, we did not observe significant inhibition of archaeal AMO activity by 1-heptyne, although the AMO from "*Ca.* Nitrosotalea sinensis" was notably more sensitive to inhibition by C_2-C_5 1-alkynes compared to AMO from "*Ca.* Nitrosocosmicus franklandus". Additionally, 1-hexyne had a significant inhibitory effect on NO_2^- production by "*Ca.* Nitrosotalea sinensis" but not by "*Ca.* Nitrosocosmicus franklandus" (Fig. 3.2 A and B).

A considerable amount of research has focused on determining the environmental drivers that influence AOA and AOB ecology and their relative contribution to nitrification. Environmental factors, including substrate availability, pH, O_2 availability and temperature, have been suggested to influence the ecological niche differentiation of ammonia oxidisers and to control ammonia oxidation rates in distinct ecosystems (see Chapter 1.5). The resistance of "*Ca.* Nitrosocosmicus franklandus" and "*Ca.* Nitrosotalea sinensis" to inhibition by 1-octyne (C_8) further validates the use of 1-octyne to distinguish between AOA and AOB nitrifying activity in soils and to reveal the environmental factors influencing niche differentiation (Lu *et al.*,2015; Taylor *et al.,* 2017; Hink *et al.*,2017). Determining patterns in the

distribution of AOA and AOB in the environment could improve land and water management to mitigate the negative impacts associated with nitrification (Refer to Chapter 1.2).

3.10.2 Inhibition of AMO by phenylacetylene

Evidence from field studies indicated that phenylacetylene inhibited nitrification activity by AOA (Im *et al.*, 2011). Here, we examined phenylacetylene inhibition in pure culture with the terrestrial AOA strain "*Ca.* Nitrosocosmicus franklandus". Our data show that in "*Ca.* Nitrosocosmicus franklandus", phenylacetylene is a specific inhibitor of AMO, as it had no effect on hydroxylamine-dependent NO_2^- production (Fig. 3.6). Kinetic analysis suggested that phenylacetylene does not compete with NH_3 for the same AMO binding site, since increasing the native substrate (NH_4^+) concentration did not protect against inhibition (Fig. 3.4 A). In contrast, higher concentrations of NH_4^+ did provide a protective effect when "*Ca.* Nitrosocosmicus franklandus" was incubated with acetylene, indicating acetylene and NH_3 compete for the same binding site (Fig. 3.5, Table 3.2). The recovery of AMO activity following complete inhibition by phenylacetylene incorporated a significant lag phase, similar to that observed for acetylene, suggesting that inhibition by these alkynes was irreversible, and that cells required *de novo* protein synthesis of new AMO to re-establish NH_4^+-oxidising activity (Fig. 3.7). Irreversible inhibition could indicate that the binding cavity of the AMO from "*Ca.* Nitrosocosmicus franklandus" is large enough to enable the orientation and subsequent activation of phenylacetylene, and that phenylacetylene and acetylene essentially both act as suicide substrates. Curiously though, the data suggest that phenylacetylene does not interact with the same binding site on the AMO as NH_3 and acetylene.

Phenylacetylene is an irreversible inhibitor of AMO from *N. europaea* (Hyman and Wood, 1985; Bennett *et al.,* 2016). Here we demonstrated that phenylacetylene does not compete with NH_3 for the same binding site (Fig. 3.4 B). It has been proposed that the AMO from *N. europaea* may contain two distinct binding sites, one that specifically binds NH_3 and hydrocarbons $\leq C_3$ and a second that binds larger hydrocarbons, with oxidation occurring at either site (Keener and Arp, 1993; Keener *et al.,* 1998). Alternatively, different hydrocarbons might be able to access the active site of the AMO from two different directions (Keener *et al.,*1998). It has also been suggested that the pMMO contains two distinct binding sites, one which binds small substrates such as methane and ethane, and another which binds larger non-growth substrates (Miyaji *et al.,* 2011). Although the location and nuclearity (the number of metals atoms) of the active site for methane oxidation is still under debate, it does appear that the pMMO contains multiple metal-binding sites (Lieberman and Rosenzweig, 2005; Chan and Yu, 2008; Cao *et al.,* 2018; Lu *et al.,* 2019; Ross *et al.,* 2019; Ro *et al.,* 2019), or potential active sites, and therefore it is possible that different hydrocarbons are oxidised at distinct sites on the pMMO. The non-competitive nature of phenylacetylene inhibition, with respect to NH_3, of the AMO from "*Ca.* Nitrosocosmicus franklandus" provides early indications that distinct binding sites may be present on the archaeal AMO, or that there are two separate routes by which substrates can access the archaeal AMO active site.

Kinetic analysis of phenylacetylene inhibition of AMO of "*Ca.* Nitrosocosmicus franklandus" and *N. europaea* revealed that phenylacetylene most likely interacts with the AMOs via distinct mechanisms. Specifically, phenylacetylene inhibition of AMO from *N. europaea* had characteristics of uncompetitive inhibition, where both the $K_{m(app)}$ and $V_{max(app)}$ decreased with increasing concentrations of

phenylacetylene, indicating that the inhibitor only has affinity for the enzyme-substrate complex. Potentially, the binding of NH_3 induces a structural change in the AMO binding cavity, enabling phenylacetylene to bind at a putative secondary (non-NH_3) site. Phenylacetylene inhibition of the AMO from "*Ca.* Nitrosocosmicus franklandus" did not show the same characteristics as in *N. europaea* (Table 3.1), demonstrating that the interaction between phenylacetylene and the active site differed between the distinct AMO types.

Both AMO- and pMMO-expressing microorganisms have received interest for their potential use in bioremediation due to their capability to co-oxidize persistent organic pollutants such as halogenated alkanes and alkenes and chlorinated hydrocarbons (Sayavedra-Soto *et al.,* (2010); Semrau, 2011). Unlike the bacterial AMO, the oxidation of aromatic compounds has not been observed by the pMMO (Burrows *et al.*, 1984; Keener *et al.*, 1998; Lontoh *et al.*, 1999; Lontoh *et al.*, 2000). Lontoh *et al.,* (2000) showed that pMMO from *M. capsulatus* (Bath) and several strains of methanotrophs were relatively resistant to phenylacetylene inhibition, with whole cell pMMO activity still present at 1 mM phenylacetylene. It is possible that aromatic compounds are simply too bulky to gain access to, or be orientated at, the pMMO active site (Ng *et al.,* 2008). In contrast, the sMMO can co-oxidise many aromatic compounds, including mono- and di-aromatics (Jiang *et al.,* 2010). Although *N. europaea* appears to lack the ability to completely mineralise aromatic pollutants, it may initiate degradation of aromatic compounds and provide oxidation products that can be transformed by other microorganisms (Keener and Arp, 1994). There is evidence that the archaeal AMO, unlike the pMMO, is capable of transforming aromatic compounds. Recently, Men *et al.,* (2016) demonstrated that the AOA strain *N. gargensis* was capable of co-metabolising two tertiary amines, mianserin and

ranitidine (both pharmaceutical drugs), with the initial oxidative reaction most likely carried out by the AMO.

This research offers new insights into the structure and substrate range of AMO from archaea using alkyne inhibitors, in comparison with other members of the CuMMO family. The subsequent study (Chapter 4) investigates the inhibition and subsequent co-oxidation of an alternative archaeal AMO substrate. Examining alternative substrate/inhibitor reactions can provide additional information about archaeal AMO stereoselectivity, advances our understanding of the enzyme structure and can improve predicted structural models for archaeal AMO.

4. The oxidation of C1 compounds by ammonia oxidising archaea

4.1 Introduction

Enzymes belonging to the CuMMO superfamily can oxidise a range of substrates (Discussed in Chapter 1.8 and in Chapter 3). It has been proposed that the downstream metabolic steps are what defines the functional role of microbes using these enzymes (Holmes *et al.,* 1995; Pester *et al.,* 2011). For instance, the bacterial pMMO and AMO can both oxidise methane to methanol and NH_3 to hydroxylamine. Methanotrophs further catabolise methanol to formaldehyde and formate using different dehydrogenases and similarly, ammonia oxidisers produce nitric oxide and nitrite from hydroxylamine (Murrell, 1992; Caranto and Lancaster, 2017). Methanol/formaldehyde and hydroxylamine provide the internal source of energy and reductant for methanotrophs and NH_3 oxidisers, respectively (Khadka *et al.,* 2018). NH_3 and methane oxidation are major processes in the global nitrogen and carbon cycle and frequently occur together in sediments, such as the aerobic zone above methanogenic activity (Hyman and Wood, 1983). Whilst the pMMO and AMO demonstrate clear specificity for one substrate, possibly due to their source of reducing equivalents, it is interesting to consider the degree of "crossover" and synergy between carbon and nitrogen cycling of as a result of the 'promiscuous' nature of the pMMO and AMO.

Methane is the second most abundant greenhouse gas, with up to 884 Tg of methane being emitted annually from various natural and anthropogenic sources (Saunois *et al.,* 2016). With a global warming potential 84 times that of carbon dioxide over a 20-year period, the removal of methane has become a major focus of climate change science (IPCC, 2018; Guerrero-Cruz *et al.,* 2021). Soils can act as a natural

biofilter for methane emissions, largely due to the activities of methanotrophs which oxidise approximately 30 Tg $year^{-1}$ (Kallistova *et al.,* 2017). Methanotrophs fall into the classes of *Alphaproteobacteria* and *Gammaproteobacteria,* and the phyla *Verrucomicrobia* and NC10 (Kalyuzhnaya *et al.,* 2019). The pMMO is expressed by most methanotrophs, except from *Methylocella* spp. and a few strains from the *Methyloferula* and *Methyloceanibacter* genera which only have the iron-dependent sMMO (Semrau *et al.,* 2010; Farhan Ul Haque *et al.,* 2020). In methanotrophs that possess both forms of MMO, the expression and activity of these enzymes is controlled by intracellular copper concentrations, which is known as the "copper switch" (Nielsen *et al.,* 1997; Semrau *et al.,* 2010).

Methanotrophs often have a rich inventory for the metabolism of various forms of inorganic nitrogen, and many encode a hydroxylamine oxidoreductase homologue (mHAO) (Hanson and Hanson, 1996; Poret-Peterson *et al.,* 2008; Stein and Klotz, 2011; Versantvoort *et al.,* 2020). Unlike AOB, which transport electrons from hydroxylamine oxidation to the quinone pool to conserve energy and support cellular growth, the mHAO prevents the toxic accumulation of hydroxylamine following the oxidation of NH_3 (Klotz and Stein, 2008). Nitrification by methanotrophs can produce significant amounts of nitrous oxide (Lee *et al.,* 2009) and some methanotrophs have been shown to denitrify during hypoxia in the presence of nitrite (Campbell *et al.,* 2011; Kits *et al.,* 2015; Mohammadi *et al.,* 2017). NH_3 behaves as a competitive inhibitor of the pMMO (O'Neill and Wilkinson, 1977; Carlsen *et al.,*1990) and can have relatively low dissociation constants (K_i values). *M. capsulatus,* for example, was found to have a K_i for NH_3 as low as 8.4 μM, depending on pH (Carlsen *et al.,* 1990), which is comparable to the K_m of several AOBs (Suzuki *et al.,* 1974; Qiang and Bakken, 1999). In addition to being an inhibitor of methane oxidation, ammonium can

also serve as a nutrient and stimulate methanotrophic growth (Bodelier and Laanbroek, 2004; Bodelier 2011; Daebeler *et al.,* 2014). Consequently, the dynamics between stimulation and inhibition of methanotrophic activity by ammonium is very interesting and is likely influenced by the genetic potential of methanotrophs to cope with its oxidised products (Stein *et al.,* 2012).

Methane and methanol oxidation by pure cultures of AOB has been confirmed in several key studies (Jones and Morita 1982, Hyman and Wood 1983; Voysey and Wood, 1987; Ward, 1987). *N. europaea* has a relatively poor affinity for methane, with a K_i of 2 mM, however cells can produce considerable quantities of methanol when incubated with methane and in the presence of a source of reductant (NH_3 and/or hydroxylamine) (Hyman and Wood, 1983, Taher and Chandran, 2013). Heavy isotope tracer experiments also found that ^{13}C-formaldehyde and ^{13}C-formate were detectable in *N. europaea* cell suspensions following the addition of ^{13}C-methane and ^{13}C-methanol (Voysey and Wood, 1987). The marine AOB *Nitrosococcus oceani* is more sensitive to methane inhibition and has a considerably lower K_i (6.6 μM) compared to *N. europaea* (Ward, 1987). Both AOB strains produced $^{14}CO_2$ from ^{14}C-methane and ^{14}C-methanol and incorporated methane and methanol derived carbon into cellular biomass (Jones and Morita, 1982; Ward, 1987 and 1990). For *N oceani,* 80% of the ^{14}C-methanol added could be accounted for in the sum biomass and CO_2, with CO_2 the major product of methane and methanol oxidation (Ward, 1987 and 1990). In contrast, only trace amounts of $^{14}CO_2$ were produced from methanol oxidation by *N. europaea* (Voysey and Wood, 1987). How methanol is metabolised by *N. europaea* and *N. oceani* is currently unknown. There is no known methanol dehydrogenase (MDH) genes in the genomes of AOB (Voysey and Wood, 1987; Stein *et al.,* 2007). Some studies have suggested that AOB do not contribute to methanotrophy when

presented with environmentally relevant levels of methane (Jiang and Bakken, 1999; Zheng *et al.,* 2014). However, recently there has been a surge in research investigating the use of NH_3 oxidisers in the bioconversion of methane to methanol, with promising results (Zhang *et al.*, 2021; Su *et al.,* 2019; Taher and Chandran, 2013).

The oxidation of C_1 compounds by AOA has not been investigated and similar to AOB, MDH appears to absent from genomes. Interestingly, "*Ca.* Nitrosocosmicus exaquare" encodes genes associated with C_1 metabolism, including formate dehydrogenase and glutathione-dependent formaldehyde dehydrogenase, although it has not been determined if they are functional (Sauder *et al.,* 2017). The inhibition of AOA by linear 1-alkynes (Taylor *et al.,* 2013 and 2015; Wright *et al.*, 2020) strongly suggests that the archaeal AMO substrate range will include short-chain-length hydrocarbons: $\leq C_5$. Additionally, many AOA, particularly those associated with marine and acidophilic environments, have a greater affinity for NH_3 compared to AOB, and therefore perhaps they have a greater affinity for methane too (Jung *et al.,* 2021). Given their abundance and distribution (Chapter 1, Section 1.3), AOA could potentially represent global players in C_1 compound turnover in the environment. The first aim of this project was to investigate the inhibition of the AMO from "*Ca.* Nitrosocosmicus franklandus" by methane and methanol. Secondly, we explored methane and methanol metabolism in "*Ca.* Nitrosocosmicus franklandus" using ^{13}C-labelling experiments. The major questions we were seeking to answer was: (1) is the AMO from "*Ca.* Nitrosocosmicus franklandus" capable of oxidising methane or methanol at environmentally relevant levels and (2) was methanol further metabolised to produce CO_2 and/or be incorporated into cellular biomass. The experiments detailed in this chapter were either performed by myself or Barbora Oudova and are stated in the subsequent sections of this chapter.

4.2 Methane inhibition

4.2.1 Inhibition of NH_3-dependent NO_2^- production by CH_4 during growth

Experiments were designed to (1) establish the sensitivity of NH_3-dependent NO_2^- production by whole cells during growth in the presence of methane (Fig. 4.1) and (2) to determine if the inhibition could be overcome by culturing "*Ca.* Nitrosocosmicus franklandus" in the presence of higher concentrations of NH_4^+ (Fig. 4.2). For the first assay, washed and concentrated cells were inoculated into media containing 2 mM NH_4^+ and NO_2^- was sampled after 5 days. Only the cultures incubated with 20% methane showed significant inhibition of NO_2^- production relative to the control ($p < 0.01$, one-way ANOVA, Fig. 4.1). There was no significant difference between the control and the 20% N_2 treatment, verifying that the reduction of O_2 in the headspace is not the cause of the inhibition.

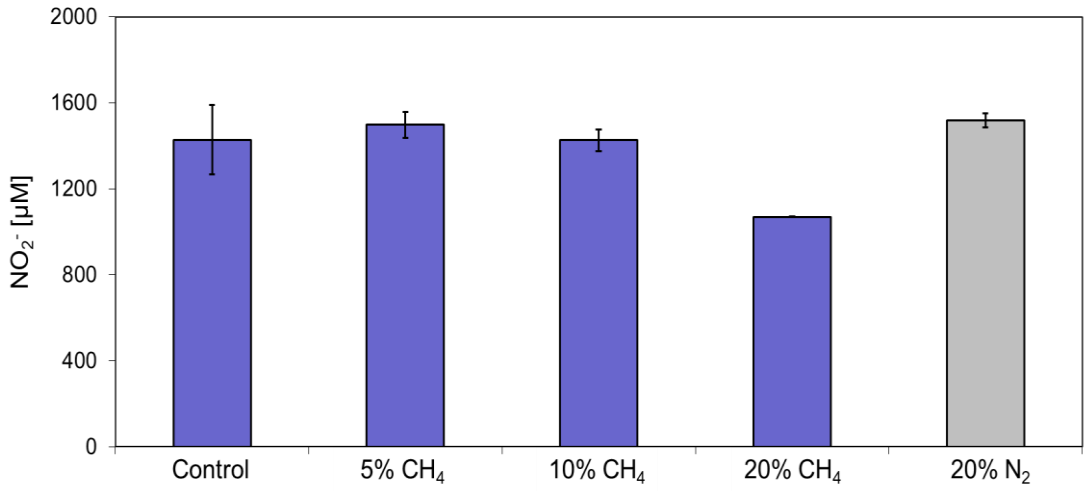

FIG 4.1 NO_2^- accumulation by "*Ca.* Nitrosocosmicus franklandus" cultures in the presence of methane or N_2 in the headspace. Concentrated cells were inoculated into media containing 2 mM NH_4^+ and NO_2^- was sampled after five days. Error bars represent SE (n = 3).

Next, the effect of increasing the NH_4^+ concentration on the inhibition of NO_2^- production by 20% methane was examined. Incubating the cultures with ≥ 10 mM

NH_4^+ prevented the inhibition of NO_2^- production by methane (Fig. 4.2), this was the first indication that methane most likely behaved as a competitive inhibitor of NH_3 oxidation by the AMO. The lower rates of NO_2^- production in the presence of 20 and 40 mM NH_4^+ was attributed to the NH_4^+ tolerance of this strain (Fig. 4.2E and 4.2F). Lehtovirta-Morley *et al.,* (2016b) showed that the maximum specific growth rate of "*Ca.* Nitrosocosmicus franklandus" began to decrease at NH_4^+ concentrations ≥10 mM.

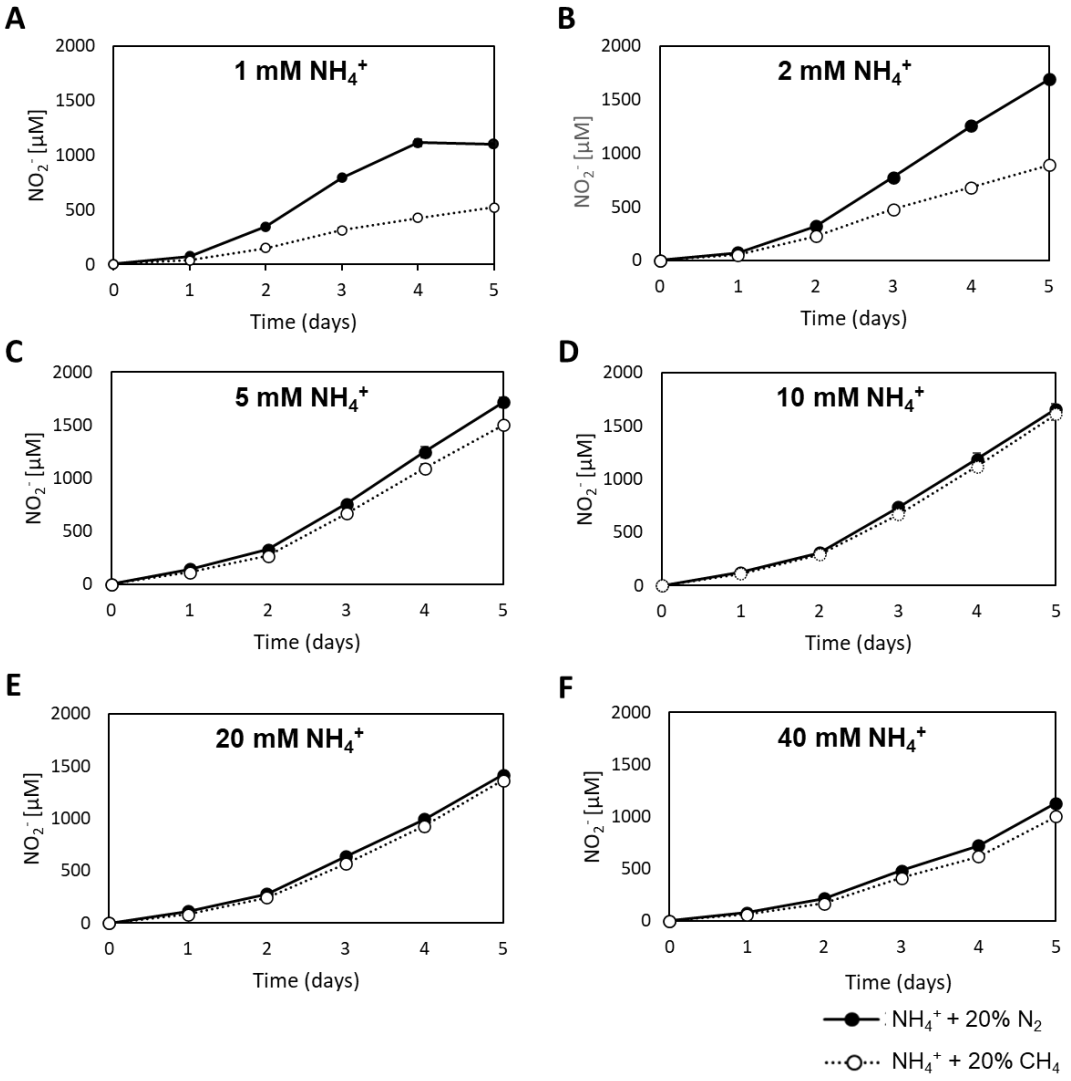

FIG 4.2 NO_2^- accumulation by "*Ca.* Nitrosocosmicus franklandus" cultures in the presence of 20% methane or N_2 in the headspace. Cells were inoculated into media containing difference concentrations of NH_4^+ and NO_2^- was sampled every 24 h for five days. Error bars represent SE (n = 3).

4.2.2 NH_3 and hydroxylamine oxidation activity in the presence of methane

Results from Section 4.2.1 suggested that methane was a competitive inhibitor of NH_3 oxidation. However, since these were growth assays, other factors could have influenced the results and the data obtained may not fully reflect the response of AMO to methane. Therefore, short-term whole-cell enzyme activity assays were designed to explore the inhibition of the AMO from "*Ca.* Nitrosocosmicus franklandus" by methane and to calculate the kinetic parameters (Section 4.2.3). Due to the low solubility of methane (1.4×10^{-3} M / atm, (Wilhelm *et al.*, 1977)) the activity assays were performed with shaking (120 rpm).

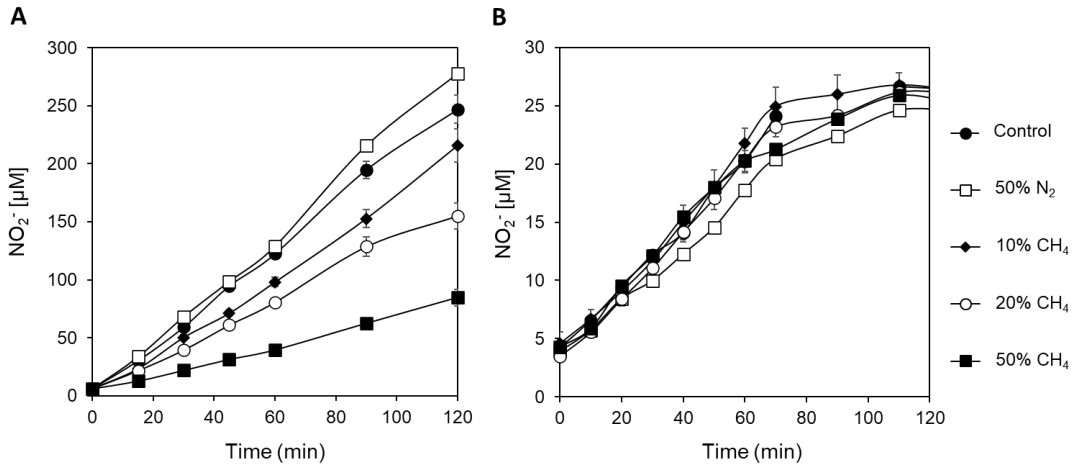

FIG 4.3 NO_2^- production by "*Ca.* Nitrosocosmicus franklandus" in the presence of **A)** 1 mM NH_4^+ and **B)** 0.2 mM hydroxylamine in response to different concentrations of methane in the headspace. Error bars represent SE (n = 3).

Initial 1 h assays with concentrated cell suspensions were used to determine the effect of methane on NH_3 oxidation in the presence of 1 mM NH_4^+ (Fig. 4.3A). Methane inhibition of NH_3-dependent NO_2^- production was comparable to those obtained with the growth assay (Fig. 4.2A), with 20% CH_4 inhibiting NO_2^- production by approximately 2-fold compared to the 20% N_2 control (Fig. 4.3A). Methane did not significantly decrease the rate of NO_2^- production from hydroxylamine (Fig. 4.3B),

making it unlikely that methane or its oxidised products affected enzymatic reactions downstream of the AMO in the NH_3 oxidation pathway during these short incubations. The concentration of methane used in these experiments ranged from 0.14 – 0.70 mM (10 – 50% headspace). These are comparable to the concentrations used to inhibit NH_3 oxidation by *N. europaea* in the study by Hyman and Wood (1983). NH_3 oxidation by *N. oceani* was more sensitive to methane with strong inhibition occurring at <0.1 mM (Jones and Morita, 1992; Ward, 1987).

4.2.3 Kinetic analysis of CH_4 inhibition

4.2.3.1 Determining the mechanism of CH_4 inhibition

NH_3-dependent NO_2^- production by "*Ca.* Nitrosocosmicus franklandus" followed Michaelis-Menten type saturation kinetics in the absence of inhibitors (Eq. 1, Chapter 3). To determine the mechanism of methane inhibition, the kinetic parameters ($K_{m(app)}$ and $V_{max(app)}$) were calculated in the presence and absence of methane using hyperbolic regression analysis (Fig. 4.4). Methane concentrations were selected to give partial inhibition of NH_3-oxidising activity and were derived from the data shown in Fig. 4.3A.

$$v = \frac{V_{\max\,(\mathrm{app})}\,[S]}{[S]+K_{\mathrm{m(app)}}} \quad (1)$$

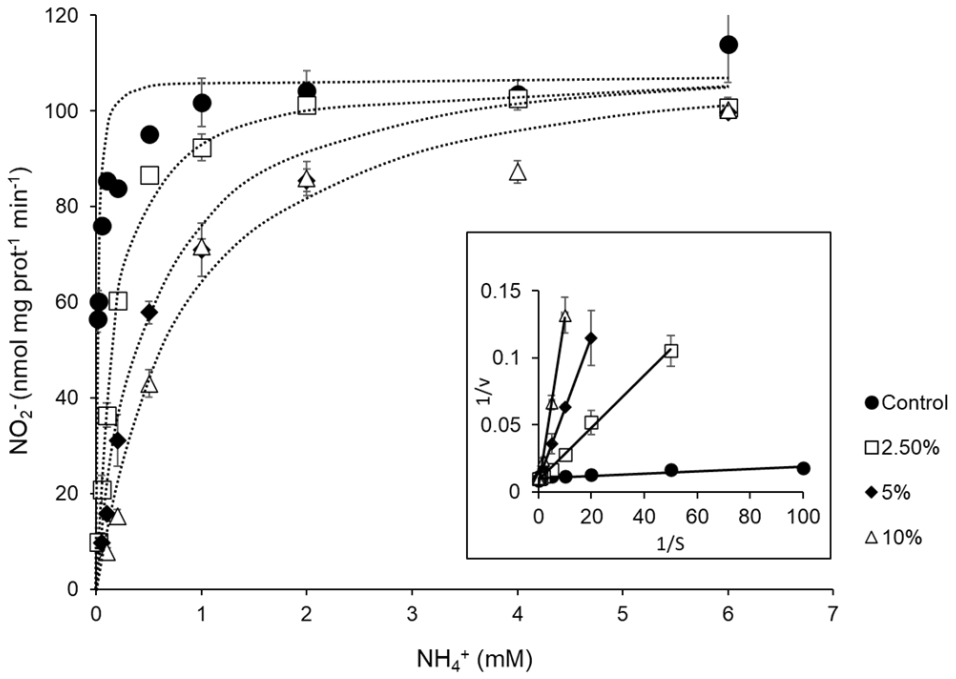

FIG 4.4 Michaelis-Menten hyperbolic plot showing the initial rate of NO_2^- production by "*Ca.* Nitrosocosmicus franklandus" to methane as a function of NH_4^+ concentration. Inhibition was overcome by increasing concentrations of NH_4^+, indicating competitive inhibition. Inset shows the Lineweaver-Burk plot for methane as an inhibitor of NH_4^+-dependent NO_2^- production. The slopes for each methane concentration intercept the 1/v axis at the same point, signifying competitive inhibition. Error bars represent SE (n = 3).

As anticipated, increasing the NH_4^+ concentration alleviated the inhibitory effects of methane to the point that when cells were incubated with >6 mM NH_4^+, the rate of NO_2^- production was no longer inhibited (Fig. 4.4). Additionally, the $K_{m(app)NH4+}$ markedly increased from 12.2 ± 2.4 μM to 771.9 ± 107.8 μM in the presence of 0 and 10% methane respectively, whilst the maximum rate ($V_{max(app)}$) of NO_2^- production did not change significantly ($p < 0.01$) (Table 4.1). This convincingly demonstrated that NH_3 (substrate (S)) and methane (inhibitor (I)) competed for the same binding site on the AMO enzyme from "*Ca.* Nitrosocosmicus franklandus" (Fig. 4.5A). The $K_{m(app)}$ and $V_{max(app)}$ values calculated from the Lineweaver-Burk plot (Fig. 4.4 inset) were not significantly different from those calculated using the hyperbolic plot ($p < 0.01$).

Competitive inhibition is described by Eq. 2. This equation is identical to the Michaelis-Menten equation (Eq. 1) except that the presence of the inhibitor (methane) increases the K_m by the factor [1 + ([I]/K_i)].

$$v = \frac{V_{\max\,(app)}\,[S]}{[S]+K_{m(app)}(1+\frac{[I]}{K_i})} \quad (2)$$

Table 4.1 Kinetic parameters of NH_3-dependent NO_2^- production by "*Ca.* Nitrosocosmicus franklandus" in the presence of methane. SE of three replicates is in parentheses (n = 3).

Methane (%)	$K_{m(app)NH4+}$ (μM)	$V_{max(app)}$ (nmol mg prot^{-1} min^{-1})	$K_{m(app)NH3}$ (μM)
0	12.2 (2.4)	101.3 (2.4)	0.129
2.5	169.7 (13.1)	108.0 (1.8)	1.8
5	483.0 (58.8)	107.2 (3.9)	5.12
10	771.9 (107.8)	112.4 (4.7)	8.18

The mode of methane inhibition is consistent with the conclusions made in Chapter 3, in that the AMO from "*Ca.* Nitrosocosmicus franklandus" likely has at least two binding sites, one that binds and oxidises small substrates: NH_3, acetylene and methane for instance, and another which binds and oxidises larger substrates (Fig. 4.5B). Differences in the $K_{m(app)}$ for "*Ca.* Nitrosocosmicus franklandus" reported in this chapter and in Chapter 3 in the absence of inhibitors (control) are likely due to the effect of shaking the cell suspensions, however the values obtained are still very comparable.

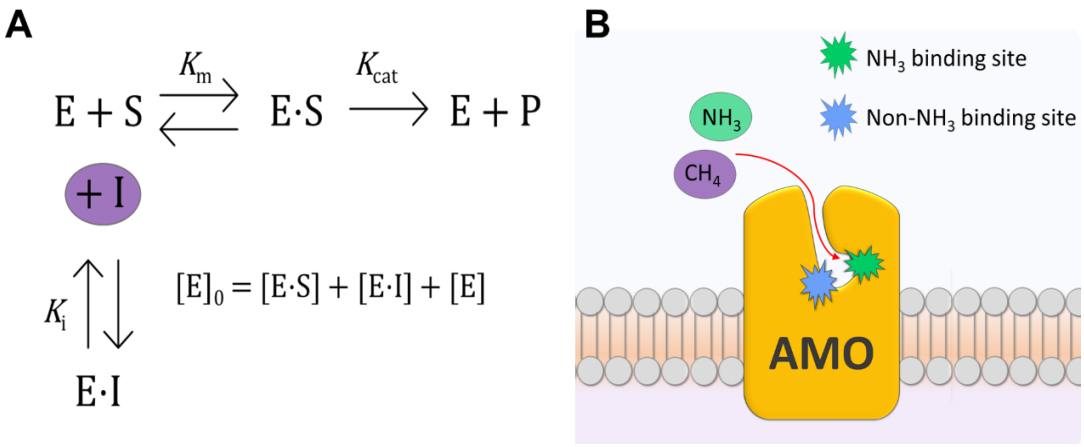

FIG 4.5 A) Schematic of competitive inhibition. Total enzyme concentration ($[E]_0$) equals the sum of enzyme bound to both the substrate($[E{\cdot}S]$) and the inhibitor ($[E{\cdot}I]$) plus free enzyme ($[E]$). Adapted from Silverman (2000). **B)** Proposed model for methane inhibition of NH_3 oxidation by the AMO from "*Ca.* Nitrosocosmicus franklandus". Methane and NH_3 compete for the same binding site on the AMO.

Methane was found to be a competitive inhibitor of the AMO from the AOB *N. europaea* and *N. oceani* since high NH_4^+ concentrations prevented inhibition. However, the kinetics appeared more complex for these strains compared to "*Ca.* Nitrosocosmicus franklandus". In the presence of methane, both hyperbolic regression and the resulting Lineweaver-Burk plots for NH_3 oxidation by *N. oceani* did not follow Michaelis-Menten type kinetics and were sigmoidal. Ward (1987, 1990) suggested the AMO from *N. oceani* has multiple NH_3 binding sites and that methane binds cooperatively, indicating the binding of methane induces allosteric effects that prevents NH_3 binding to that site but increases the affinity for NH_3 at other sites. Methane inhibition of whole-cell *N. europaea* and cell-free extracts was also reported to be sigmoidal at low NH_4^+ concentrations (Suzuki *et al.*, 1976; Hyman and Wood, 1983).

4.2.3.2 Calculating the inhibitor dissociation constant (K_i) for methane

The next step was to calculate the K_i for the enzyme-inhibitor (*EI*) complex (Eq. 3, Fig. 4.5B). In this instance, the K_i reflected the affinity of AMO from "*Ca.* Nitrosocosmicus franklandus" for binding methane, and consequently the reduction in its NH_3 oxidising activity.

$$K_i = \frac{[E]\times[I]}{[EI]} \quad (3)$$

The K_i was estimated using three different methods:

(i) The Lineweaver-Burk plot

The K_i can be calculated by replotting the Lineweaver-Burk plot (Eq. 4). [*I*] is the concentration of the inhibitor, in this case methane. $V_{max(app)}/K_{m(app)}$ describes how the AMO behaved at low NH_3 concentrations. If the K_i is small, it pushes the equilibrium to *EI*, indicating the binding of methane is strong (Eq. 3). Methane was a competitive inhibitor of NH_3 oxidation, so the $V_{max(app)}$ remained the same whilst $K_{m(app)}$ increased, therefore decreasing $V_{max(app)}/K_{m(app)}$. The K_i was determined by plotting the $K_{m(app)}/V_{max(app)}$ (the reciprocal of $V_{max(app)}/ K_{m(app)}$) versus [*I*] and was calculated to be 0.3% methane, which equals approximately 4.5 μM (Fig. 4.6A and B).

$$\frac{1}{v} = \frac{K_m}{V_{max}}\left(\frac{1}{[S]}\right)\left(1 + \frac{[I]}{K_i}\right) + \frac{1}{V_{max}} \quad (4)$$

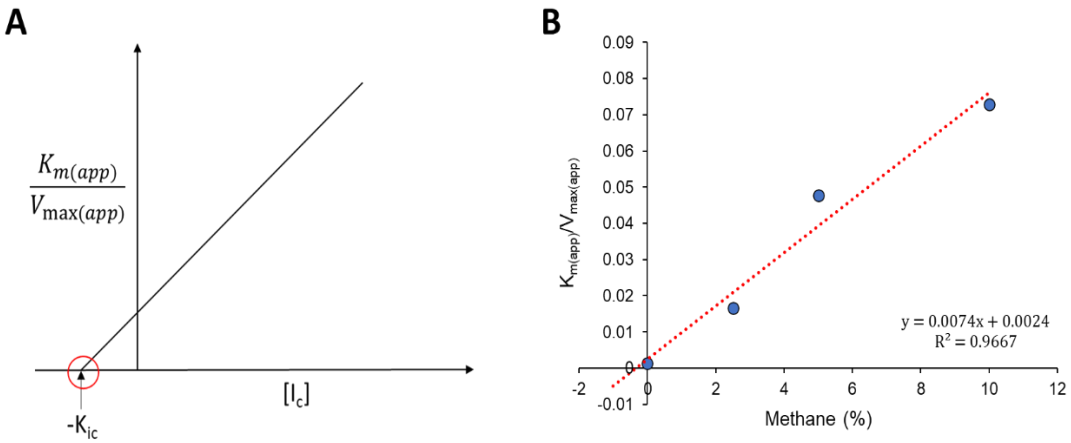

FIG 4.6 A) Schematic of the $K_{m(app)}/V_{max(app)}$ versus [*I*] plot used to calculate K_i. **B)** The values of $K_{m(app)}/V_{max(app)}$ plotted against the methane concentrations used in this study.

(ii) Fixed substrate concentration

The K_i can also be calculated from a fixed substrate concentration [*S*] using Eq. 5. In this method, *v* is the rate of NO_2^- production without methane and v^{obs} is the rate of NO_2^- production in the presence of methane. The $K_{m(app)}$ is without methane. The K_i can be obtained by plotting $v\text{-}v^{obs}/v^{obs}$ versus [*I*] and calculating the value from the slope (Fig. 4.7 A and B). The fixed substrate concentration was 5.3 µM NH_3 (calculated from the dissociation of NH_3/NH_4^+ at pH 7.3 using the Henderson Hasselbach equation) and the K_i was calculated to be 0.2% methane or approximately 2.8 µM.

$$\frac{v-v^{obs}}{v^{obs}} = \frac{K_m}{[S]+K_m} \times \frac{1}{K_i} \times [I] \qquad (5)$$

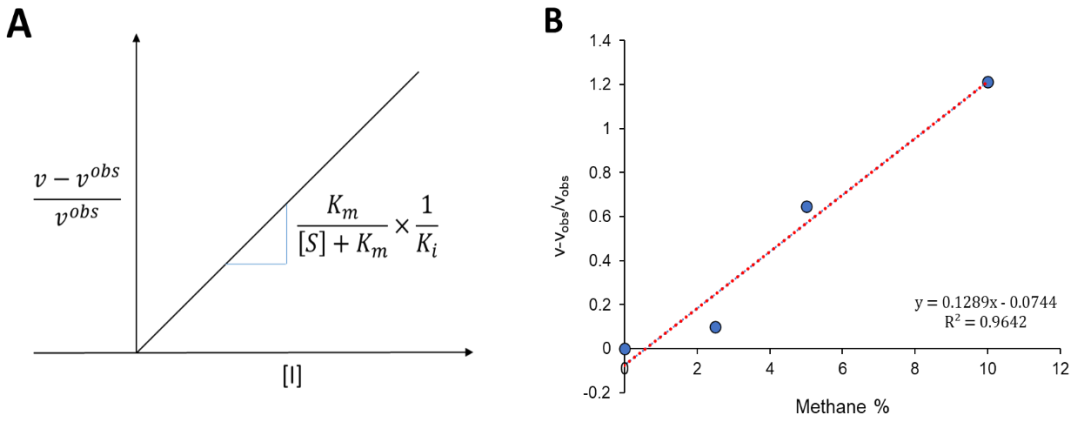

FIG 4.7 A) Schematic of the v-v^{obs}/v^{obs} versus [I] plot. K_i can then be calculated from the slope. **B)** The values of v-v^{obs}/v^{obs} versus the methane concentrations used in this study.

Solving K_i for methane from the slope (Fig. 4.7B):

$$0.1289 = \frac{K_m}{[S]+K_m} \times \frac{1}{K_i} = \frac{0.129\ \mu M}{5.3\ \mu M + 0.129\ \mu M} = 0.0238$$

$$0.1289 = \frac{0.0238}{K_i}$$

$$K_i = \frac{0.0238}{0.1289}$$

K_i = 0.2% = 2.8 µM

(iii) Calculating the K_i from the K_m

Finally, the K_i was calculated from the $K_{m(app)}$ in the presence of methane, which is denoted by K'_m (Eq. 6). The method was used by Hyman and Wood (1983) and Ward (1987) to determine the K_i for *N. europaea* and *N. oceani*, respectively. Methane was converted from % headspace concentration to µM using Henry's Law and the K_i was estimated to be 2.2 ± 0.32 µM (mean ± S.D).

$$K_i = \frac{K_m\,(1+[I])}{K'_m} \qquad (6)$$

All three methods produced very similar K_i values, ranging from 2.2 to 4.5 µM, which are lower than those previously reported for AOB. For *N. oceani*, a K_i of 6.6 µM was obtained, although the significance of this value was uncertain due to the

complex behaviour of methane inhibition in this strain (Ward, 1987). The K_i for *N. europaea* was considerably different depending on whether cell extracts or whole cells were used, with values of 50 or 2,000 μM respectively (Suzuki *et al.*,1976; Hyman and Wood, 1983). Again, there is some deliberation required over how to interpret these values since, in the presence of methane, neither whole cells nor cell extracts of *N. europaea* obeyed Michaelis-Menten type saturation kinetics. Ward (1987 and 1990) suggested that methane behaves as an allosteric inhibitor of the AMO from *N. oceani*, although for *N. europaea*, the depletion of reductant caused by the oxidation of methane instead of NH_3 was proposed to be the cause of non-linear secondary plots (Hyman and Wood, 1984; Keener and Arp, 1993). Additionally, methanol, the product of methane oxidation, has also been found to be an alternate substrate oxidised by the AMO from *N. europaea*, which could further complicate the kinetics (Voysey and Wood, 1987; Hyman and Wood, 1984). Intriguingly, unlike the AOB, NH_3 oxidation by methane inhibited "*Ca.* Nitrosocosmicus franklandus" cells did appear to follow simple Michaelis-Menten type kinetics (Fig. 4.4), and R^2 values from methane inhibited linear regressions were >0.99 (Fig. 4.4 inset).

The K_i of an inhibitor can be analogous to its K_m as a substrate. However, this is under certain conditions where K_m equals K_s (substrate dissociation/association constant), which is the equivalent of K_i. If substrate binding is faster than the rate at which E·S is turned into product (k_{cat}), then K_m and K_s are the same (Silverman, 2000). It is not possible to know if this is the case for methane inhibition/oxidation in a whole-cell system, and only experiments with purified AMO would be able to determine this. It could be possible to investigate the kinetic parameters of alternative substrate reactions by the AMO in whole cells using an external source of reductant. This is further explored in Chapter 5. Whilst the K_i values estimated for "*Ca.* Nitrosocosmicus

franklandus" are substantially higher than atmospheric methane concentrations (<3 nM) (Conrad, 1996), they are well within the range of $K_{m(app)}$ values reported for methane uptake by some cultivated "low-affinity" methanotrophs (Joergensen and Degn, 1983). Certainly, there are many environments that contain methane concentrations within and above the K_i calculated here, for instance in wetland sediments and landfill cover soils which are associated with high methanogenic activity (Laanbroek, 2010; Jones and Nedwell, 1983). It also needs emphasising that methane inhibition of nitrifiers is very multifaceted. The oxidation of hydroxylamine, the product of NH_3 oxidation, provides the only known source of internal reducing equivalents to sustain AMO activity. Consequently, methane inhibition, or oxidation, will slow the rate of NH_3 turnover by the AMO by reducing the supply of reductant. Therefore, methane could hugely influence NH_3 oxidation activity in the environment. *N. europaea* has a much lower affinity for both methane and NH_3 compared to "*Ca.* Nitrosocosmicus franklandus". Potentially, NH_3 oxidisers with a high affinity for NH_3 could also have a relatively high affinity for methane. It would be interesting to see if NH_3 oxidisers with 'high affinity' AMOs also have novel metabolic repertoires to mitigate the effects of methane, or other alternative substrates/inhibitors, on energy production. Possibly by having multiple NH_3 oxidation sites as suggested by Ward (1990) and evident from data from Chapter 3.

4.3 Methanol inhibition

Methanol is oxidised by the AMO from several different strains of AOB (Ward, 1987; Voysey and Wood, 1987). In ^{13}C-tracer experiments carried out by Barbora Oudova, described in Section 4.4, methanol appeared to be a substrate for the AMO from "*Ca.* Nitrosocosmicus franklandus". Consequently, the mode of methanol inhibition on NH_3 oxidation by "*Ca.* Nitrosocosmicus franklandus" was investigated.

The results discussed here are from experiments designed and carried out by Barbora Oudova. Kinetic parameters ($K_{m(app)}$, $V_{max(app)}$ and K_i) were calculated according to the methods used for methane inhibition (Section 4.2.3).

Like methane, methanol appeared to be a competitive inhibitor of the NH_3 oxidation by the AMO from "*Ca.* Nitrosocosmicus franklandus", apparent from the increase in $K_{m(app)}$ at increasing methanol concentrations but no significant effect on the $V_{max(app)}$. The K_i for methanol ranged from 7.4 to 16.4 μM depending on which method was used for the calculation (Section 4.2.3.2). As discussed for methane, it is difficult to interpret what the K_i value represents, as it may not be comparable to K_m. Additionally, methanol oxidation presumably drains the supply of reductant to the AMO. It has also been highlighted that formaldehyde, the product of methanol oxidation, can react with hydroxylamine to form formaldoxime which inhibits hydroxylamine oxidation by *N. europaea* (Voysey and Wood, 1987). Nevertheless, the K_i calculated for methanol is very low, almost in the range of the K_m calculated for the purified methanol dehydrogenase (MDH) from the methylotrophic denitrifying bacteria *Hyphomicobium denitrificans*, which ranges from 0.3 to 10.5 μM (Nojri *et al.*, 2006). Other purified MDHs have a much higher K_m, well into the millimolar range. Methanol concentrations in the environment are extremely variable, however high concentrations can be expected in the proximity to plants as most of the methanol released is associated with degradation of plant polymers (Kolb, 2009).

4.4 Methane and methanol metabolism

4.4.1 Detection of methanol from methane oxidation

Experiments described in this section were designed to assess methane as a substrate for the AMO from "*Ca.* Nitrosocosmicus franklandus" and to explore C_1

metabolism downstream of the AMO. Hyman and Wood (1983) reported that under an atmosphere of 50% methane, *N. europaea* produced 0.5 mM methanol in 1 h. Experiments performed by Barbora Oudova to detect methanol production by "*Ca.* Nitrosocosmicus franklandus" under an atmosphere of 20 and 50% methane, using alcohol oxidase followed by the Nash assay for the detection of formaldehyde (Nash, 1953), were inconclusive (data not shown). It is possible that "*Ca.* Nitrosocosmicus franklandus" can oxidise methanol via a non-specific alcohol dehydrogenase. Subsequently, ^{13}C-isotope labelling experiments were used to examine if methane and methanol was oxidised to produce CO_2, and if methane/methanol derived carbon was incorporated into cellular biomass.

4.4.2 Enrichment of cellular biomass and CO_2 from methane and methanol oxidation

Results from the preliminary ^{13}C-methane tracer experiments are presented here and further data from ^{13}C-methane and methanol experiments performed by Barbora Oudova are discussed thereafter. "*Ca.* Nitrosocosmicus franklandus" cells were harvested from cultures grown to mid-exponential phase, washed and concentrated before inoculation into fresh media. Cultures were grown under a headspace of 20% ^{13}C-methane (99%), 20% N_2 (unlabelled control) or 0.1% ^{13}C-CO_2 (99%) and supplemented with more NH_4^+ following the accumulation of 1 mM NO_2^- (refer to Chapter 2, Section). ^{13}C-CO_2 treatments confirmed the cells could metabolise and incorporate ^{13}C-carbon into cellular biomass. The ^{13}C labelling of cellular biomass was analysed by EA-IRMS and ^{13}C-CO_2 by GasBench IRMS.

Table 4.3 Data from the initial ^{13}C-labelling experiment. Values for unlabelled control treatments represent the natural abundance of ^{13}C. SE is in parentheses (n = 3).

Treatment	Cell yield (cells μM^{-1} NO_2^-)	^{13}C-cellular biomass (Atom%)
Control	5.21×10^3 (0.36×10^3)	1.0778 (0.0008)
20% ^{13}C-methane	4.59×10^3 (0.036×10^3)	1.2289 (0.0085)
0.1% ^{13}C-CO_2	4.75×10^3 (0.49×10^3)	8.9140 (0.5632)

For the first experiment, "*Ca.* Nitrosocosmicus franklandus" cultures were grown for 25 days, with an additional 2 mM NH_4^+ added on day 10 after they became substrate limited (Fig. 4.8, Table 4.3). It was puzzling that NO_2^- production by cultures incubated with 20% ^{13}C-methane was no longer inhibited after the second addition of NH_4^+. This was not expected based on the results of the previous growth experiments (Fig. 4.2). Cultures incubated with 0.1% ^{13}C-CO_2 and ^{13}C-methane yielded slightly less biomass per μM of NO_2^- produced compared to the control (Table 4.3). The cells incorporated both ^{13}C-CO_2 and ^{13}C-methane derived carbon into cellular biomass, evident from the increase in ^{13}C relative to the unlabelled control treatment (natural abundance, Table 4.3). Biomass from unlabelled cells contained approximately 1.08 atom % ^{13}C. Cells incubated with methane were significantly ^{13}C-enriched (~1.23 ± 0.01 atom %) compared to the unlabelled control cells (Fig. 4.8). ^{13}C-CO_2 data were omitted from Fig. 4.8 to allow for the direct comparison between unlabelled biomass and cells incubated with ^{13}C-methane.

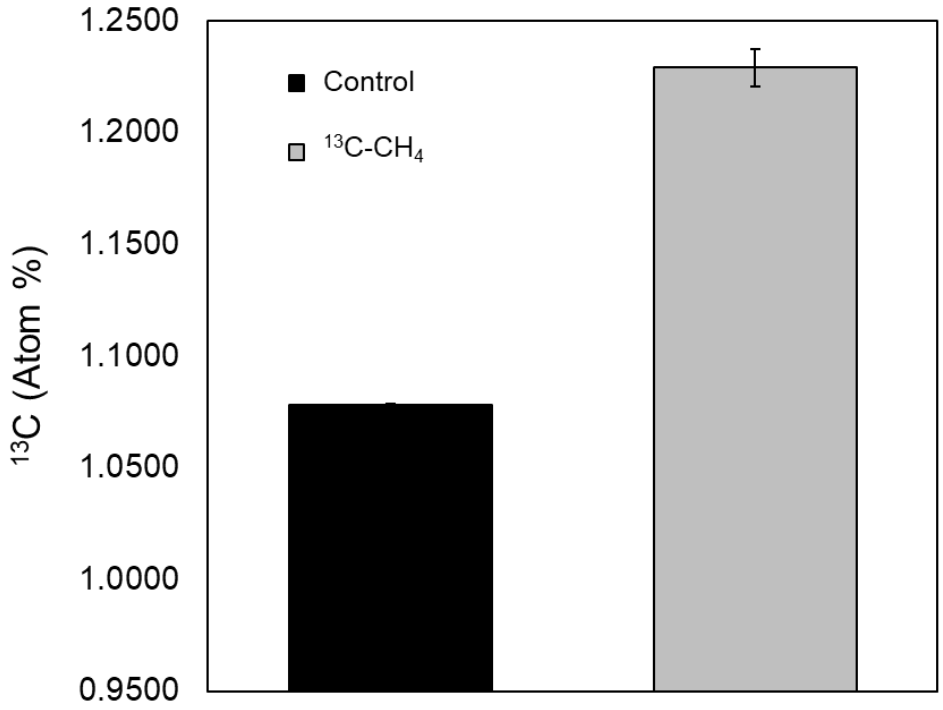

Fig. 4.8 Comparison of ^{13}C-labelling of cellular biomass from unlabelled cells versus cells incubated with ^{13}C-methane. Error bars represent SE (n = 3).

For the second experiment (Table 4.4), additional replicates of each treatment were grown in the presence of 40 mM NH_4^+, with the anticipation that the high NH_4^+ concentration would prevent methane gaining access to the AMO binding site (refer to Fig. 4.2). Cultures were prepared as described above. Cultures incubated with 1 mM NH_4^+ were spiked with a further 1 mM on day 5. After 14 days the cultures had accumulated approximately 2 mM NO_2^-, a similar concentration as to what was accumulated in the first experiment, and cells were harvested for analysis as described (Chapter 2, Section 2.3). The cell yields were notably lower compared to the first experiment (Table 4.4), particularly in the cultures incubated in the presence of 40 mM NH_4^+. This concentration was therefore deemed too high for growth and subsequent experiments by Barbora Oudova were performed with 20 mM NH_4^+. The

cultures were grown in the absence of additional bicarbonate, to prevent dilution of the $^{13}C/^{12}C$ ratio (refer to Chapter 2, Section). It is likely these cultures were carbon-limited which prevented cell division, though it is curious this was not the case for the first experiment. Additional experiments by Barbora Oudova found a minimum of 0.4 mM $NaHCO_3$ was required in the medium for substantial growth.

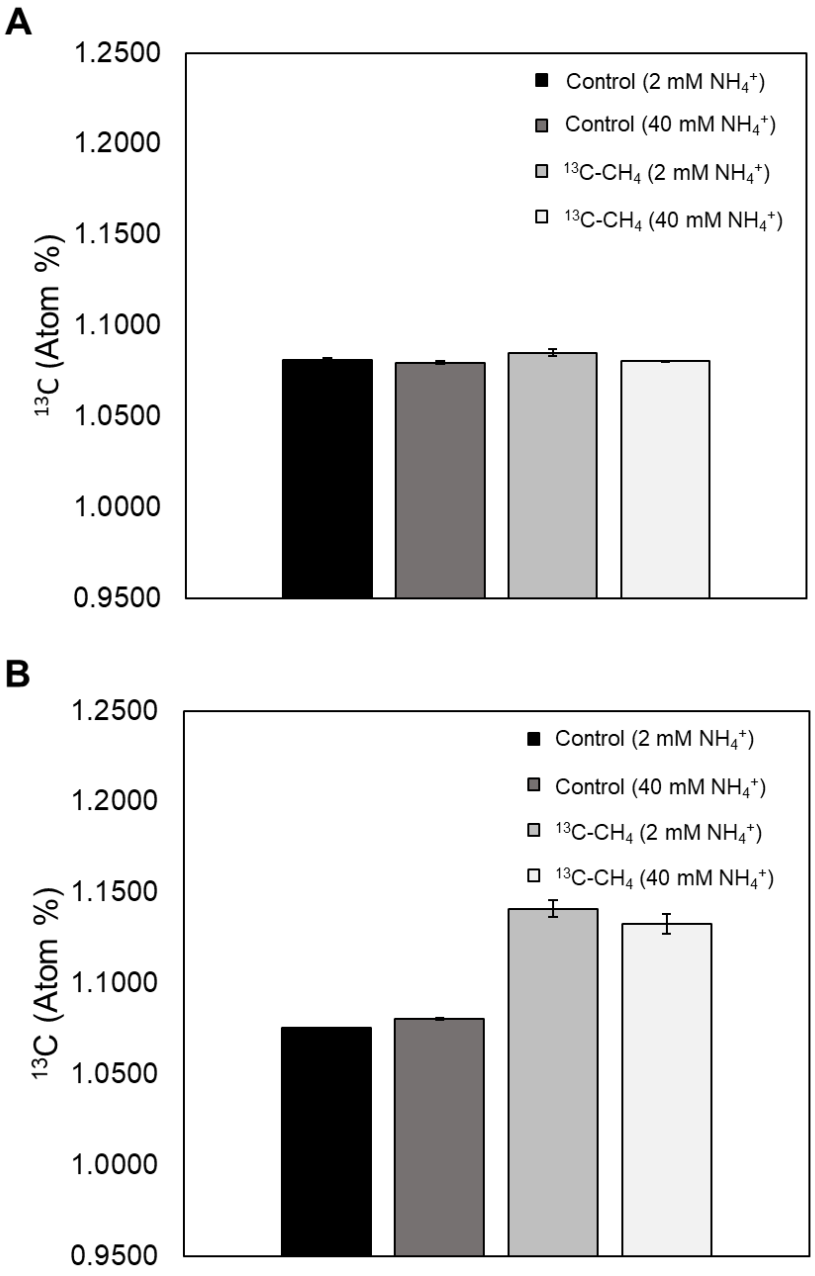

Fig. 4.9 Comparison of ^{13}C-labelling of **A)** cellular biomass and **B)** headspace CO_2 from unlabelled cultures and cultures incubated with ^{13}C-methane, either in the presence of 2 or 40 mM NH_4^+. Error bars represent SE.

Table 4.4 Data from the second ^{13}C labelling experiment. Values for unlabelled control treatments represent the natural abundance of ^{13}C. SE is in parentheses (n = 3).

Treatment	Total NH_4^+ added (mM)	Cell yield (cells μM^{-1} NO_2^-)	^{13}C-cellular biomass (Atom%)	^{13}C-CO_2 (Atom%)	CO_2 [ppmv]
Control	2	2.47×10^3 (0.65×10^3)	1.0813 (0.0009)	1.0756 (0.0001)	140 (7)*
	40	0.64×10^3 (0.31×10^3)	1.0796 (0.0006)	1.0806 (0.0005)	269 (28)*
20% ^{13}C-methane	2	0.93×10^3 (0.30×10^3)	1.0851 (0.0018)	1.1411 (0.0046)	2256 (211)
	40	0.22×10^3 (0.18×10^3)	1.0805 (0.0001)	1.1329 (0.0056)	124 (14)*
0.1% ^{13}C-CO_2	2	1.72×10^3 (0.43×10^3)	2.6176 (0.5509)	11.4965 (0.7566)	1086 (82)
	40	0.31×10^3 (0.20×10^3)	1.3752 (0.0887)	4.4851 (0.4210)	256 (22)*

*CO_2 below the level of quantification (~330 ppmv)

Insufficient growth is most likely the reason the cells did not attain the same amount of ^{13}C-labelling as the first experiment during incubations with both ^{13}C-methane and ^{13}C-CO_2. Some labelling was achieved by cultures incubated with 20% ^{13}C-methane and 2 mM NH_4^+ (1.085 ± 0.002), but it was scarcely above the natural abundance (Table 4.4, Fig. 4.9A). There was a substantial enrichment in methane derived ^{13}C-CO_2, but intriguingly, cells incubated with 2 and 40 mM NH_4^+ were both highly enriched, 1.141 ± 0.005 and 1.133 ± 0.006 atom % respectively (Table 4.4, Fig. 4.9B). This was unexpected since NH_4^+ concentrations ≥5 mM was shown to prevent methane inhibition, and presumably oxidation too. The possibility that "*Ca.* Nitrosocosmicus franklandus" has another mechanism for oxidising methane cannot be ruled out. However, this is very unlikely because experiments performed by Barbora Oudova showed that the addition of acetylene prevented the enrichment of methane derived ^{13}C-CO_2. Additionally, hydroxylamine oxidation was not affected by methane (Fig. 4.3B), suggesting that methane oxidation was AMO-dependent. Another peculiarity of this experiment was the very low concentration of CO_2 in the headspace in all treatments, with the exception of cultures incubated with 20% ^{13}C-methane or 0.1% ^{13}C-CO_2 and in the presence of 2 mM NH_4^+ (Table 4.4). When this is factored into the labelling by methane, only ~0.066 ppmv total CO_2 was labelled in the 40 mM NH_4^+ treatment compared to ~1.38 ppmv labelled CO_2 in the treatments with 2 mM NH_4^+, suggesting the high ammonium concentrations does prevent methane oxidation via competition for the same active site.

4.5 Summary

Overall, the results presented in this chapter have led to the proposal that the AMO from "*Ca.* Nitrosocosmicus franklandus" can co-oxidise methane and methanol, with these compounds competing with ammonia for the same active site. Additionally,

both compounds appear to be metabolised to produce CO_2 and incorporate methane and methanol derived carbon into cellular biomass. This project has been continued by Barbora Oudova who has carried out further experiments investigating both methane and methanol metabolism in "*Ca.* Nitrosocosmicus franklandus".

5. The role of nitric oxide in the archaeal ammonia oxidation pathway

5.1 Introduction

This study began by exploring a possible source of external reductant for alternative substrate oxidations, such as methane and methanol, by the AMO from "*Ca.* Nitrosocosmicus franklandus". It subsequently developed into a more detailed exploration of the similarities and differences between the archaeal and bacterial NH_3 oxidation pathways.

The NH_3 oxidation pathway in AOB is now reasonably well characterised, owing to recent work by Caranto and Lancaster (2017) who demonstrated that both hydroxylamine and nitric oxide (NO) are obligatory intermediates, although the enzyme catalysing the oxidation of NO to NO_2^- is currently unknown (Eq. 1 and 2, reviewed in Chapter 1, Section 1.7.1). Possible candidates include nitrosocyanin, encoded by *ncyA*, and *NirK* (Caranto and Lancaster, 2017; Zorz *et al.,* 2018). Nitrite reductase (NirK) normally reduces NO_2^- to NO, however under specific conditions, this enzyme has been shown to function in reverse. It should be noted that the conversion of NO to NO_2^- was only shown *in vitro* and there is no guarantee that NirK could function in reverse under physiological conditions (Wijma *et al.,* 2004). Hydroxylamine oxidation is catalysed by the periplasmic multi-heme enzyme hydroxylamine oxidoreductase (HAO) and generates three electrons, two of which are cycled back to AMO to sustain its activity (Fig. 5.1).

$$NH_3 + O_2 + 2e^- + 2H^+ \rightarrow NH_2OH + H_2O \quad (1)$$

$$NH_2OH \rightarrow NO + 3e^- + 3H^+ \quad (2)$$

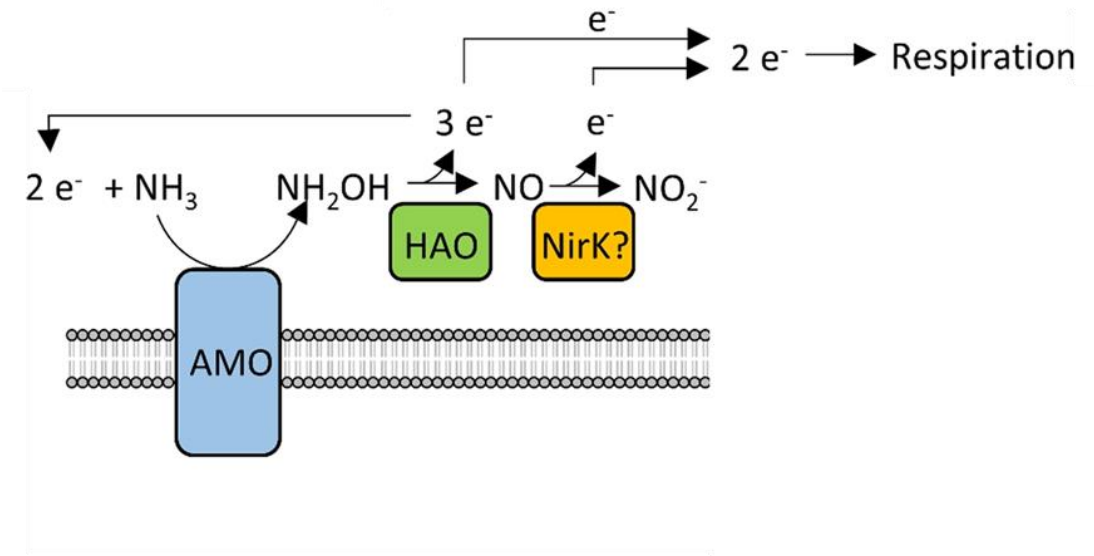

FIG 5.1 The NH_3 oxidation pathway for *N. europaea* according to the three-step model proposed by Caranto and Lancaster (2017). Figure from Lehtovirta-Morley (2018).

The HAO is homotrimeric, with each monomer consisting of a single catalytic P_{460} cofactor, supported by seven other *c*-type hemes (Coleman and Lancaster, 2020). HAO oxidises hydroxylamine to NO via a sequence of Fe-nitrosyl intermediates. NO rapidly dissociates from HAO and is rapidly oxidised to NO_2^- via the unidentified NO oxidoreductase (NOO) enzyme (Smith *et al.*, 2019). Hydrazine, which is a key intermediate in anammox catabolism, is an alternative substrate for the HAO and is presumed to be oxidised to N_2 (Eq. 3, Anderson, 1964, Logan and Hooper, 1995). As with hydroxylamine, electrons from hydrazine oxidation can serve as reducing equivalents for the AMO. Subsequently, hydrazine has been used as an external supply of reductant to fuel alternative substate oxidations by the bacterial AMO (Hyman and Wood, 1984; Hyman *et al.*, 1988; Hyman *et al.*, 1990; Rasche *et al.*, 1991; Juliette *et al.*, 1993; Keener and Arp, 1993 and 1994).

$$N_2H_4 \rightarrow N_2 + 4H^+ + 4e^- \quad (3)$$

The overall stoichiometry of NH_3 oxidation by AOA is indistinguishable from that of AOB (Eq. 4, Martens-Habbena *et al.,* 2009), which would suggest the biochemistry should be similar too.

$$1NH_3 + 1.5O_2 \rightarrow 1NO_2^- + H_2O + H^+ \quad (4)$$

There is strong evidence indicating that hydroxylamine is the product of NH_3 oxidation by the archaeal AMO (Vajrala *et al.,* 2013). However, no HAO homologue exists in AOA and AOA do not have the genetic repertoire to fully synthesise *c*-type hemes, thus AOA have a completely novel mechanism for the oxidation of hydroxylamine (Walker *et al.,* 2010). A potential candidate is the periplasmic multicopper oxidase (MCO1), however these enzymes are not encoded by all genera of AOA (Kerou *et al.,* 2016; Herbold *et al.,* 2017). Like AOB, NO appears to play a major role in the archaeal NH_3 oxidation pathway. However, given that AOA are much more sensitive to NO-scavengers, such as 2-phenyl-4,4,5,5-tetramethylimidazoline-1-oxyl 3-oxide (PTIO), compared to AOB, NO will likely have a different function in the archaeal pathway (Yan *et al.,* 2012; Shen *et al.,* 2013; Sauder *et al.,* 2016). Several models for the archaeal NH_3 oxidation pathway have been proposed. Perhaps the two most widely accepted to date are a two-step pathway (Kozlowski *et al.,* 2016) and a three-step pathway that is similarly to that of AOB (Lehtovirta-Morley, 2018). In the two-step model, a novel copper-based HAO (Cu-HAO) accepts both hydroxylamine and NO as co-reactants, resulting in a five-electron oxidation and the production of two molecules of NO_2^-. One NO_2^- is then reduced to NO, possibly by NirK, which is required for the previous reaction (Fig. 5.2a). In the three-step pathway, hydroxylamine is oxidised to NO and subsequently to NO_2^-, as suggested for AOB. However, in this model, the rate of hydroxylamine oxidation exceeds that of NO oxidation, and the presence of free NO is required to induce NO oxidising activity

(Fig. 5.2b). Both the two-step and three-step models are consistent with the sensitivity of AOA to NO-scavengers.

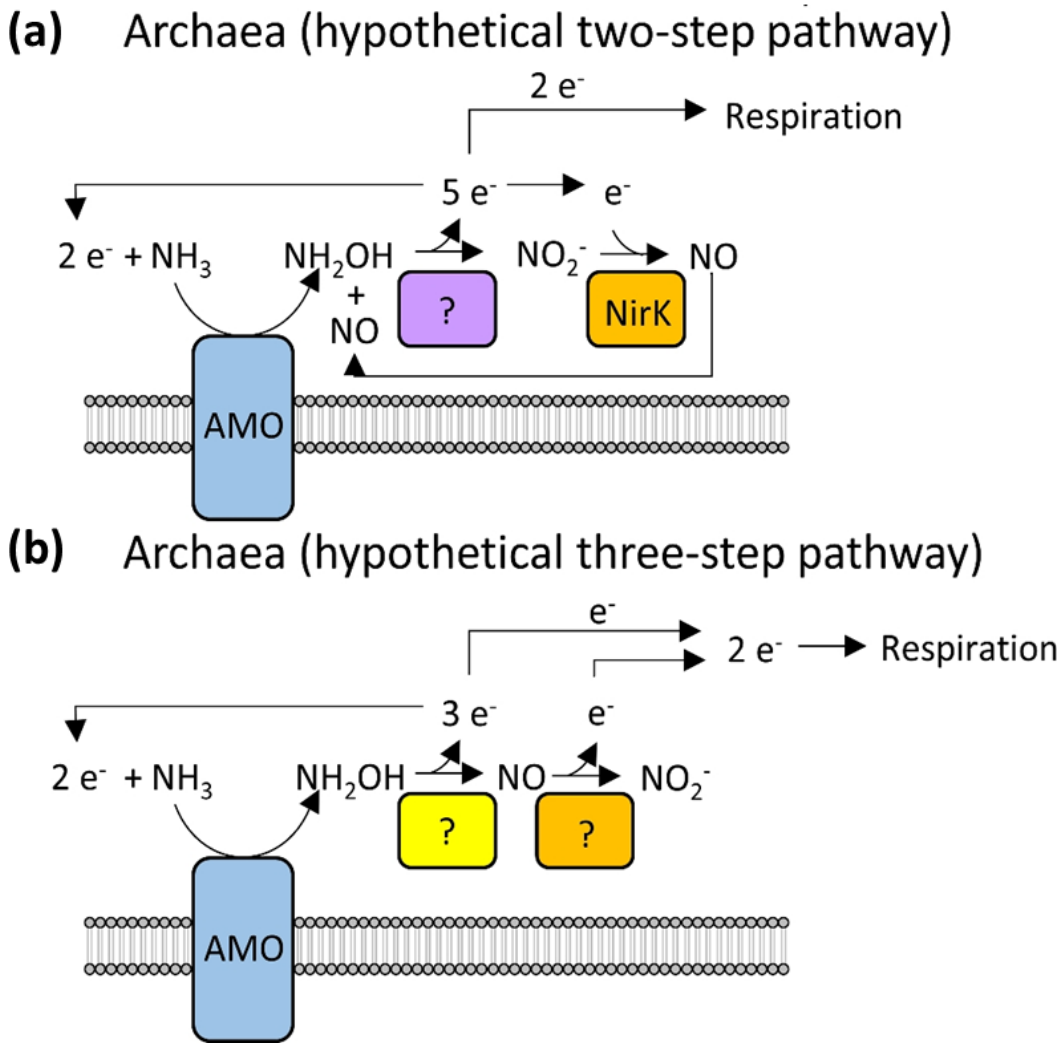

FIG 5.2 The hypothesised archaeal NH_3 oxidation pathways. **(a)** the two-step model proposed by Kozlowski *et al.,* (2016) and **(b)** the three-step model proposed by Lehtovirta-Morley (2018). Figures from Lehtovirta-Morley (2018).

The first aims of this study were to investigate if (1) hydrazine was a substrate for "*Ca.* Nitrosocosmicus franklandus" and (2) if hydrazine could be used as the sole source of external reducing power for AMO, enabling methanol oxidation in the absence of NH_3. The results from these experiments prompted further investigations into the role of NO in the archaeal NH_3 oxidation pathway. This was carried out by

comparing the effect of the NO-scavenger PTIO on NH_3 and hydroxylamine oxidation by "*Ca.* Nitrosocosmicus franklandus" and *N. europaea* by following O_2 uptake. This project was a collaboration between myself and Arne Schatteman.

5.2 Hydrazine oxidation by "*Ca.* Nitrosocosmicus franklandus"

Hydrazine oxidation by "*Ca.* Nitrosocosmicus franklandus" was first confirmed using O_2 uptake assays with hydrazine as the sole substrate. Initial hydrazine concentrations ranged from 0.2 to 1.0 mM and the rate of hydrazine dependent O_2 uptake appeared to increase until saturated at 0.6 mM, with a maximum initial rate of 4.7 μmol O_2 mg $prot^{-1}$ h^{-1} (calculated from first 100 sec following hydrazine addition, Fig. 5.3a). Abiotic hydrazine induced-O_2 consumption was negligible (Schatteman, unpublished). For *N. europaea*, 0.6 mM hydrazine was also found to be saturating (Hyman and Wood, 1984) and the O_2 uptake rate calculated from this experiment was considerably higher than for "*Ca.* Nitrosocosmicus franklandus" at 14.33 μmol O_2 mg $prot^{-1}$ h^{-1} (Fig. 5.3b). Noticeably, the rate of hydrazine dependent O_2 uptake by "*Ca.* Nitrosocosmicus franklandus" was not linear, as it was for *N.* europaea, suggesting something was limiting. Both hydrazine and hydroxylamine dependent O_2 uptake by "*Ca.* Nitrosocosmicus franklandus" ceased after approximately 30 and 50 μM (90 and 150 nmoles) O_2 was consumed respectively (Fig. 5.3a). In contrast, hydrazine and hydroxylamine oxidation by *N. europaea* continued until the O_2 was depleted (Fig. 5.3b).

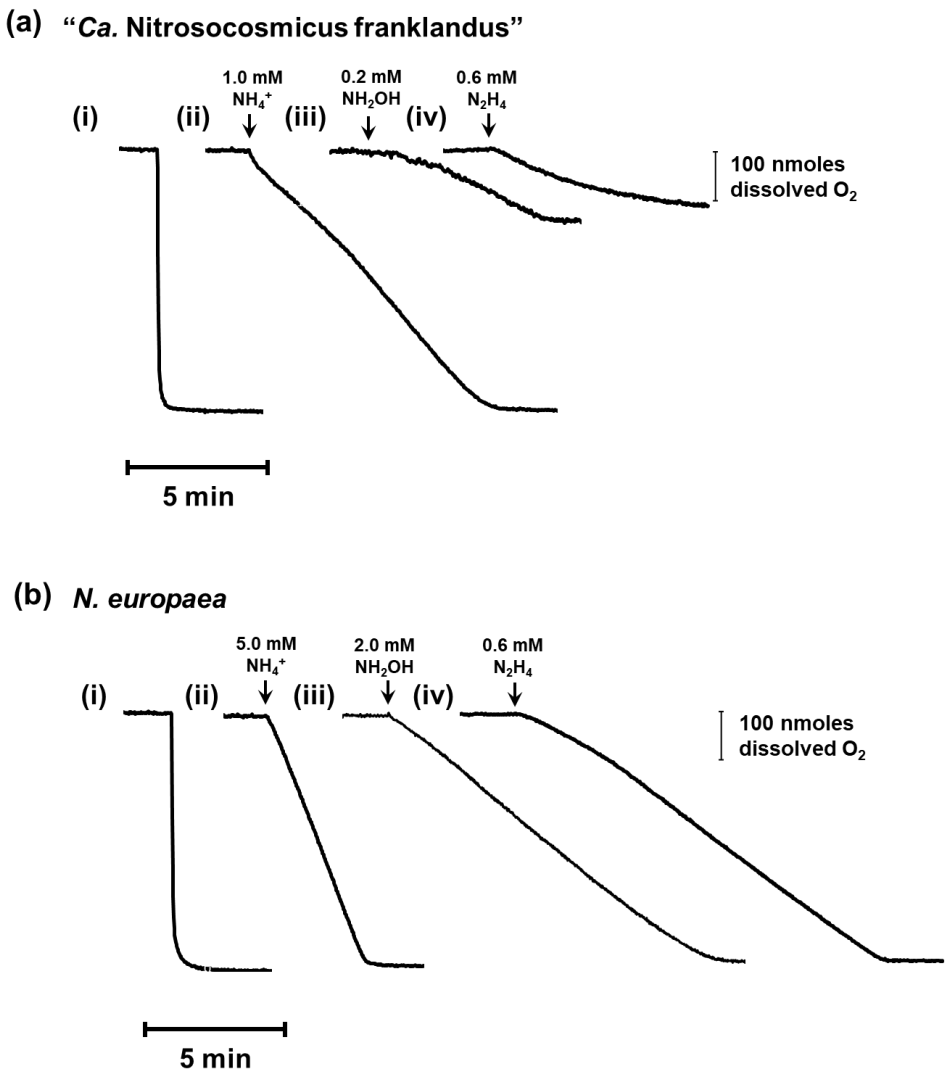

FIG 5.3 Substrate induced O_2 uptake by **(a)** "*Ca.* Nitrosocosmicus franklandus" and **(b)** *N. europaea* measured on a Clark type O_2 electrode according to the method described in Chapter 2, Section 2.7. Trace **(i)** shows the time course for the chemical reduction of O_2 by sodium dithionite. Traces **(ii)**, **(iii)** and **(iv)** show the time course for O_2 uptake following the addition of NH_4^+, hydroxylamine (NH_2OH) and hydrazine (N_2H_4) respectively.

Further work by Arne Schatteman established that the addition of hydrazine to "*Ca.* Nitrosocosmicus franklandus" generated ATP, making hydrazine one of the few compounds metabolised by AOA to yield energy (Schatteman *et al.*, in review).

5.3 Hydrazine as an external source of reductant for methanol oxidation by "*Ca.* Nitrosocosmicus franklandus" and *N. europaea*

Experiments detailed in Chapter 4 established that both methane and methanol are alternative substrates oxidised by the AMO from "*Ca.* Nitrosocosmicus franklandus". These oxidations required the co-oxidation of NH_3 to generate reducing equivalents for AMO activity. The following experiments explored substrate-dependent O_2 uptake by "*Ca.* Nitrosocosmicus franklandus" in the absence of NH_3, with hydrazine supplied as an external source of reductant. A key aim was to calculate kinetic parameters ($K_{m(app)}$ and $V_{max(app)}$) for alternative substrate oxidations by AMO. Methane oxidation was originally tested but its low solubility caused the displacement of O_2 when added to the O_2 electrode chamber. Methanol, on the other hand is much more soluble and hydrazine has been shown to provide the reducing power for methanol oxidation by *N. europaea* in the absence of NH_3 (Voysey and Wood, 1987). Experiments were therefore carried out with methanol as the substrate and repeated with *N. europaea* cells as a control for the experimental set-up. "*Ca.* Nitrosocosmicus franklandus" cells were supplemented with 1 mM methanol, based on methanol inhibition experiments carried out by Barbora Oudova (manuscript in prep.). *N. europaea* were given 10 mM methanol to be comparable with the results of Voysey and Wood (1987). Both "*Ca.* Nitrosocosmicus franklandus" and *N. europaea* were given a final concentration of 0.6 mM hydrazine (Refer to Section 5.2).

Table 5.1 The rate of O_2 uptake by "*Ca.* Nitrosocosmicus franklandus" following the addition of NH_4^+, methanol, hydrazine and hydroxylamine

Substrate additions	Rate of O_2 uptake (μmol O_2 mg $prot^{-1}$ h^{-1})
1 mM NH_4Cl	7.9
1 mM CH_3OH	0.4
0.2 mM NH_2OH	2.6
1 mM CH_3OH + 0.2 mM NH_2OH	2.3
0.6 mM N_2H_4	4.7
1 mM CH_3OH + 0.6 mM N_2H_4	4.7

Table 5.1 lists the substrate additions/combinations and the corresponding O_2 uptake rates by "*Ca.* Nitrosocosmicus franklandus". The NH_4^+-dependent O_2 uptake rate was typical for this strain. There was a very slow, almost negligible, rate in O_2 uptake when "*Ca.* Nitrosocosmicus franklandus" was spiked with 1 mM methanol, which was anticipated in the absence of reductant. The addition of hydrazine to cells spiked with methanol did not promote an increase in O_2 uptake rate above the rate of hydrazine alone. Curiously, neither did hydroxylamine, a presumed source of reducing power for the archaeal AMO. Furthermore, the rate of hydrazine induced O_2 uptake was nearly two-fold faster than hydroxylamine, although it should be noted this was initial (100 s after substrate addition) and the rate of hydrazine oxidation decreased faster than hydroxylamine oxidation.

Table 5.2 The rate of O_2 uptake by *N. europaea* following the addition of NH_4^+, methanol and hydrazine

	Rate of O_2 uptake (μmol O_2 mg $prot^{-1}$ h^{-1})	
Substrate additions	**No acetylene**	**With acetylene***
5 mM NH_4Cl	43.5	0.4
10 mM CH_3OH	0.6	0.6
0.6 mM N_2H_4	13.5	14.9
10 mM CH_3OH + 0.6 mM N_2H_4	20.6	13.9

***Cells were pre-incubated with 20 μM acetylene

In contrast, the addition of hydrazine to *N. europaea* cells with methanol increased the rate of O_2 uptake by *N. europaea* cells by 7.1 μmol O_2 mg $prot^{-1}$ h^{-1} compared to hydrazine alone. Neatly, preincubating *N. europaea* cells spiked with methanol and hydrazine with 20 μM acetylene for 1 h led to no significant increase in O_2 uptake above that of hydrazine alone, confirming the AMO was responsible for methanol oxidation. The results agree with that of Voysey and Wood (1987) with the exception that in this experiment, there was no methanol oxidation in the absence of hydrazine. This was likely because of differences in the cell preparation. Voysey and Wood (1987) washed and concentrated *N. europaea* cells before immediately putting on ice. In our experimental set-up, cells were harvested, washed and rested for 1 h at 30°C to ensure all residual NH_3 was oxidised, however any internal reserves of reductant could have been depleted during this time.

5.4 The inhibition of NH_3 and hydroxylamine oxidation by PTIO

Recent studies have shown that the energy metabolism of AOA requires free NO, however, the exact function of NO has yet to be explained. The following O_2 uptake assays were designed to assess and compare the effect of the NO-scavenger PTIO on both NH_3 and hydroxylamine oxidation by "*Ca.* Nitrosocosmicus franklandus" and *N. europaea* to further understand the role of NO in the archaeal NH_3 oxidation pathway. A final concentration of 0.2 mM PTIO was added to cells to be consistent with previous studies investigating the inhibition of NH_3 oxidation by PTIO (Martens-Habbena *et al.*, 2015; Kozlowski *et al.*, 2016).

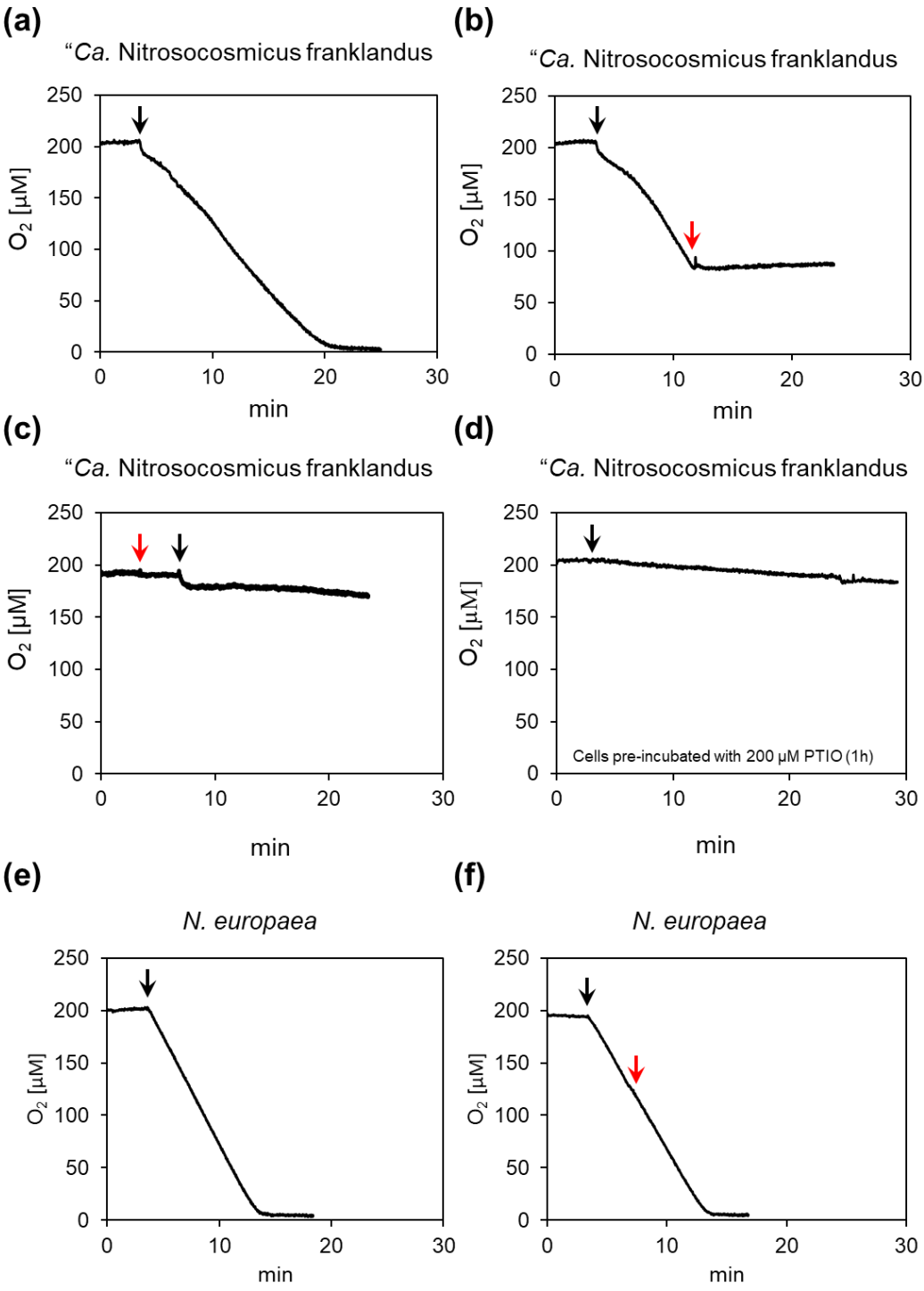

FIG 5.4 NH_4^+ induced O_2 uptake by "*Ca.* Nitrosocosmicus franklandus" **(a-d)** and *N. europaea* **(e, f)**. Black arrows indicate the addition of NH_4^+ at 1 and 5 mM for "*Ca.* Nitrosocosmicus franklandus" and *N. europaea,* respectively. Red arrows indicate the addition of 0.2 mM PTIO. Cell concentration were approximately 6×10^8 and 3×10^8 cells mL^{-1} for "*Ca.* Nitrosocosmicus franklandus" and *N. europaea,* respectively.

Figure 5.4 shows the effect of PTIO on NH_4^+-dependent O_2 uptake by "*Ca.* Nitrosocosmicus franklandus" and *N. europaea*. Panels (a) and (e) are the O_2 uptake traces in the absence of PTIO for "*Ca.* Nitrosocosmicus franklandus" and *N. europaea* respectively. The initial rapid uptake of O_2 by "*Ca.* Nitrosocosmicus franklandus" following the addition of 1 mM NH_4^+ is typical for this strain (Fig. 5.4a). O_2 consumption by "*Ca.* Nitrosocosmicus franklandus" ceased immediately after cells were spiked with 0.2 mM PTIO (Fig. 5.4b). Subsequent experiments investigated the effect of adding PTIO before NH_4^+ as well as preincubating cells with PTIO (Fig. 5.4c and d). Interestingly, when cells were given NH_4^+ after PTIO there was an initial spike in O_2 consumption before it ceased for approximately 5 min, followed by a lower rate (1.13 μM min^{-1}, Fig. 5.4c). The initial rapid rate was potentially caused by the same phenomenon that occurs after the addition of NH_4^+ in the absence of PTIO (Fig. 5.4a and b). This did not occur when cells were preincubated with PTIO but there was a very similar rate in O_2 uptake (1.14 μM min^{-1}, Fig. 5.5d). With *N. europaea*, the NH_4^+-induced O_2 uptake rate increased slightly from 6.26 to 7.83 μM min^{-1} following the addition of PTIO (Fig. 5.4f).

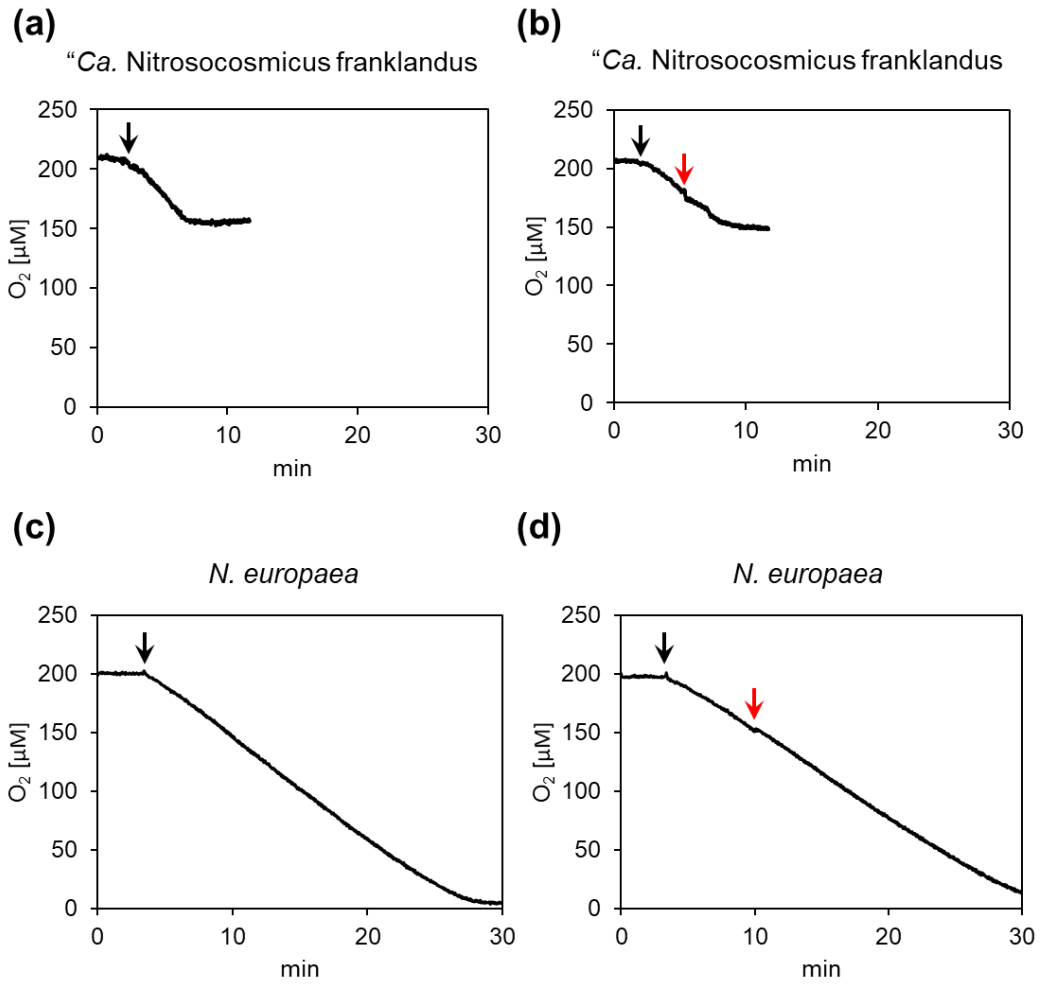

FIG 5.5 Hydroxylamine dependent O_2 uptake by "*Ca.* Nitrosocosmicus franklandus" **(a, b)** and *N. europaea* **(c, d)**. Black arrows indicate the addition of hydroxylamine at 0.2 and 2 mM for "*Ca.* Nitrosocosmicus franklandus" and *N. europaea,* respectively. Red arrows indicate the addition of 0.2 mM PTIO. Cell concentration were approximately 6×10^8 and 3×10^8 cells mL^{-1} for "*Ca.* Nitrosocosmicus franklandus" and *N. europaea*.

Next, the effect of PTIO on hydroxylamine-induced O_2 uptake by "*Ca.* Nitrosocosmicus franklandus" and *N. europaea* was tested (Fig. 5.5). As described in Section 5.2, hydroxylamine oxidation by "*Ca*. Nitrosocosmicus franklandus" ceased after approximately 50 µM O_2 had been consumed (Fig. 5.5a). When "*Ca.* Nitrosocosmicus franklandus" cells were given PTIO the O_2 uptake trace was perturbed, but unlike for NH_4^+-dependent O_2 uptake, hydroxylamine-dependent O_2

uptake did continue until ~50 μM O_2 was consumed (Fig. 5.5b). PTIO had no effect on the rate of hydroxylamine induced O_2 uptake by *N. europaea* (Fig. 5.5d).

5.5 The effect of NO additions on O_2 uptake by "*Ca.* Nitrosocosmicus franklandus"

NO appears to be important for the function of AMO from "*Ca.* Nitrosocosmicus franklandus", possibly as a source of reductant, or perhaps by interacting with the enzyme itself. Therefore, NO could be the missing ingredient for alternative substrate oxidations by "*Ca.* Nitrosocosmicus franklandus" in the absence of ammonia and it is interesting to consider if the addition of an NO-donor would stimulate methanol oxidation, for example. Whilst the addition of alternative substrates was not tested in this study, the addition of an NO-donor on O_2 uptake by "*Ca.* Nitrosocosmicus franklandus" was investigated. The data presented below are preliminary and was only attempted once, however this pilot experiment offered the opportunity to further investigate the function of NO in the archaeal NH_3 oxidation pathway.

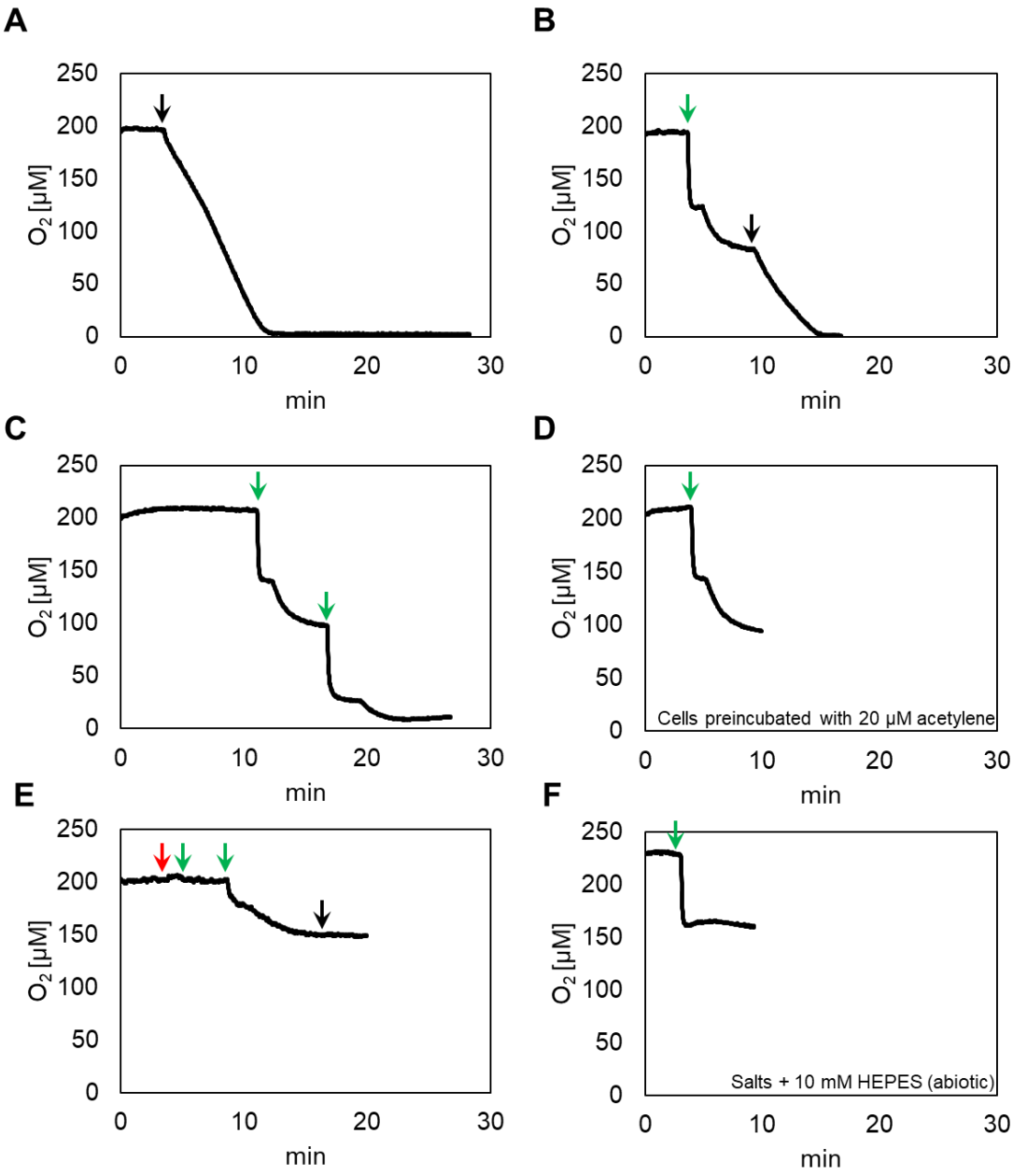

FIG 5.6 The effect of PROLI-NONOate on O_2 uptake by "*Ca.* Nitrosocosmicus franklandus". NH_4^+ (Black arrows) and PROLI-NONOate (green arrows) were added to cells at a final concentration of 1 mM unless stated. PTIO (red arrows) was added at 0.2 mM. The cell concentration was 8×10^8 cells ml^{-1}. Panel **A** shows NH_4^+ induced O_2 uptake. Panel **B** shows the O_2 trace after the addition of PROLI-NONOate followed by NH_4^+. In Panel **C**, cells were spiked twice with PROLI-NONOate. In panel **D**, the effect of PROLI-NONOate was tested on cells that were pre-incubated with 20 µM acetylene to inhibit AMO activity. In panel **E**, PTIO was added and immediately followed by 0.2 mM PROLI-NONOate, then an additional 1 mM PROLI-NONOate and then NH_4^+. Panel **F** shows O_2 uptake by PROLI-NONOate in cell-free medium.

PROLI-NONOate spontaneously dissociates at neutral pH to form 1 mol proline and 2 mol NO, with a $t_{1/2}$ of 1.8 sec at 37°C. Initially, cells were spiked with 10 μM PROLI-NONOate, which resulted in a very short but rapid drop in O_2, followed by a very slow rate in O_2 uptake (0.84 μM min^{-1}) (data not shown). Subsequently, 1 mM PROLI-NONOate was added which resulted in a greater, rapid drop in O_2 (~60 μM) followed by a second rate with an initial uptake rate of ~25 μM min^{-1} (Fig. 5.6 B-D). This rapid drop in O_2 was determined to be abiotic (Fig. 5.5 F) and was almost certainly caused by NO reacting with O_2 and forming nitrogen dioxide (NO_2), which can then react with water to form nitric acid (HNO_3). Fig. 5.6 B shows the O_2 uptake after the addition of 1 mM PROLI-NONOate, followed by 1 mM NH_4^+. NH_4^+-dependent O_2 uptake proceeded at a similar rate to that in the absence of PROLI-NONOate (Fig. 5.6 A), demonstrating the N-species released by NO reactions (the majority likely being HNO_3) had no adverse effect on AMO function. Additionally, cells could be spiked with NO until all the O_2 was depleted (Fig. 5.6 C). The effect of PROLI-NONOate on O_2 uptake was similar when cells were preincubated with 20 μM acetylene, suggesting that O_2 consumption was not due to AMO activity (Fig. 5.6 D) and therefore was mostly likely due to the activity of another enzyme/mechanism in the ammonia oxidation pathway. It is recognised that NH_4^+ should have been added after PROLI-NONOate-induced O_2 uptake had ceased to demonstrate the AMO was fully inhibited by acetylene (Fig. 5.6 D). Finally, there was no O_2 uptake when cells were spiked with 0.2 mM PTIO before 0.2 mM PROLI-NONOate, confirming that PTIO is an effective scavenger of NO (Fig. 5.6 E). A further addition of 1 mM PROLI-NONOate restored O_2 uptake, however the addition of NH_4^+ resulted in no rate, which could suggest that PTIO directly inhibits AMO. However, it was noted that the colour of the cell suspension turned dark yellow/brown following the addition of NH_4^+, which

was possibly caused by a reaction with HNO_3 and potentially rendering the enzymes inactive.

5.6 Discussion

A key discovery from this study was that hydrazine is a substrate for "*Ca.* Nitrosocosmicus franklandus", with O_2 consumption coupled with ATP production. In addition to NH_3, this adds hydrazine to a short list of substrates that can be used by AOA for energy transduction and includes hydroxylamine, urea and cyanate; with the latter two being first converted to NH_3 (Lu *et al.*, 2012; Palatinszky *et al.*, 2015; Schatteman *et al.*, in review). Further work by Schatteman *et al.*, (in review) demonstrated that N_2 was a product of hydrazine oxidation by "*Ca*. Nitrosocosmicus franklandus". The oxidation of hydrazine to N_2 is known to be catalysed by HAO enzymes (Logan and Hooper, 1996; Schalk *et al.*, 1998). Therefore, it is conceivable that the archaeal machinery responsible for hydroxylamine oxidation is also capable of oxidising hydrazine, especially in light of recent experiments by Schatteman *et al.*, (in review) exploring hydrazines as inhibitors of the archaeal NH_3 oxidation pathway. Unlike *N. europaea*, hydrazine oxidation by "*Ca.* Nitrosocosmicus franklandus" was not linear and decreased over time, suggesting that something became limiting or there was product inhibition (Fig. 5.3a). Furthermore, when Schatteman *et al.*, (in review) spiked "*Ca.* Nitrosocosmicus franklandus" cells with additional hydrazine no further O_2 uptake was induced. This contrasts with hydroxylamine oxidation, where 0.2 mM hydroxylamine could be continuously added until all the O_2 was depleted. Considering the two-step model for archaeal NH_3 oxidation, where hydroxylamine and NO are co-reactants for a putative Cu-HAO (Fig 5.3a, Kozlowski *et al.*, 2016), NO could be the limiting factor during hydrazine oxidation (Schatteman *et al.*, in review).

It was demonstrated in Chapter 4 that methanol was a substrate for the AMO from "*Ca.* Nitrosocosmicus franklandus", however this required the co-oxidation of NH_3. Therefore, it was tested if hydrazine could act as an external source of reductant for methanol oxidation. This was ineffective (Table 5.1), plausibly because the generation of NO is necessary for AOA energy metabolism, either as a co-reactant or potentially as a source of reducing power itself (Fig. 5.2 A and B). The addition of hydroxylamine did not promote methanol oxidation either, which was puzzling since hydroxylamine oxidation should produce NO, either directly or from the reduction of NO_2^- depending on the model. In comparison, O_2 uptake by *N. europaea* increased considerably when cells were given methanol and hydrazine (Table 5.2), replicating the results of Voysey and Wood (1987). This did not occur when cells were preincubated with acetylene and the rate of O_2 uptake was comparable to hydrazine alone (Table 5.2), explicitly demonstrating that the AMO from *N. europaea* was responsible for methanol oxidation. The results agree with the modelled pathway for NH_3 oxidation by *N. europaea* (Fig. 5.1A, Eq. 1 and 2), where electrons derived from HAO oxidations are transferred to AMO via the quinone pool to sustain activity without the participation of NO.

Due to its reactivity, NO normally exists in very low concentrations within cells, however, NO is both produced and consumed in measurable nanomolar quantities by AOA and evidence from this work as well as previous studies has suggested that free-NO is essential for archaeal ammonia oxidation (Martens-Habbena *et al.*, 2015; Sauder *et al.*, 2016; Kozlowski *et al.*, 2016). This was explored further by investigating the effect of PTIO on both NH_3 and hydroxylamine dependent O_2 consumption by "*Ca.* Nitrosocosmicus franklandus". Experiments were repeated with *N. europaea* for comparison and to make correlations with the proposed NH_3 oxidation

pathways (Fig. 5.1 and 5.2). It should be highlighted that most of the previous studies investigating the inhibitory effect of PTIO have focussed on growth of AOA and AOB, and comparably little has been done exploring the inhibition of ammonia oxidising activity by PTIO, apart from the study by Kozlowski *et al.*, (2016) with *N. viennensis*. PTIO did not perturb either NH_3- or hydroxylamine-dependent O_2 uptake by *N. europaea*, which was anticipated since NO production and consumption was proposed to be tightly coupled in *N. europaea* (Fig. 5.1, Caranto and Lancaster, 2017; Lancaster *et al.*, 2018). However, PTIO has been shown to have a less inhibitory effect on AOB compared to AOA (Shen *et al.*, 2013; Martens-Habbena *et al.*, 2015; Sauder *et al.*, 2016), and there is the possibility that the concentration used here was simply not high enough to have any pronounced effect on ammonia or hydroxylamine oxidising activity by *N. europaea*.

PTIO had an unequivocal impact on NH_3 oxidation by "*Ca.* Nitrosocosmicus franklandus", but not so much on hydroxylamine oxidation, which presents drawbacks with both archaeal NH_3 oxidation models that are highlighted in this study. Considering the two-step pathway (Fig. 5.2 A), the addition of PTIO should completely stop both NH_3 and hydroxylamine oxidation since NO is a co-substrate for the unknown hydroxylamine oxidising enzyme/complex, and therefore required for the only step of the pathway generating reducing equivalents. If AOA carry out NH_3 oxidation via the three-step model (Fig. 5.2 B), like *N. europaea*, NH_3 and hydroxylamine oxidation by "*Ca.* Nitrosocosmicus franklandus" should not be inhibited by PTIO. However, the scavenging of free NO would prevent NO_2^- production.

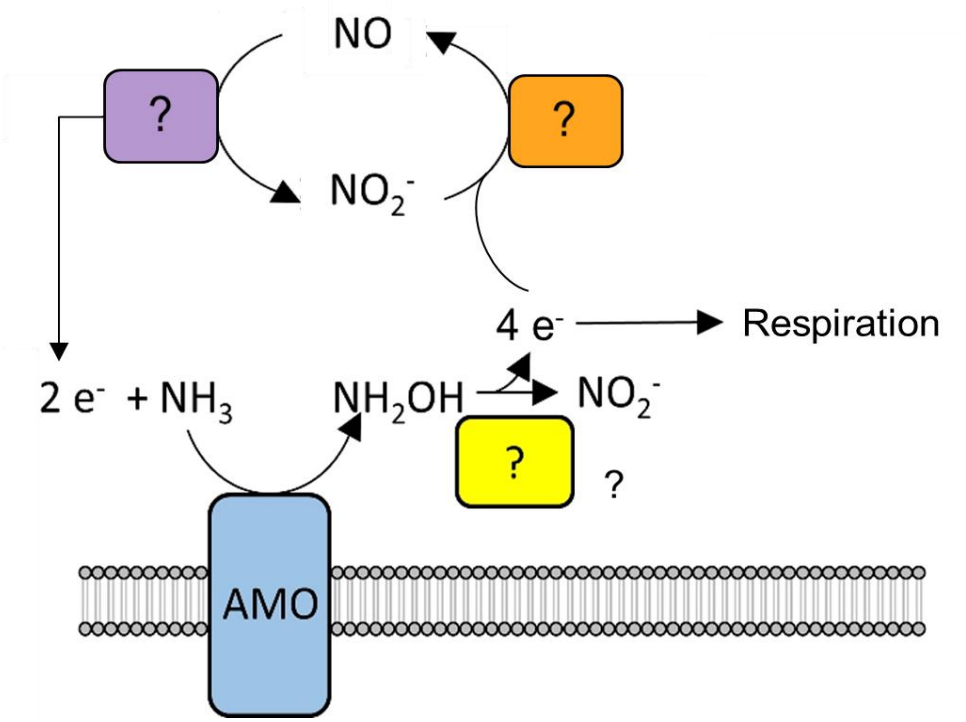

FIG 5.7 Archaeal NH_3 oxidation pathway proposed by Stahl and de la Torre (2012) with NO acting as a redox shuttle.

Whilst considering the role of NO in the archaeal NH_3 oxidation pathway, it is interesting to revisit an earlier model proposed by Stahl and de la Torre (2012) where NO functions as a redox shuttle (Fig. 5.7, Eq. 5 and 6). NO_2^- is reduced by a putative copper-containing NirK, producing NO which is subsequently re-oxidised to NO_2^-, possibly by a putative purple cupredoxin, transferring electrons to the AMO (Hosseinzadeh *et al.*, 2016).

$$2NO_2^- + 2e^- + 4H^+ \rightarrow 2NO + 2H_2O \quad (5)$$

$$2NO + O_2 + NH_3 + H_2O \rightarrow NH_2OH + 2NO_2^- + 2H^+ \quad (6)$$

The addition of PTIO in this instance would stop NH_3 oxidation by preventing the supply of electrons however hydroxylamine oxidation should unaffected. It is difficult say this was the case for hydroxylamine oxidation by "*Ca.* Nitrosocosmicus franklandus" since the O_2 uptake trace is very short, but it was perturbed (Fig. 5.5 B).

If hydroxylamine oxidation is affected by PTIO, but not inhibited completely, it could suggest that the enzyme responsible does require NO to participate but not as a co-reactant, as suggested for the two-step pathway (Fig. 5.2 A).

Curiously, whilst PTIO inhibited the growth of *N. viennensis*, Kozlowski *et al.,* (2016) found that it did not have an inhibitory effect NH_4^+ oxidising activity, as it does with "*Ca.* Nitrosocosmicus franklandus" (Fig. 5.4). It was postulated that PTIO was unable to chelate rapidly cycling NO by *N. viennensis* at the high cell densities used in their experiments (how many cells). Additionally, Kozlowski *et al.,* (2016) found the initial rapid uptake in O_2 by *N. viennensis* following the addition of NH_4^+, corresponded with a spike in NO production. "*Ca.* Nitrosocosmicus franklandus" also demonstrates a very similar O_2 uptake trace following the addition of NH_4^+, and it would be interesting to ascertain if this was coupled to NO production (E.g., Fig. 5.3 A). In contrast, *N. maritimus* did not demonstrate the same O_2 profiles as *N. viennensis* and "*Ca.* Nitrosocosmicus franklandus" and NO accumulation occurred at a steady state (Martens-Habbena *et al.,* 2015). Notably, with "*Ca.* Nitrosocosmicus franklandus" the addition of PTIO immediately before NH_4^+ resulted in a spike in O_2 consumption followed by a slow rate of uptake. Conversely, this profile was absent when cells were pre-incubated with PTIO (Fig.5.4 C and D). This could support the notion of Kozlowski *et al.,* (2016) that PTIO scavenging is not as effective at high cell densities and/or requires time to gain access through the cell wall. The specificity of PTIO as an NO scavenger has been previously questioned, and it may react with other nitrogenous compounds (Pfeiffer *et al.,* 1997).

AOA are much more sensitive to externally added hydroxylamine compared to AOB. For example, the rate of hydroxylamine oxidation by "*Ca.* Nitrosocosmicus franklandus" begins to decrease at concentrations >0.2 mM and the addition of 1 mM

hydroxylamine to *N. maritimus* cultures completely inhibited activity (Vajrala *et al.,* 2013). AOB, on the other hand, tolerate considerably higher concentrations of hydroxylamine (Soler-Jofra *et al.,* 2020). As well as concentration thresholds, hydroxylamine-dependent O_2 uptake also proceeds very differently between AOA and AOB. In the presence of 2 mM, *N. europaea* oxidise hydroxylamine until O_2 was depleted from the electrode chamber (E.g., Fig. 5.3 B). AOA only oxidise approximately 50 μM, given a ratio of 1:1 for hydroxylamine and O_2, after which activity stops (Fig. 5.3 A, Vajrala *et al.,* 2013; Martens-Habbena *et al,* 2015; Kozlowski *et al.,* 2016). When "*Ca.* Nitrosocosmicus franklandus" was spiked with additional hydroxylamine after O_2 consumption had ceased, the activity was restored (Schatteman *et al.,* in review). This could suggest that externally added hydroxylamine reacts abiotically, most likely with NO_2^-, based on experimental evidence by Steiglmeier *et al.,* (2014), to produce N_2O. Hydroxylamine oxidation by "*Ca.* Nitrosocosmicus franklandus" is also unusual compared to *N. viennensis* and *N. maritimus* because it is not stoichiometric with NO_2^- production (Chapter 3, Fig. 3.6, Chapter 4, Fig. 4.3). In fact, O_2 consumption is consistently 2-fold higher than NO_2^- production. It has been shown that under acidic conditions *Nitrosocosmicus oleophilus* might be able to enzymatically denitrify nitrite to N_2O using a putative cytochrome P450 NO reductase (Jung *et al.,* 2019). "*Ca.* Nitrosocosmicus franklandus" also encodes a putative cytochrome P450 and perhaps this process would mop-up excess electrons generated by hydroxylamine oxidation since the AMO would be inactive. Although, the conditions in these experiments were not acidic and further experimentation would be required to explore the possibility of denitrifying activity by "*Ca.* Nitrosocosmicus franklandus".

The final experiment described in this chapter explored the addition of an NO-donor directly to "*Ca.* Nitrosocosmicus franklandus" cells. To knowledge, this has not been performed before for any whole cell AOA or AOB culture and the results, although very preliminary, were intriguing. The NO-donor PROLI-NONOate was added to cells at a very high concentration (1 mM), and some of the dissociated NO reacted with O_2 to form approximately 120 µM NO_2. The NO_2 could react with H_2O to form HNO_3. After the initial abiotic drop in O_2 in the electrode chamber, there was a second biological rate of O_2 consumption (Fig 5.6). It is remarkable that at this concentration and given the reactivity of NO, there was activity at all. Perhaps the cells were not viable anymore, but the enzyme(s) responsible for the O_2 uptake are still functional. The addition of PROLI-NONOate also did not appear to have an inhibitory effect on the AMO as NH_4^{+-} dependent O_2 uptake proceeded at a similar rate to the control and PROLI-NONOate-dependent O_2 uptake after cells were preincubated with acetylene also confirmed the AMO was not responsible for this activity (Fig. 5.6c). It should be noted that spiking the cells with NH_4^+ following the addition of PROLI-NONOate and PTIO resulted in no further O_2 uptake, which potentially indicates PTIO directly inhibits AMO. This requires further investigation and other NO-scavengers such as caffeic acid, curcumin, methylene blue hydrate and Trolox (Sauder *et al.*, 2016) could also be considered/tested as alternatives in future experiments.

It is perplexing that with the same overall stoichiometry (Eq. 4), there are many dissimilarities in the biochemistry of ammonia oxidation of AOA and AOB, in particular the role of NO. NO is biologically a very reactive and highly toxic molecule but is also used as a signalling molecule and is an intermediate in the microbial nitrogen cycle (Hu *et al.*, 2019). There is now substantial evidence that free-NO (i.e., able to be scavenged) is essential for AOA energy metabolism, but not necessarily for

AOB. This work has provided insights regarding the hypothesised ammonia oxidation pathways and has provided a case for re-evaluating the possibility that NO could function as an electron shuttle. If NO does function to provide reductant to the archaeal AMO, it is interesting to consider the evolution of this, particularly considering that both the bacterial AMO and pMMO draw electrons from the quinone pool (Shiemke *et al.*, 2004). This is further discussed in Chapter 6. In addition, the results presented here highlight the need to explore the biochemistry of ammonia oxidation in multiple strains. This is exemplified by the differences between PTIO inhibition of ammonia oxidation by "*Ca.* Nitrosocosmicus franklandus" and *N. viennensis*, which phylogenetically are quite closely related, but not identical in terms of physiology. Whether archaeal ammonia oxidation proceeds as a two- or three-step pathway and the specific role of NO will require further experimentation.

6. Summary and prospects

6.1 The physiology and biochemistry of AOA

Since ammonia oxidation by mesophilic archaea was first confirmed 16 years ago with the isolation and characterisation of the marine strain *Nitrosopumilus maritimus* SCM1 (Könneke *et al.,* 2005), an abundance of research papers has been published on the ecology of archaeal and bacterial ammonia oxidisers, specifically the environmental niches they inhabit (Merbt *et al.,* 2012; Thion & Prosser, 2014; Qin *et al.,* 2016; Palomo *et al.,*2018; Zhou *et al.,* 2020; Séneca *et al.,* 2020). Understanding the drivers of ammonia oxidising activity in the environment is of paramount importance since it could help mitigate the negative impacts associated with nitrification such as the release of N_2O and nitrate into the atmosphere and groundwater, respectively (Prosser *et al.,* 2020). Being chemolithotrophs, ammonia oxidisers also have a prominent role in carbon fixation too, particularly AOA which make up a large proportion of microbial biomass on Earth (Karner *et al.,* 2001; Leininger *et al.,* 2006; Pitcher *et al.,* 2011; Offre *et al.,* 2013). Chapter 1 reviews the physiology of AOA and how it can underpin their overall ecology. This is an ever-unfolding field of research as more ammonia oxidisers are isolated or highly enriched in culture. For example, the first molecular ecology surveys and the extremely high substrate affinity of *N. maritimus* (Martens-Habbena *et al.,* 2009) as well as the isolation of acidophilic AOA (Lehtovirta-Morley *et al.,* 2011) originally suggested that AOA dominated ammonia oxidation activity in oligotrophic environments, whilst AOB, with comparably lower substrate affinity were prolific in eutrophic habitats. However, this was recently challenged with the isolation of members of the *Nitrosocosmicus* genus, which tolerate high ammonium concentrations and have growth characteristics similar to that of AOB (Lehtovirta-Morley *et al.,* 2016b; Jung

et al., 2016; Sauder *et al.,* 2017; Alves *et al.,* 2019). Comammox bacteria often thrive in oligotrophic environments and isolates have been shown to have a very high affinity for ammonia (Kits *et al.,* 2017; Jung *et al.,* 2021). Most recently, oligotrophic and acidophilic AOB have also been isolated or highly enriched which demonstrate very low apparent K_m's for NH_3 (Sedlacek *et al.,* 2019; Picone *et al.,* 2021). A new study by Jung and colleagues (2021) compared the ammonia oxidation kinetic properties of multiple AOA, AOB and comammox strains and demonstrated that their apparent affinity for NH_3 is closely linked to the environmental niche these strains occupy. Knowledge of the physiological competitiveness of AOM for NH_3 in combination with their preferred abiotic conditions (pH, salinity, temperature) will enable better modelling of nitrifying activities in the environment.

Currently, the most prevalent archaeal ammonia oxidisers in the environment are not yet available in culture (Alves *et al.,* 2018). The isolation of ammonia oxidisers is notoriously difficult owing to the risk of them losing the tight partnerships with other microbes that detoxify the inhibitory intermediates and the products of their metabolism, protect from oxidative stress, and participate in reciprocal feeding (Stein, 2019). Additionally, AOA are slow growing, therefore isolation is time-consuming, and they can be easily outcompeted by faster growing AOB. However, studies with isolated or enriched AOA strains have highlighted that even closely related strains often differ in their physiology. For example, the acidophilic AOA "*Ca.* Nitrosotalea devanaterra" and "*Ca.* Nitrosotalea sinensis" respond very differently to the addition of organic acids during growth (Lehtovirta-Morley *et al.,* 2014). Similarly, this study found that "*Ca.* Nitrosocosmicus franklandus" and *Nitrososphaera viennensis* differed in their response to the presence of the NO-scavenger, PTIO, during ammonia oxidation (Chapter 5). This emphasises the importance of conducting culture-

dependent studies with multiple AOA strains, especially when investigating core metabolisms. This could also be said for ammonia oxidisers in general. The accepted ammonia oxidation pathway for AOB has been resolved in *Nitrosomonas europaea.* Aside from the fact that this strain is not particularly prevalent in the environment, it is certainly not going to be the same strain isolated by Winogradsky over 130 years ago (Winogradsky, 1890) because of adaptation to growth under laboratory conditions. Therefore, perhaps the biochemistry of ammonia oxidation by *N. europaea* is not representative of all AOB.

Conversely, the study of multiple ammonia oxidising isolates can also reveal similarities in physiology and biochemistry. This was demonstrated in Chapter 3, where the reduced sensitivity of the archaeal AMO to inhibition by longer-chain-length alkynes seems to be conserved across the representatives of four different AOA lineages; *Nitrososphaera*, *Nitrosopumilus*, *Nitrosotalea* and *Nitrosocosmicus*. This further advocates the use of 1-octyne to differentiate between archaeal and bacteria ammonia oxidising activities in the environment (detailed in Chapter 3).

6.2 Thoughts on the biochemistry of energy metabolism in AOA

Ammonia oxidisers have evolved specialised systems of electron carriers to deliver reductant to the quinone pool in order to generate proton motive force (PMF) and ATP using ammonia as the sole energy source (Stein and Klotz, 2016; Stein, 2019). Additionally, they have unique metabolisms enabling them to deal with the toxic intermediates generated by ammonia oxidation, which include hydroxylamine, NO and nitrite (Stein, 2019). The AMO is the only enzyme known to be shared by all three clades of ammonia oxidisers and the overall ammonia oxidation pathway is thought to differ considerably between archaeal and bacterial ammonia oxidisers

(described in Chapter 5). The ammonia oxidation pathway of AOA is particularly perplexing since the mechanism of hydroxylamine oxidation is unknown. Along with other hydroxylamine oxidising candidate enzymes that are described in Chapter 1, Section 1.7 and in Chapter 5, recently there has been evidence for the activity of a putative Cu-containing NirK in AOA energy metabolism. Cu-NirK is one of the most highly recovered transcripts from AOA (meta)transcriptomes and highly abundant in proteome analyses (Hollibough *et al.,* 2011; Lund *et al.,* 2012; Williams *et al.,* 2012; Santoro *et al.,* 2015; Kerou *et al.,* 2016). Conventionally, NirK catalyses the reduction of nitrite to NO, and therefore it may have a key role in NO production, which we know is an essential metabolite for archaeal ammonia oxidation (refer to Chapter 5). In addition, a putative Cu-NirK from *N. viennensis* heterologously expressed in *Escherichia coli* demonstrated the ability to oxidise hydroxylamine, but with an extremely slow rate of turnover (nearly 1/100 of the rate of NO_2^- reduction, Kobayashi *et al.,* 2018). There is no other evidence in literature to suggest that NirK could oxidise hydroxylamine (Stein, 2019) and the low activity casts doubts on this occurrence, however, the putative archaeal Cu-NirK appears to be unique based on amino acid sequence (Bartossek *et al.,* 2010). NirK typically consists of two copper binding sites connected by a structural motif site which is termed the "trigger loop" (Li *et al.,* 2015; Horrel *et al.,* 2016). The archaeal NirK contains significant variations in this region, including multiple amino acid insertions, suggesting that it may have a completely novel function (Tolar *et al.,* 2017), possibly even bifunctional. Certainly, more needs to be done on the biochemical characterisation of the archaeal Cu-NirK. One caveat is that members of the *Nitrosocaldus* genus and the sponge symbiont *Cenarchaeum symbiosum* do not encode *nirK* (Hallam *et al.,* 2006; de la Torre *et al.,* 2008; Abby *et al.,* 2018; Daebeler *et al.,* 2018).

There were originally two key hypotheses for the archaeal ammonia oxidation pathway. In the two-step model a novel copper containing HAO accepts both hydroxylamine and NO as co-substrates, resulting in a five-electron oxidation to form two molecules of nitrite. Subsequently, the reduction of one NO_2^- to NO, potentially catalysed by NirK, is required for the previous reaction (Kozlowski *et al.,* 2016). One problem with this model is that it does not agree with tracer experiments using ^{18}O labelled water, which show that only one O atom from water is incorporated into NO_2^- (Santoro et al., 2011; Buchwald et al., 2012). Secondly, the scavenging of NO by PTIO should abolish both ammonia and hydroxylamine oxidising activity. However, hydroxylamine oxidation by "*Ca.* Nitrosocosmicus franklandus", albeit perturbed, still continued in the presence of PTIO in experiments described in Chapter 5. Similarly, ammonia and hydroxylamine oxidising activity by "*Ca.* Nitrosocosmicus franklandus" in the presence of PTIO do not agree with the three-step model, since in the scavenging of NO should not have an inhibitory effect on AMO. In fact, the model that best fits with the data presented in Chapter 5 is the pathway suggested by Stahl and de la Torre (2012), where NO functions as a redox shuttle. Further experiments with both "*Ca.* Nitrosocosmicus franklandus" and other AOA representatives should be performed to explore this pathway further. Additional studies could focus on the release of NO by AOA and AOB into the environment. NO, like N_2O, is a climate active gas, however little work has been carried out investigating the contributions of AOA and AOB to NO emissions.

6.3 The structure, function and substrate range of the archaeal AMO

Active AMO is difficult to purify, and its structure and function are largely unexplored in archaea. Chapter 3 provided insights into the structure of the archaeal AMO active site(s) and its potential substrate range by characterising the inhibition of

archaeal AMOs to specific alkyne inhibitors and comparing with other members of the CuMMO family, namely the bacterial AMO and pMMO. "*Ca.* Nitrosocosmicus franklandus" and "*Ca.* Nitrosotalea sinensis" demonstrated a reduced sensitivity to inhibition by larger 1-alkynes compared to *N. europaea.* Additionally, the archaeal 1-alkyne inhibition profiles were similar to that of pMMO expressing *Methylococcus capsulatus.* Together, this suggested that the archaeal AMO has a narrower hydrocarbon substrate range compared to the bacterial AMO, as previously reported for other genera of AOA. Phenylacetylene inhibited the archaeal and bacterial AMO at different threshold concentrations and by different mechanisms of inhibition, highlighting structural differences between the two forms of monooxygenase. However, inhibition kinetics revealed phenylacetylene did not compete with ammonia for the same binding site, indicating the presence of multiple binding sites on both the archaeal and bacterial AMO. Overall, Chapter 3 highlights the use of inhibitors to investigate the biochemistry of enzymes that are not amenable to purification. Future work could investigate the structure of the archaeal AMO binding cavity further by studying the steric effects of different substrates and inhibitors, which would improve predicted structural models.

Chapter 4 explored the inhibition of NH_3 oxidation by "*Ca.* Nitrosocosmicus franklandus" by methane and subsequently by methanol. Both compounds inhibited the AMO from "*Ca.* Nitrosocosmicus franklandus" competitively, which supports the suggestion that small substrates/inhibitors bind at the same site as ammonia. "*Ca.* Nitrosocosmicus franklandus" was found to have a relatively low $K_{i(app)}$ for both methane and methanol, lower than previously estimated for AOB. Additionally, in contrast to AOB, inhibition by methane and methanol adhered to simple Michaelis-Menten kinetics, a novel phenomenon considering the biochemistry of AOA rarely

conforms to a known mechanism, as demonstrated in other chapters. In terms of biogeochemical crossover, methane and methanol will almost certainly affect NH_3 oxidation by AOA in specific environments, particularly those with high concentrations of methane and/or methanol, including wetlands for example. "*Ca.* Nitrosocosmicus franklandus" also demonstrated the ability to metabolise methane and methanol to produce CO_2 and incorporate methane and methanol derived carbon into cellular biomass. Whether this strain oxidises these C_1 compounds to CO_2 prior to assimilation or assimilates carbon during metabolism has yet to be determined. Further work will need to be carried out to elucidate the pathway for C_1 compound metabolism in "*Ca.* Nitrosocosmicus franklandus". Furthermore, an *in-situ* study, such as a stable isotope probing (SIP) experiment (Macey *et al.,* 2020), could be used to assess the contribution of AOA to methane and methanol oxidation.

It is interesting to consider the evolution of aerobic ammonia oxidation and the CuMMO superfamily. CuMMO require molecular O_2, therefore it logical that ammonia oxidation looks to have evolved after the evolution of oxygenic photosynthesis approximately 2.3 billion years ago (Ga) (Ward *et al.,* 2021). AOB originated <1 Ga, with major radiations occurring within the last 500 million years (Ma), suggesting that AOA played the dominant role in ammonia oxidation prior to this (Ward *et al.,* 2021). The pMMO appears to have been acquired by methanotrophs via lateral gene transfer (LGT) from an ancestor of the AOB lineage *Nitrosococcus* (Khadha *et al.,* 2018). Intriguingly, there is isotopic evidence that aerobic ammonia oxidation may have occurred before 2.3 Ga (Garvin *et al.,* 2009). No metabolism has been discovered where ammonia is oxidised in the absence of O_2, using NO as a potential terminal electron acceptor. However, prior to 'The Great Oxygenation Event' NO was the strongest oxidant available on Earth, therefore it is plausible that early

microbes could have used external NO as a terminal electron acceptor (Ward *et al.*, 2021; Hu *et al.*, 2019; Canfield *et al.*, 2010). It is interesting to then consider the supply of electrons required for CuMMO activity in the context of their evolutionary history. The bacterial AMO and pMMO derive electrons from the quinone pool (Shiemke *et al.*, 2004), however, the source of reductant is less well defined for the archaeal AMO. Potentially, the archaeal AMO could accept electrons from NO shuttling, as described by Stahl and de la Torre (2012), which would eliminate the need to draw electrons directly from the quinone pool.

6.4 Final thoughts

This thesis contributes some novel insights into AOA biochemistry energy metabolism and using purely culture-dependent studies. The isolation and characterisation of new archaeal ammonia oxidisers, in terms of their physiology and biochemistry, will further broaden our knowledge about these hugely important microbes that contribute significantly to both the biogeochemical cycling of nitrogen and carbon.

7. References

Abby SS, Melcher M, Kerou M, Krupovic M, Stieglmeier M, Rossel C, Pfeifer K, Schleper C. 2018. *Candidatus* Nitrosocaldus cavascurensis, an ammonia oxidizing, extremely thermophilic archaeon with a highly mobile genome. *Front Microbiol* **9**:28.

Alves RJE, Minh BQ, Urich T, von Haeseler A, Schleper C. 2018. Unifying the global phylogeny and environmental distribution of ammonia-oxidising archaea based on amoA genes. *Nat commun* **9**:1-17.

Alves RJE, Kerou M, Zappe A, Bittner R, Abby SS, Schmidt HA, Pfeifer K, Schleper C. 2019. Ammonia oxidation by the arctic terrestrial thaumarchaeote *Candidatus* Nitrosocosmicus arcticus is stimulated by increasing temperatures. *Front Microbiol* **10**:1571.

Aylward FO, Santoro AE. 2020. Heterotrophic Thaumarchaea with small genomes are widespread in the dark ocean. *mSystems* **5**:e00415-20.

Amin SA, Moffett JW, Martens-Habbena W, Jacquot JE, Han Y, Devol A, Ingalls AE, Stahl DA, Armbrust EV. 2013. Copper requirements of the ammonia-oxidizing archaeon *Nitrosopumilus maritimus* SCM1 and implications for nitrification in the marine environment. *Limnol Oceanogr* **58**:2037-2045.

Anderson J. 1964. The metabolism of hydroxylamine to nitrite by *Nitrosomonas*. *Biochem J* **91**:8–17

Andrade SL, Dickmanns A, Ficner R, Einsle O. 2005. Crystal structure of the archaeal ammonium transporter Amt-1 from *Archaeoglobus fulgidus*. *Proc Natl Acad of Sci* **102**:14994-14999.

Arcondéguy T, Jack R, Merrick M. 2001. PII signal transduction proteins, pivotal players in microbial nitrogen control. *Microbiol Mol Biol Rev* **65**:80-105.

Arp DJ, Sayavedra-Soto LA, Hommes NG. 2002. Molecular biology and biochemistry of ammonia oxidation by *Nitrosomonas europaea*. *Arch Microbiol* **178**:250-255.

Bale NJ, Palatinszky M, Rijpstra WIC, Herbold CW, Wagner M, Sinninghe Damsté JS. 2019. Membrane lipid composition of the moderately thermophilic ammonia-oxidizing archaeon "*Candidatus* Nitrosotenuis uzonensis" at different growth temperatures. *Appl Environl Microbiol* **85**:e01332-19.

Bartossek R, Nicol GW, Lanzen A, Klenk HP, Schleper C. 2010. Homologues of nitrite reductases in ammonia-oxidizing archaea: diversity and genomic context. *Environ Microbiol* **12**:1075-1088.

Bates ST, Berg-Lyons D, Caporaso JG, Walters WA, Knight R, Fierer N. 2011. Examining the global distribution of dominant archaeal populations in soil. *ISME J* **5**:908-917.

Bayer B, Vojvoda J, Offre P, Alves RJ, Elisabeth NH, Garcia JA, Volland JM, Srivastava A, Schleper C, Herndl GJ. 2016. Physiological and genomic characterization of two novel marine thaumarchaeal strains indicates niche differentiation. *ISME J* **10**:1051-1063.

Bédard C, Knowles R. 1989. Physiology, biochemistry, and specific inhibitors of CH_4, NH_4^+, and CO oxidation by methanotrophs and nitrifiers. *Microbiol Mol Biol Rev* **53**:68-84.

Beeckman F, Motte H, Beeckman T. 2018. Nitrification in agricultural soils: impact, actors and mitigation. *Curr Opin Biotechnol* **50**:166-173.

Bennett K, Sadler NC, Wright AT, Yeager C, Hyman MR. 2016. Activity-based protein profiling of ammonia monooxygenase in *Nitrosomonas europaea*. *Appl Environl Microbiol* **82**:2270-2279.

Berney M, Greening C, Conrad R, Jacobs WR, Cook GM. 2014. An obligately aerobic soil bacterium activates fermentative hydrogen production to survive reductive stress during hypoxia. *Proc Natl Acad of Sci* **111**:11479-11484.

Berube PM, Stahl DA. 2012. The divergent $AmoC_3$ subunit of ammonia monooxygenase functions as part of a stress response system in *Nitrosomonas europaea*. *J Bacteriol* **194**:3448-3456.

Bodelier PL, Laanbroek HJ. 2004. Nitrogen as a regulatory factor of methane oxidation in soils and sediments. *FEMS Microbiol Ecol* **47**:265-277.

Bodelier PL. 2011. Interactions between nitrogenous fertilizers and methane cycling in wetland and upland soils. *Curr Opin Environ Sustain* **3**:379-388.

Bollmann A, Bullerjahn GS, McKay RM. 2014. Abundance and diversity of ammonia-oxidizing archaea and bacteria in sediments of trophic end members of the Laurentian Great Lakes, Erie and Superior. *PLoS One 9*:e97068.

Bouskill, N.J., Eveillard, D., Chien, D., Jayakumar, A. and Ward, B.B., 2012. Environmental factors determining ammonia-oxidizing organism distribution and diversity in marine environments. *Environ Microbiol* **14**:714-729.

Bristow LA, Dalsgaard T, Tiano L, Mills DB, Bertagnolli AD, Wright JJ, Hallam SJ, Ulloa O, Canfield DE, Revsbech NP, Thamdrup B. 2016. Ammonium and nitrite oxidation at nanomolar oxygen concentrations in oxygen minimum zone waters. *Proc Natl Acad Sci* **113**:10601-10606.

Brochier-Armanet C, Boussau B, Gribaldo S, Forterre P. 2008. Mesophilic Crenarchaeota: proposal for a third archaeal phylum, the Thaumarchaeota. *Nat Rev Microbiol* **6**:245-252.

Brusseau GA, Tsien HC, Hanson RS, Wackett LP. 1990. Optimization of trichloroethylene oxidation by methanotrophs and the use of a colorimetric assay to detect soluble methane monooxygenase activity. *Biodegrad* **1**:9-29.

Buchwald C, Santoro AE, McIlvin MR, Casciotti KL. 2012. Oxygen isotopic composition of nitrate and nitrite produced by nitrifying cocultures and natural marine assemblages. *Limnol Oceanogr* **57**:1361-1375.

Burrows KJ, Cornish A, Scott D, Higgins IJ. 1984. Substrate specificities of the soluble and particulate methane monooxygenases of *Methylosinus trichosporium* OB3b. *Microbiol* **130**:3327-3333.

Burton S.A, Prosser JI. 2001. Autotrophic ammonia oxidation at low pH through urea hydrolysis. *Appl Environ Microbiol* **67**:2952-2957.

Camejo PY, Santo Domingo J, McMahon KD, Noguera DR. 2017. Genome-enabled insights into the ecophysiology of the comammox bacterium "*Candidatus* Nitrospira nitrosa". *Msystems* **2**:e00059-17.

Campbell MA, Nyerges G, Kozlowski JA, Poret-Peterson AT, Stein LY, Klotz MG. 2011. Model of the molecular basis for hydroxylamine oxidation and nitrous oxide production in methanotrophic bacteria. *FEMS Microbiol Lett* **322**:82-89.

Canfield DE, Glazer AN, Falkowski PG. 2010. The evolution and future of Earth's nitrogen cycle. *Science* **330**:192-196.

Cao H, Auguet JC, Gu JD. 2013. Global ecological pattern of ammonia-oxidizing archaea. *PloS One* **8**:e52853.

Cao TP, Choi JM, Kim SW, Lee SH. 2018. The crystal structure of methanol dehydrogenase, a quinoprotein from the marine methylotrophic bacterium *Methylophaga aminisulfidivorans* MP^T. *J Microbiol* **56**:246-254.

Caranto JD, Lancaster KM. 2017. Nitric oxide is an obligate bacterial nitrification intermediate produced by hydroxylamine oxidoreductase. *Proc Natl Acad Sci* **114**:8217-8222.

Carini P, Dupont CL, Santoro AE. 2018. Patterns of thaumarchaeal gene expression in culture and diverse marine environments. *Environ Microbiol* **20**:2112-2124.

Carlsen HN, Joergensen L, Degn H. 1991. Inhibition by ammonia of methane utilization in *Methylococcus capsulatus* (Bath). *Appl Microbiol Biotechnol* **35**:124-127.

Chan SI, Yu SSF. 2008. Controlled oxidation of hydrocarbons by the membrane-bound methane monooxygenase: The case for a tricopper cluster. *Acc Chem Res* **41**:969-979.

Chen XP, Zhu YG, Xia Y, Shen JP, He JZ. 2008. Ammonia-oxidizing archaea: important players in paddy rhizosphere soil? *Environ Microbiol* **10**:1978-1987.

Colby J, Stirling DI, Dalton H. 1977. The soluble methane monooxygenase of *Methylococcus capsulatus* (Bath). Its ability to oxygenate n-alkanes, n-alkenes, ethers, and alicyclic, aromatic and heterocyclic compounds. *Biochem J* **165**:395-402.

Conrad R. 1996. Soil microorganisms as controllers of atmospheric trace gases (H_2, CO, CH_4, OCS, N_2O, and NO). *Microbiol Rev* **60**:609-640.

Crombie AT, Murrell JC. 2014. Trace-gas metabolic versatility of the facultative methanotroph *Methylocella silvestris*. *Nature* **510**:148-151.

Culpepper MA, Rosenzweig AC. 2012. Architecture and active site of particulate methane monooxygenase. *Crit Rev Biochem Mol Biol* **47**:483-492.

Daebeler A, Bodelier PL, Yan Z, Hefting MM, Jia Z, Laanbroek HJ. 2014. Interactions between Thaumarchaea, *Nitrospira* and methanotrophs modulate autotrophic nitrification in volcanic grassland soil. *ISME J* **8**:2397-2410.

Daebeler A, Herbold CW, Vierheilig J, Sedlacek CJ, Pjevac P, Albertsen M, Kirkegaard RH, De La Torre JR, Daims H, Wagner M. 2018. Cultivation and genomic analysis of "*Candidatus* Nitrosocaldus islandicus," an obligately thermophilic, ammonia-oxidizing thaumarchaeon from a hot spring biofilm in Graendalur Valley, Iceland. *Front Microbiol* **9**:193.

Daims H, Lebedeva EV, Pjevac P, Han P, Herbold C, Albertsen M, Jehmlich N, Palatinszky M, Vierheilig J, Bulaev A, Kirkegaard RH. 2015. Complete nitrification by *Nitrospira* bacteria. *Nature* **528**:504-509.

Dalsgaard T, Thamdrup B, Canfield DE. 2005. Anaerobic ammonium oxidation (anammox) in the marine environment. *Res Microbiol* **156**:457-464.

Dalton H. 1977. Ammonia oxidation by the methane oxidising bacterium *Methylococcus capsulatus* strain Bath. *Arch Microbiol* **114**:273-279.

De Boer W, Gunnewiek PK, Veenhuis M, Bock E, Laanbroek HJ. 1991. Nitrification at low pH by aggregated chemolithotrophic bacteria. *Appl Environl Microbiol* **57**:3600-3604.

De Boer W, Kowalchuk GA. 2001. Nitrification in acid soils: micro-organisms and mechanisms. *Soil Biol Biochem* **33**:853-866.

DeLong EF. 1992. Archaea in coastal marine environments. *Proc Natl Acad Sci* **89**:5685-5689.

Diamond S, Lavy A, Crits-Christoph A, Carnevali PBM, Sharrar A, Williams KH, Banfield JF. 2021. Soils and sediments host novel archaea with divergent monooxygenases implicated in ammonia oxidation. *bioRxiv*.

Dunfield PF, Khmelenina VN, Suzina NE, Trotsenko YA, Dedysh SN. 2003. *Methylocella silvestris* sp. nov., a novel methanotroph isolated from an acidic forest cambisol. *Int J Syst Evol Microbiol* **53**:1231-1239.

Enthaler S, von Langermann J, Schmidt T. 2010. Carbon dioxide and formic acid: the couple for environmental-friendly hydrogen storage? *Energy Environ Sci* **3**:1207-1217.

Ellerbeck M, Schüßler A, Brucker D, Dafinger C, Loos F, Brachmann A. 2013. Characterization of three ammonium transporters of the glomeromycotan fungus *Geosiphon pyriformis*. *Eukaryot Cell* **12**:1554-1562.

Elling FJ, Könneke M, Lipp JS, Becker KW, Gagen EJ, Hinrichs KU. 2014. Effects of growth phase on the membrane lipid composition of the thaumarchaeon *Nitrosopumilus maritimus* and their implications for archaeal lipid distributions in the marine environment. *Geochim Cosmochim Acta* **141**:579-597.

Elling FJ, Becker KW, Könneke M, Schröder JM, Kellermann MY, Thomm M, Hinrichs KU. 2016. Respiratory quinones in Archaea: phylogenetic distribution and application as biomarkers in the marine environment. *Environ Microbiol* **18**:692-707.

Elling FJ, Könneke M, Nicol GW, Stieglmeier M, Bayer B, Spieck E, de la Torre JR, Becker KW, Thomm M, Prosser JI, Herndl GJ. 2017. Chemotaxonomic characterisation of the thaumarchaeal lipidome. *Environ Microbiol* **19**:2681-2700.

Erisman JW, Sutton MA, Galloway J, Klimont Z, Winiwarter W. 2008. How a century of ammonia synthesis changed the world. *Nature Geosci* **1**:636-639.

Falkowski PG, Fenchel T, Delong EF. 2008. The microbial engines that drive Earth's biogeochemical cycles. *Science* **320**:1034-1039.

Haque MFU, Xu HJ, Murrell JC, Crombie A. 2020. Facultative methanotrophs–diversity, genetics, molecular ecology and biotechnological potential: a mini-review. *Microbiol* **166**:894.

Fiencke C, Bock E. 2006. Immunocytochemical localization of membrane-bound ammonia monooxygenase in cells of ammonia oxidizing bacteria. *Arch Microbiol* **185**:99-106.

Forchhammer K. 2008. PII signal transducers: novel functional and structural insights. *Trends Microbiol* **16**:65-72.

Francis CA, Roberts KJ, Beman JM, Santoro AE, Oakley BB. 2005. Ubiquity and diversity of ammonia-oxidizing archaea in water columns and sediments of the ocean. *Proc Natl Acad Sci* **102**:14683-14688.

Francis CA, Beman JM, Kuypers MM. 2007. New processes and players in the nitrogen cycle: the microbial ecology of anaerobic and archaeal ammonia oxidation. *ISME J* **1**:19-27.

Fuhrman JA, McCallum K, Davis AA. 1992. Novel major archaebacterial group from marine plankton. *Nature* **356**:148-149.

Garvin J, Buick R, Anbar AD, Arnold GL, Kaufman AJ. 2009. Isotopic evidence for an aerobic nitrogen cycle in the latest Archean. *Science* **323**:1045-1048.

Giguere AT, Taylor AE, Suwa Y, Myrold DD, Bottomley PJ. 2017. Uncoupling of ammonia oxidation from nitrite oxidation: impact upon nitrous oxide production in non-cropped Oregon soils. *Soil Biol Biochem* **104**:30-38.

Gilch S, Vogel M, Lorenz MW, Meyer O, Schmidt I. 2009. Interaction of the mechanism-based inactivator acetylene with ammonia monooxygenase of *Nitrosomonas europaea*. *Microbiol* **155**:279-284.

González-Cabaleiro R, Curtis TP, Ofiţeru ID. 2019. Bioenergetics analysis of ammonia-oxidizing bacteria and the estimation of their maximum growth yield. *Water Res* **154**:238-245.

Gorman-Lewis D, Martens-Habbena W, Stahl DA. 2019. Cu (II) adsorption onto ammonia-oxidizing bacteria and archaea. *Geochim Cosmochim Acta* **255**:127-143.

Greening C, Biswas A, Carere CR, Jackson CJ, Taylor MC, Stott MB, Cook GM, Morales SE. 2016. Genomic and metagenomic surveys of hydrogenase distribution indicate H_2 is a widely utilised energy source for microbial growth and survival. *ISME J* **10**:761-777.

Gubry-Rangin C, Hai B, Quince C, Engel M, Thomson BC, James P, Schloter M, Griffiths RI, Prosser JI, Nicol GW. 2011. Niche specialization of terrestrial archaeal ammonia oxidizers. *Proc Natl Acad Sci* **108**:21206-21211.

Guerrero-Cruz, S., Vaksmaa, A., Horn, M.A., Niemann, H., Pijuan, M. and Ho, A., 2021. Methanotrophs: Discoveries, Environmental Relevance, and a Perspective on Current and Future Applications. *Frontiers in Microbiology*, *12*, p.1057.

Gwak JH, Jung MY, Hong H, Kim JG, Quan ZX, Reinfelder JR, Spasov E, Neufeld JD, Wagner M, Rhee SK. 2020. Archaeal nitrification is constrained by copper complexation with organic matter in municipal wastewater treatment plants. *ISME J* **14**:335-346.

Hallam SJ, Konstantinidis KT, Putnam N, Schleper C, Watanabe YI, Sugahara J, Preston C, de la Torre J, Richardson PM, DeLong EF. 2006. Genomic analysis of the uncultivated marine crenarchaeote *Cenarchaeum symbiosum*. *Proc Natl Acad Sci* **103**:18296-18301.

Hanson RS, Hanson TE, 1996. Methanotrophic bacteria. *Microbiol Rev* **60**:439-471.

Hatzenpichler R, Lebedeva EV, Spieck E, Stoecker K, Richter A, Daims H, Wagner M. 2008. A moderately thermophilic ammonia-oxidizing crenarchaeote from a hot spring. *Proc Natl Acad Sci* **105**:2134-2139.

Hayatsu M, Tago K, Uchiyama I, Toyoda A, Wang Y, Shimomura Y, Okubo T, Kurisu F, Hirono Y, Nonaka K, Akiyama H. 2017. An acid-tolerant ammonia-oxidizing γ-proteobacterium from soil. *ISME J* **11**:1130-1141.

Head IM, Hiorns WD, Embley TM, McCarthy AJ, Saunders JR. 1993. The phylogeny of autotrophic ammonia-oxidizing bacteria as determined by analysis of 16S ribosomal RNA gene sequences. *Microbiol* **139**:1147-1153.

van Heeswijk WC, Westerhoff HV, Boogerd FC. 2013. Nitrogen assimilation in *Escherichia coli*: putting molecular data into a systems perspective. *Microbiol Mol Biol Rev* ***77***:628-695.

Helling RB. 1994. Why does *Escherichia coli* have two primary pathways for synthesis of glutamate? *J Bacteriol* **176**:4664-4668.

Herbold CW, Lehtovirta-Morley LE, Jung MY, Jehmlich N, Hausmann B, Han P, Loy A, Pester M, Sayavedra-Soto LA, Rhee SK, Prosser JI. 2017. Ammonia-oxidising archaea living at low pH: insights from comparative genomics. *Environ Microbiol* **19**:4939-4952.

Hink L, Nicol GW, Prosser JI. 2017. Archaea produce lower yields of N_2O than bacteria during aerobic ammonia oxidation in soil. *Environ Microbiol* **19**:4829-4837.

Hink L, Gubry-Rangin C, Nicol GW, Prosser JI. 2018. The consequences of niche and physiological differentiation of archaeal and bacterial ammonia oxidisers for nitrous oxide emissions. *ISME J* **12**:1084-1093.

Hollibaugh JT, Gifford S, Sharma S, Bano N, Moran MA. 2011. Metatranscriptomic analysis of ammonia-oxidizing organisms in an estuarine bacterioplankton assemblage. *ISME J* **5**:866-878.

Holmes AJ, Costello A, Lidstrom ME, Murrell JC. 1995. Evidence that particulate methane monooxygenase and ammonia monooxygenase may be evolutionarily related. *FEMS Microbiol Lett* **132**:203-208.

Hommes NG, Sayavedra-Soto LA, Arp DJ. 2003. Chemolithoorganotrophic growth of *Nitrosomonas europaea* on fructose. *J Bacteriol* **185**:6809-6814.

Hosseinzadeh P, Tian S, Marshall NM, Hemp J, Mullen T, Nilges MJ, Gao YG, Robinson H, Stahl DA, Gennis RB, Lu Y. 2016. A purple cupredoxin from *Nitrosopumilus maritimus* containing a mononuclear type 1 copper center with an open binding site. *J Am Che Soc* **138**:6324-6327.

Hu Z, Wessels HJ, van Alen T, Jetten MS, Kartal B. 2019. Nitric oxide-dependent anaerobic ammonium oxidation. *Nature Commun*, **10**:1-7.

Huang L, Chakrabarti S, Cooper J, Perez A, John SM, Daroub SH, Martens-Habbena W. 2021. Ammonia-oxidizing archaea are integral to nitrogen cycling in a highly fertile agricultural soil. *ISME Comm* **1**:1-12.

Hurley SJ, Elling FJ, Könneke M, Buchwald C, Wankel SD, Santoro AE, Lipp JS, Hinrichs KU, Pearson A. 2016. Influence of ammonia oxidation rate on thaumarchaeal lipid composition and the TEX_{86} temperature proxy. *Proc Natl Acad Sci* **113**:7762-7767.

Hyman MR, Wood PM, 1983. Methane oxidation by *Nitrosomonas europaea*. *Biochem J* **212**:31-37.

Hyman MR, Wood PM. 1985. Suicidal inactivation and labelling of ammonia monooxygenase by acetylene. *Biochem J* **227**:719-725.

Hyman MR, Murton IB, Arp DJ. 1988. Interaction of ammonia monooxygenase from *Nitrosomonas europaea* with alkanes, alkenes, and alkynes. *Appl Environ Microbiol* **54**:3187-3190.

Hyman MR, Kim CY, Arp DJ. 1990. Inhibition of ammonia monooxygenase in *Nitrosomonas europaea* by carbon disulfide. *J Bacteriol* **172**:4775-4782.

Hyman MR, Arp DJ. 1992. $^{14}C_2H_2$-and $^{14}CO_2$-labeling studies of the *de novo* synthesis of polypeptides by *Nitrosomonas europaea* during recovery from acetylene and light inactivation of ammonia monooxygenase. *J Biol Chem* **267**:1534-1545.

Hynes RK, Knowles R. 1982. Effect of acetylene on autotrophic and heterotrophic nitrification. *Can J Microbiol* **28**:334-340.

Ingalls AE, Shah SR, Hansman RL, Aluwihare LI, Santos GM, Druffel ER, Pearson A. 2006. Quantifying archaeal community autotrophy in the mesopelagic ocean using natural radiocarbon. *Proc Natl Acad Sci* **103**:6442-6447.

Im J, Lee SW, Bodrossy L, Barcelona MJ, Semrau JD. 2011. Field application of nitrogen and phenylacetylene to mitigate greenhouse gas emissions from landfill cover soils: effects on microbial community structure. *Appl Microbiol Biotechnol* 89:189-200.

Jetten MSM, Cirpus I, Kartal B, van Niftrik LAMP, Van De Pas-Schoonen KT, Sliekers O, Haaijer S, Van der Star W, Schmid M, van de Vossenberg JLCM, Schmidt I. 2005. 1994–2004: 10 years of research on the anaerobic oxidation of ammonium. *Biochem Soc Trans* **33**:119-123.

Jia Z, Conrad R. 2009. Bacteria rather than Archaea dominate microbial ammonia oxidation in an agricultural soil. *Environ Microbiol* **11**:1658-1671.

Jiang QQ, Bakken LR, 1999. Nitrous oxide production and methane oxidation by different ammonia-oxidizing bacteria. *Appl Environ Microbiol* **65**:2679-2684.

Jiang H, Chen Y, Jiang P, Zhang C, Smith TJ, Murrell JC, Xing XH. 2010. Methanotrophs: multifunctional bacteria with promising applications in environmental bioengineering. *Biochem Eng J* **49**:277-288.

Joergensen L, Degn, H. 1983. Mass spectrometric measurements of methane and oxygen utilization by methanotrophic bacteria. *FEMS Microbiol Lett* **20**:331-335.

Jones HA, Nedwell DB. 1993. Methane emission and methane oxidation in land-fill cover soil. *FEMS Microbiol Eco* **11**:185-195.

Jones RD, Morita RY. 1983. Methane oxidation by *Nitrosococcus oceanus* and *Nitrosomonas europaea*. *Appl Environ Microbiol* **45**:401-410.

Juliette LY, Hyman MR, Arp DJ. 1993. Inhibition of ammonia oxidation in *Nitrosomonas europaea* by sulfur compounds: thioethers are oxidized to sulfoxides by ammonia monooxygenase. *Appl Environ Microbiol* 59:3718-3727.

Jung MY, Well R, Min D, Giesemann A, Park SJ, Kim JG, Kim SJ, Rhee SK, 2014. Isotopic signatures of N_2O produced by ammonia-oxidizing archaea from soils. *ISME J* **8**:1115-1125.

Jung MY, Kim JG, Sinninghe Damsté JS, Rijpstra WIC, Madsen EL, Kim SJ, Hong H, Si OJ, Kerou M, Schleper C, Rhee SK. 2016. A hydrophobic ammonia-oxidizing archaeon of the *Nitrosocosmicus* clade isolated from coal tar-contaminated sediment. *Environ Microbiol Rep* **8**:983-992.

Jung MY, Gwak JH, Rohe L, Giesemann A, Kim JG, Well R, Madsen EL, Herbold CW, Wagner M, Rhee SK. 2019. Indications for enzymatic denitrification to N_2O at low pH in an ammonia-oxidizing archaeon. *ISME J* **13**:2633-2638.

Jung MY, Sedlacek CJ, Kits KD, Mueller AJ, Rhee SK, Hink L, Nicol GW, Bayer B, Lehtovirta-Morley L, Wright CL, de la Torre JR, Herbold CW, Pjevac P, Daims H, Wagner M. 2021. Ammonia-oxidizing archaea possess a wide range of cellular ammonia affinities. *ISME J* doi:

Karner MB, DeLong EF, Karl DM. 2001. Archaeal dominance in the mesopelagic zone of the Pacific Ocean. *Nature*, **409**:507-510.

Kallistova AY, Merkel AY, Tarnovetskii, I Y, Pimenov NV. 2017. Methane formation and oxidation by prokaryotes. *Microbiol* **86**:671-691.

Kalyuzhnaya MG, Gomez OA, Murrell JC. 2019. The methane-oxidizing bacteria (methanotrophs). In Taxonomy, genomics and ecophysiology of hydrocarbon-degrading microbes. Edited by McGenity TJ. Cham: Springer *Nature* 1-34.

Keener WK, Arp DJ. 1993. Kinetic studies of ammonia monooxygenase inhibition in *Nitrosomonas europaea* by hydrocarbons and halogenated hydrocarbons in an optimized whole-cell assay. *Appl Environ Microbiol* **59**:2501-2510.

Keener WK, Arp DJ. 1994. Transformations of aromatic compounds by *Nitrosomonas europaea*. *Appl Environ Microbiol* **60**:1914-1920.

Keener WK, Russell SA, Arp DJ. 1998. Kinetic characterization of the inactivation of ammonia monooxygenase in *Nitrosomonas europaea* by alkyne, aniline and cyclopropane derivatives. *Biochem Biophys Acta* **1388**:373-385.

Kerou M, Offre P, Valledor L, Abby SS, Melcher M, Nagler M, Weckwerth W, Schleper C. 2016. Proteomics and comparative genomics of *Nitrososphaera viennensis* reveal the core genome and adaptations of archaeal ammonia oxidizers. *Proc Natl Acad Sci* **113**:7937-7946.

Van Kessel MA, Speth DR, Albertsen M, Nielsen PH, den Camp HJO, Kartal B, Jetten MS, Lücker S. 2015. Complete nitrification by a single microorganism. *Nature* **528**:555-559.

Khadka R, Clothier L, Wang L, Lim CK, Klotz MG, Dunfield PF. 2018. Evolutionary history of copper membrane monooxygenases. *Front Microbiol* **9**:2493.

Kim JG, Park SJ, Damsté JSS, Schouten S, Rijpstra WIC, Jung MY, Kim SJ, Gwak JH, Hong H, Si OJ, Lee S. 2016. Hydrogen peroxide detoxification is a key mechanism for growth of ammonia-oxidizing archaea. *Proc Natl Acad Sci* **113**:7888-7893.

Kits KD, Campbell DJ, Rosana AR, Stein LY. 2015. Diverse electron sources support denitrification under hypoxia in the obligate methanotroph *Methylomicrobium* album strain BG8. *Front Microbiol* **6**:1072.

Kits KD, Klotz MG, Stein LY. 2015. Methane oxidation coupled to nitrate reduction under hypoxia by the Gammaproteobacterium *Methylomonas denitrificans*, sp. nov. type strain FJG1. *Environ Microbiol* **17**:3219-3232.

Kits KD, Sedlacek CJ, Lebedeva EV, Han P, Bulaev A, Pjevac P, Daebeler A, Romano S, Albertsen M, Stein LY, Daims H. 2017. Kinetic analysis of a complete nitrifier reveals an oligotrophic lifestyle. *Nature* **549***:*269-272.

Kitzinger K, Padilla CC, Marchant HK, Hach PF, Herbold CW, Kidane AT, Könneke M, Littmann S, Mooshammer M, Niggemann J, Petrov S. 2019. Cyanate and urea are substrates for nitrification by Thaumarchaeota in the marine environment. *Nature Microbiol* **4**:234-243.

Klotz MG, Stein LY. 2008. Nitrifier genomics and evolution of the nitrogen cycle. *FEMS Microbiol Lett* **278**:146-156.

Kobayashi S, Hira D, Yoshida K, Toyofuku M, Shida Y, Ogasawara W, Yamaguchi T, Araki N, Oshiki M. 2018. Nitric oxide production from nitrite reduction and hydroxylamine oxidation by copper-containing dissimilatory nitrite reductase (NirK) from the aerobic ammonia-oxidizing archaeon, *Nitrososphaera viennensis*. *Microbes Environ* **33**:428-434.

Koch H, van Kessel MA, Lücker S. 2019. Complete nitrification: insights into the ecophysiology of comammox *Nitrospira*. *Appl Microbiol Biotechnol* **103**:177-189.

Kolb S. (2009). Aerobic methanol-oxidizing bacteria in soil. *FEMS Microbiol Lett* **300**:1-10.

Könneke M, Bernhard A E, José R, Walker CB, Waterbury JB, Stahl DA. 2005. Isolation of an autotrophic ammonia-oxidizing marine archaeon. *Nature* **437**:543-546.

Könneke M, Schubert DM, Brown PC, Hügler M, Standfest S, Schwander T, von Borzyskowski LS, Erb TJ, Stahl DA Berg IA. 2014. Ammonia-oxidizing archaea use the most energy-efficient aerobic pathway for CO2 fixation. *Proc Natl Acad Sci* **111**:8239-8244.

Kozlowski JA, Price J, Stein LY. 2014. Revision of N_2O-producing pathways in the ammonia-oxidizing bacterium *Nitrosomonas europaea* ATCC 19718. *Appl Environ Microbiol* **80**:4930-4935.

Kozlowski JA, Stieglmeier M, Schleper C, Klotz MG, Stein LY. 2016a. Pathways and key intermediates required for obligate aerobic ammonia-dependent chemolithotrophy in bacteria and Thaumarchaeota. *ISME J* **10**:1836-1845.

Kozlowski, JA, Kits KD, Stein LY. 2016b. Comparison of nitrogen oxide metabolism among diverse ammonia-oxidizing bacteria. *Front Microbiol* **7**:1090.

Kuypers MM, Marchant HK, Kartal B. 2018. The microbial nitrogen-cycling network. *Nature Rev Microbiol* **16**:263-276.

Laanbroek HJ. 2010. Methane emission from natural wetlands: interplay between emergent macrophytes and soil microbial processes. A mini-review. *Ann Bot* **105**:141-153.

Lancaster KM, Caranto JD, Majer SH, Smith MA. 2018. Alternative bioenergy: updates to and challenges in nitrification metalloenzymology. *Joule* **2**:421-441.

Lawton TJ, Ham J, Sun T, Rosenzweig AC. 2014. Structural conservation of the B subunit in the ammonia monooxygenase/particulate methane monooxygenase superfamily. *Proteins* **82**:2263-2267.

Lee SW, Im J, DiSpirito AA, Bodrossy L, Barcelona MJ, Semrau JD. 2009. Effect of nutrient and selective inhibitor amendments on methane oxidation, nitrous oxide production, and key gene presence and expression in landfill cover soils: characterization of the role of methanotrophs, nitrifiers, and denitrifiers. *Appl Microbiol Biotechnol* **85**:389-403.

Lehtovirta-Morley LE, Stoecker K, Vilcinskas A, Prosser JI, Nicol GW. 2011. Cultivation of an obligate acidophilic ammonia oxidizer from a nitrifying acid soil. *Proc Natl Acad Sci* **108**:15892-15897.

Lehtovirta-Morley LE, Verhamme DT, Nicol GW, Prosser JI. 2013. Effect of nitrification inhibitors on the growth and activity of *Nitrosotalea devanaterra* in culture and soil. *Soil Biol Biochem* **62**:129-133.

Lehtovirta-Morley LE, Ge C, Ross J, Yao H, Nicol GW, Prosser JI. 2014. Characterisation of terrestrial acidophilic archaeal ammonia oxidisers and their inhibition and stimulation by organic compounds. *FEMS Microbiol Eco* **89**:542-552.

Lehtovirta-Morley LE, Sayavedra-Soto LA, Gallois N, Schouten S, Stein LY, Prosser JI, Nicol GW. 2016a. Identifying potential mechanisms enabling acidophily in the ammonia-oxidizing archaeon "*Candidatus* Nitrosotalea devanaterra". *Appl Environ Microbiol* **82**:2608-2619.

Lehtovirta-Morley LE, Ross J, Hink L, Weber EB, Gubry-Rangin C, Thion C, Prosser JI, Nicol GW. 2016b. Isolation of '*Candidatus* Nitrosocosmicus franklandus', a novel ureolytic soil archaeal ammonia oxidiser with tolerance to high ammonia concentration. *FEMS Microbiol Eco* **92**.

Lehtovirta-Morley LE. 2018. Ammonia oxidation: Ecology, physiology, biochemistry and why they must all come together. *FEMS Microbiol Lett* **365**:fny058.

Leininger S, Urich T, Schloter M, Schwark L, Qi J, Nicol GW, Prosser JI, Schuster SC, Schleper C. 2006. Archaea predominate among ammonia-oxidizing prokaryotes in soils. *Nature* **442**:806-809

Li Y, Chapman SJ, Nicol GW, Yao H. 2018. Nitrification and nitrifiers in acidic soils. *Soil Biol Biochem* **116**:290-301.

Li PN, Herrmann J, Tolar BB, Poitevin F, Ramdasi R, Bargar JR, Stahl DA, Jensen GJ, Francis CA, Wakatsuki S, van den Bedem H. 2018. Nutrient transport suggests an evolutionary basis for charged archaeal surface layer proteins. *ISME J* **12**:2389-2402.

Lieberman RL, Rosenzweig AC. 2005. Crystal structure of a membrane-bound metalloenzyme that catalyses the biological oxidation of methane. *Nature* **434**:177-182.

Liu S, Han P, Hink L, Prosser JI, Wagner M, Bruggemann N. 2017. Abiotic conversion of extracellular NH_2OH contributes to N_2O emission during ammonia oxidation. *Environ Sci Technol* **51**:13122-13132.

Liu T, Wang Z, Wang S, Zhao Y, Wright AL, Jiang X. 2019. Responses of ammonia-oxidizers and comammox to different long-term fertilization regimes in a subtropical paddy soil. *Euro J Soil Biol* **93**:103087.

Logan MS, Hooper AB. 1995. Suicide inactivation of hydroxylamine oxidoreductase of *Nitrosomonas europaea* by organohydrazines. *Biochem* **34**:9257-9264.

Lontoh S, DiSpirito AA, Semrau JD. 1999. Dichloromethane and trichloroethylene inhibition of methane oxidation by the membrane-associated methane monooxygenase of *Methylosinus trichosporium* OB3b. *Arch Microbiol* **171**:301-308.

Lontoh S, DiSpirito AA, Krema CL, Whittaker MR, Hooper AB, Semrau JD. 2000. Differential inhibition in vivo of ammonia monooxygenase, soluble methane monooxygenase and membrane-associated methane monooxygenase by phenylacetylene. *Environ Microbiol* **2**:485-494.

Lu L, Han W, Zhang J, Wu Y, Wang B, Lin X, Zhu J, Cai Z, Jia Z. 2012. Nitrification of archaeal ammonia oxidizers in acid soils is supported by hydrolysis of urea. *ISME J* **6**:1978-1984.

Lu X, Bottomley PJ, Myrold DD. 2015. Contributions of ammonia-oxidizing archaea and bacteria to nitrification in Oregon forest soils. *Soil Biol Biochem* **85**:54-62.

Lu YJ, Hung MC, Chang BTA, Lee TL, Lin ZH, Tsai IK, Chen YS, Chang CS, Tsai YF, Chen KHC, Chan SI. 2019. The PmoB subunit of particulate methane monooxygenase (pMMO) in *Methylococcus capsulatus* (Bath): the CuI sponge and its function. *J Inorg Biochem* **196**:110691.

Luo ZH, Narsing Rao MP, Chen H, Hua ZS, Li Q, Hedlund BP, Dong ZY, Liu BB, Guo SX, Shu WS, Li WJ. 2021. Genomic insights of "*Candidatus* Nitrosocaldaceae" based on nine new metagenome-assembled genomes, including "*Candidatus* Nitrosothermus" gen nov. and two new species of "*Candidatus* Nitrosocaldus". *Front Microbiol* **11**:3412.

Lund MB, Smith JM, Francis CA. 2012. Diversity, abundance and expression of nitrite reductase (nirK)-like genes in marine thaumarchaea. *ISME J* **6**:1966-1977.

Macey MC, Pratscher J, Crombie AT, Murrell JC. 2020. Impact of plants on the diversity and activity of methylotrophs in soil. *Microbiome* **8**:1-17.

Martens-Habbena W, Berube PM, Urakawa H, José R, Stahl DA. 2009. Ammonia oxidation kinetics determine niche separation of nitrifying Archaea and Bacteria. *Nature* **461**:976-979.

Martens-Habbena W, Stahl DA. 2011. Nitrogen metabolism and kinetics of ammonia-oxidizing archaea. *Methods Enzymol* **496**:465-487.

Martens-Habbena W, Qin W, Horak RE, Urakawa H, Schauer AJ, Moffett JW, Armbrust EV, Ingalls AE, Devol AH, Stahl DA. 2015. The production of nitric oxide by marine ammonia-oxidizing archaea and inhibition of archaeal ammonia oxidation by a nitric oxide scavenger. *Environ Microbiol* **17**:2261-2274.

McDowall JS, Murphy BJ, Haumann M, Palmer T, Armstrong FA, Sargent F. 2014. Bacterial formate hydrogenlyase complex. *Proc Natl Acad Sci* **111**:3948-3956.

McTavish HJAF, Fuchs JA, Hooper AB. 1993. Sequence of the gene coding for ammonia monooxygenase in *Nitrosomonas europaea*. *J Bacteriol* **175**:2436-2444.

Men Y, Han P, Helbling DE, Jehmlich N, Herbold C, Gulde R, Onnis-Hayden A, Gu AZ, Johnson DR, Wagner M, Fenner K. 2016. Biotransformation of two pharmaceuticals by the ammonia-oxidizing archaeon *Nitrososphaera gargensis*. *Environ Sci Technol* 50:4682-4692.

Merbt SN, Stahl DA, Casamayor EO, Martí E, Nicol GW, Prosser JI. 2012. Differential photoinhibition of bacterial and archaeal ammonia oxidation. *FEMS Microbiol Lett* **327**:41-46.

Miyaji A, Miyoshi T, Motokura K, Baba T. 2011. The substrate binding cavity of particulate methane monooxygenase from *Methylosinus trichosporium* OB3b expresses high enantioselectivity for n-butane and n-pentane oxidation to 2-alcohol. *Biotechnol Lett* 33:2241.

Mohammadi SS, Pol A, van Alen T, Jetten MS, Op den Camp HJ. 2017. Ammonia oxidation and nitrite reduction in the verrucomicrobial methanotroph *Methylacidiphilum fumariolicum* SolV. *Front Microbiol* **8**:1901.

Moissl-Eichinger C. 2011. Archaea in artificial environments: their presence in global spacecraft clean rooms and impact on planetary protection. *ISME J* **5**:209-219.

Mori JF, Chen LX, Jessen GL, Rudderham SB, McBeth JM, Lindsay MB, Slater GF, Banfield JF, Warren LA. 2019. Putative mixotrophic nitrifying-denitrifying Gammaproteobacteria implicated in nitrogen cycling within the ammonia/oxygen transition zone of an oil sands pit lake. *Front Microbiol* **10**:2435.

Mosier AC, Francis CA. 2008. Relative abundance and diversity of ammonia-oxidizing archaea and bacteria in the San Francisco Bay estuary. *Environ Microbiol* **10**:3002-3016.

Muck S, De Corte D, Clifford EL, Bayer B, Herndl GJ, Sintes E. 2019. Niche differentiation of aerobic and anaerobic ammonia oxidizers in a high latitude deep oxygen minimum zone. *Front Microbiol* **10**:2141.

Mußmann M, Brito I, Pitcher A, Damsté JSS, Hatzenpichler R, Richter A, Nielsen JL, Nielsen PH, Müller A, Daims H, Wagner M. 2011. Thaumarchaeotes abundant in refinery nitrifying sludges express *amoA* but are not obligate autotrophic ammonia oxidizers. *Proc Natl Acad Sci* **108**:16771-16776.

Murrell JC. 1992. Genetics and molecular biology of methanotrophs. *FEMS Microbiol Rev* **8**:233-248.

Nash T. 1953. The colorimetric estimation of formaldehyde by means of the Hantzsch reaction. *Biochem J* **55**:416-421.

Nakagawa T, Stahl DA. 2013. Transcriptional response of the archaeal ammonia oxidizer *Nitrosopumilus maritimus* to low and environmentally relevant ammonia concentrations. *Appl Environ Microbiol* **79**:6911-6916.

Ng KY, Tu LC, Wang YS, Chan SI, Yu SSF. 2008. Probing the hydrophobic pocket of the active site in the particulate methane monooxygenase (pMMO) from *Methylococcus capsulatus* (Bath) by variable stereoselective alkane hydroxylation and olefin epoxidation. *Chem Bio Chem* **9**:1116-1123.

Nicol GW, Schleper C. 2006. Ammonia-oxidising Crenarchaeota: important players in the nitrogen cycle? *TRENDS Microbiol* **14**:207-212.

Nicol GW, Leininger S, and Schleper C. 2011. Distribution and activity of ammonia-oxidizing archaea in natural environments, p 157–180. In Ward BB, Arp DJ, and Klotz MG (ed), *Nitrification*. ASM Press, Washington, DC.

Nielsen AK, Gerdes K, Murrell JC. 1997. Copper-dependent reciprocal transcriptional regulation of methane monooxygenase genes in *Methylococcus capsulatus* and *Methylosinus trichosporium*. *Mol Microbiol* **25**:399-409.

Nisbet EG, Dlugokencky EJ, Fisher RE, France JL, Lowry D, Manning MR, Michel SE, Warwick NJ. 2021. Atmospheric methane and nitrous oxide: challenges along the path to Net Zero. *Philos Trans R Soc A* **379**:20200457.

Nojiri M, Hira D, Yamaguchi K, Okajima T, Tanizawa K, Suzuki S. 2006. Crystal structures of cytochrome c L and methanol dehydrogenase from *Hyphomicrobium denitrificans*: structural and mechanistic insights into interactions between the two proteins. *Biochem* **45**:3481-3492.

Norton JM, Klotz MG, Stein LY, Arp DJ, Bottomley PJ, Chain PS, Hauser LJ, Land ML, Larimer FW, Shin MW, Starkenburg SR. 2008. Complete genome sequence of *Nitrosospira multiformis*, an ammonia-oxidizing bacterium from the soil environment. *Appl Environ Microbiol* **74**:3559-3572.

Nyerges G, Stein LY. 2009. Ammonia cometabolism and product inhibition vary considerably among species of methanotrophic bacteria. *FEMS Microbiol Lett* **297**:131-136.

Offre P, Spang A, Schleper C. 2013. Archaea in biogeochemical cycles. *Ann Rev Microbiol* **67**:437-457.

Offre P, Kerou M, Spang A, Schleper C. 2014. Variability of the transporter gene complement in ammonia-oxidizing archaea. *Trends Microbiol* **22**:665-675.

O'neill JG, Wilkinson JF. 1977. Oxidation of ammonia by methane-oxidizing bacteria and the effects of ammonia on methane oxidation. *Microbiol* **100**:407-412.

Ouyang Y, Norton JM, Stark JM. 2017. Ammonium availability and temperature control contributions of ammonia oxidizing bacteria and archaea to nitrification in an agricultural soil. *Soil Biol Biochem* **113**:161-172.

Ouverney CC, Fuhrman JA. 2000. Marine planktonic archaea take up amino acids. *Appl Environ Microbiol* **66**:4829-4833.

Palatinszky M, Herbold C, Jehmlich N, Pogoda M, Han P, von Bergen M, Lagkouvardos I, Karst SM, Galushko A, Koch H, Berry D. 2015. Cyanate as an energy source for nitrifiers. *Nature* **524**:105-108.

Palomo A, Pedersen AG, Fowler SJ, Dechesne A, Sicheritz-Pontén T, Smets BF. 2018. Comparative genomics sheds light on niche differentiation and the evolutionary history of comammox *Nitrospira*. *ISME J* **12**:1779-1793.

Park BJ, Park SJ, Yoon DN, Schouten S, Sinninghe Damsté JS, Rhee SK. 2010. Cultivation of autotrophic ammonia-oxidizing archaea from marine sediments in coculture with sulfur-oxidizing bacteria. *Appl Environ Microbiol* **76**:7575-7587.

Pester M, Schleper C, Wagner M, 2011. The Thaumarchaeota: an emerging view of their phylogeny and ecophysiology. *Curr Opin Microbiol* **14**:300-306.

Pfeiffer S, Leopold E, Hemmens B, Schmidt K, Werner ER, Mayer B. 1997. Interference of carboxy-PTIO with nitric oxide-and peroxynitrite-mediated reactions. *Free Radic Biol Med* **22**:787-794.

Picone N, Pol A, Mesman R, van Kessel MA, Cremers G, van Gelder AH, van Alen TA, Jetten MS, Lücker S, Den Camp HJO. 2021. Ammonia oxidation at pH 2.5 by a new gammaproteobacterial ammonia-oxidizing bacterium. *ISME J* **15**:1150-1164.

Pitcher A, Hopmans EC, Mosier AC, Park SJ, Rhee SK, Francis CA, Schouten S, Sinninghe Damsté JS. 2011. Core and intact polar glycerol dibiphytanyl glycerol tetraether lipids of ammonia-oxidizing archaea enriched from marine and estuarine sediments. *Appl Environ Microbiol* **77**:3468-3477.

Pjevac P, Schauberger C, Poghosyan L, Herbold CW, van Kessel MA, Daebeler A, Steinberger M, Jetten MS, Lücker S, Wagner M, Daims H. 2017. *AmoA*-targeted polymerase chain reaction primers for the specific detection and quantification of comammox *Nitrospira* in the environment. *Front Microbiol* **8**:1508.

Poret-Peterson AT, Graham JE, Gulledge J, Klotz MG. 2008. Transcription of nitrification genes by the methane-oxidizing bacterium, *Methylococcus capsulatus* strain Bath. *ISME J* **2**:1213-1220.

Prior SD, Dalton H. 1985. Acetylene as a suicide substrate and active site probe for methane monooxygenase from *Methylococcus capsulatus* (Bath). *FEMS Microbiol Lett* **29**:105-109.

Prosser JI, 1990. Autotrophic nitrification in bacteria. *Adv Microb Physiol* **30**:125-181.

Prosser JI, Hink L, Gubry-Rangin C, Nicol GW. 2020. Nitrous oxide production by ammonia oxidizers: Physiological diversity, niche differentiation and potential mitigation strategies. *Glob Chang Biol* **26**:103-118.

Prosser JI, Nicol GW. 2012. Archaeal and bacterial ammonia-oxidisers in soil: the quest for niche specialisation and differentiation. *Trends Microbiol* **20**:523-531.

Purkhold U, Pommerening-Röser A, Juretschko S, Schmid MC, Koops HP, Wagner M. 2000. Phylogeny of all recognized species of ammonia oxidizers based on comparative 16S rRNA and *amoA* sequence analysis: implications for molecular diversity surveys. *Appl Environ Microbiol* **66**:5368-5382.

QinW, Martens-Habbena W, Kobelt JN, Stahl DA. 2016. *Candidatus* Nitrosopumilaceae. In *Bergey's Manual of Systematics of Archaea and Bacteria*, Whitman WB, Rainey F, Kämpfer P, Trujillo M, Chun J, DeVos P, *et al.* (eds). Chichester, UK: John Wiley & Sons, pp. 1–2

Qin W, Meinhardt KA, Moffett JW, Devol AH, Virginia Armbrust E, Ingalls AE, Stahl DA. 2017. Influence of oxygen availability on the activities of ammonia-oxidizing archaea. *Environ Microbiol Rep* **9**:250-256.

Qin W, Amin SA, Lundeen RA, Heal KR, Martens-Habbena W, Turkarslan S, Urakawa H, Costa KC, Hendrickson EL, Wang T, Beck DA. 2018. Stress response of a marine ammonia-oxidizing archaeon informs physiological status of environmental populations. *ISME J* **12**:508-519.

Rasche ME, Hyman MR, Arp DJ. 1991. Factors limiting aliphatic chlorocarbon degradation by *Nitrosomonas europaea*: cometabolic inactivation of ammonia monooxygenase and substrate specificity. *Appl Environ Microbiol* **57**:2986-2994.

Ravishankara AR, Daniel JS, Portmann RW. 2009. Nitrous oxide (N_2O): the dominant ozone-depleting substance emitted in the 21st century. *Science* **326**:123-125.

Ren Y, Ngo HH, Guo W, Wang D, Peng L, Ni BJ, Wei W, Liu Y. 2020. New perspectives on microbial communities and biological nitrogen removal processes in wastewater treatment systems. *Bioresour Technol* **297**:122491.

Reyes C, Schneider D, Lipka M, Thürmer A, Böttcher ME, Friedrich MW. 2017. Nitrogen metabolism genes from temperate marine sediments. *Mar Biotechnol* **19**:175-190.

Reyes C, Hodgskiss LH, Kerou M, Pribasnig T, Abby SS, Bayer B, Kraemer SM, Schleper C. 2020a. Genome wide transcriptomic analysis of the soil ammonia oxidizing archaeon *Nitrososphaera viennensis* upon exposure to copper limitation. *ISME J* **14**:2659-2674.

Reyes C, Hodgskiss LH, Baars O, Kerou M, Bayer B, Schleper C, Kraemer SM. 2020b. Copper limiting threshold in the terrestrial ammonia oxidizing archaeon *Nitrososphaera viennensis*. *Res Microbiol* **171**:134-142.

Ro SY, Schachner LF, Koo CW, Purohit R, Remis JP, Kenney GE, Liauw BW, Thomas PM, Patrie SM, Kelleher NL, Rosenzweig AC. 2019. Native top-down mass spectrometry provides insights into the copper centers of membrane-bound methane monooxygenase. *Nature Commun* **10**:1-12.

Rodrigues-Oliveira T, Belmok A, Vasconcellos D, Schuster B, Kyaw CM. 2017. Archaeal S-layers: overview and current state of the art. *Front Microbiol* **8**:2597.

Roots P, Wang Y, Rosenthal AF, Griffin JS, Sabba F, Petrovich M, Yang F, Kozak JA, Zhang H, Wells GF. 2019. Comammox *Nitrospira* are the dominant ammonia oxidizers in a mainstream low dissolved oxygen nitrification reactor. *Water Res* **157**:396-405.

Ross MO, MacMillan F, Wang J, Nisthal A, Lawton TJ, Olafson BD, Mayo SL, Rosenzweig AC, Hoffman BM. 2019. Particulate methane monooxygenase contains only mononuclear copper centers. *Science* **364**:566-570.

Santoro AE, Casciotti KL. 2011. Enrichment and characterization of ammonia-oxidizing archaea from the open ocean: phylogeny, physiology and stable isotope fractionation. *ISME J* **5**:1796-1808.

Sauder LA, Peterse F, Schouten S, Neufeld JD. 2012. Low-ammonia niche of ammonia-oxidizing archaea in rotating biological contactors of a municipal wastewater treatment plant. *Environ Microbiol* **14**:2589-2600.

Sauder LA, Ross AA, Neufeld JD. 2016. Nitric oxide scavengers differentially inhibit ammonia oxidation in ammonia-oxidizing archaea and bacteria. *FEMS Microbiol Lett* **363**:fnw052.

Sauder LA, Albertsen M, Engel K, Schwarz J, Nielsen PH, Wagner M, Neufeld JD. 2017. Cultivation and characterization of *Candidatus* Nitrosocosmicus exaquare, an ammonia-oxidizing archaeon from a municipal wastewater treatment system. *ISME J* **11**:1142-1157.

Sander R. 2015. Compilation of Henry's law constants (version 4.0) for water as solvent. *Atmos Chem Phys* **15**:4399-4981.

Saunois M, Bousquet P, Poulter B, Peregon A, Ciais P, Canadell JG, Dlugokencky EJ, Etiope G, Bastviken D, Houweling S, Janssens-Maenhout G. 2016. The global methane budget 2000–2012. *Earth Syst Sci Data*, **8**:697-751.

Sayavedra-Soto LA, Gvakharia B, Bottomley PJ, Arp DJ, Dolan ME. 2010. Nitrification and degradation of halogenated hydrocarbons—a tenuous balance for ammonia-oxidizing bacteria. *Appl Microbiol Biotechnol* **86**:435-444.

Schatteman A, Wright CL, Crombie AT, Murrell JC, Lehtovirta-Morley LE. In review. Hydrazines as substrates and inhibitors of the archaeal ammonia oxidation pathway.

Sedlacek CJ, McGowan B, Suwa Y, Sayavedra-Soto L, Laanbroek HJ, Stein LY, Norton JM, Klotz MG, Bollmann A. 2019. A physiological and genomic comparison of *Nitrosomonas* cluster 6a and 7 ammonia-oxidizing bacteria. *Microb Eco* **78**:985-994.

Sedlacek CJ, Giguere AT, Dobie MD, Mellbye BL, Ferrell RV, Woebken D, Sayavedra-Soto LA, Bottomley PJ, Daims H, Wagner M, Pjevac P. 2020.

Transcriptomic response of *Nitrosomonas europaea* transitioned from ammonia-to oxygen-limited steady-state growth. *Msystems* **5**:e00562-19.

Séneca J, Pjevac P, Canarini A, Herbold CW, Zioutis C, Dietrich M, Simon E, Prommer J, Bahn M, Pötsch EM, Wagner M. 2020. Composition and activity of nitrifier communities in soil are unresponsive to elevated temperature and CO_2, but strongly affected by drought. *ISME J* **14**:3038-3053.

Semrau JD, DiSpirito AA, Yoon S. 2010. Methanotrophs and copper. *FEMS Microbiol Rev* **34**:496-531.

Semrau, J., 2011. Bioremediation via methanotrophy: overview of recent findings and suggestions for future research. *Frontiers in microbiology*, *2*, p.209.

Shen, T., Stieglmeier, M., Dai, J., Urich, T. and Schleper, C., 2013. Responses of the terrestrial ammonia-oxidizing archaeon Ca. Nitrososphaera viennensis and the ammonia-oxidizing bacterium Nitrosospira multiformis to nitrification inhibitors. *FEMS microbiology letters*, *344*(2), pp.121-129

Silverman RB. 2000. *The organic chemistry of enzyme-catalyzed reactions*. San Diego, CA, Academic Press. 18th Edition.

Skinner FA, Walker N. 1961. Growth of *Nitrosomonas europaea* in batch and continuous culture. *Arch Mikrobiol* **38**:339-349.

Sleytr UB, Bayley H, Sára M, Breitwieser A, Küpcü S, Mader C, Weigert S, Unger FM, Messner P, Jahn-Schmid B, Schuster B. 1997. VI. Applications of S-layers. *FEMS Microbiol Rev* **20**:151-175.

Sleytr UB, Beveridge TJ. 1999. Bacterial S-layers. *Trends Microbiol* **7**:253-260.

Shiemke AK, Arp DJ, Sayavedra-Soto LA. 2004. Inhibition of membrane-bound methane monooxygenase and ammonia monooxygenase by diphenyliodonium: implications for electron transfer. *J Bacteriol* **186**:928-937.

Smith MA, Majer SH, Vilbert AC, Lancaster KM. 2019. Controlling a burn: outer-sphere gating of hydroxylamine oxidation by a distal base in cytochrome P460. *Chem Sci* **10**:3756-3764.

Soler-Jofra A, Pérez J, van Loosdrecht MC. 2021. Hydroxylamine and the nitrogen cycle: a review. *Water Res* **190**:116723.

Spang A, Hatzenpichler R, Brochier-Armanet C, Rattei T, Tischler P, Spieck E, Streit W, Stahl DA, Wagner M, Schleper C. 2010. Distinct gene set in two different lineages of ammonia-oxidizing archaea supports the phylum Thaumarchaeota. *Trends Microbiol* **18**:331-340.

Spang A, Poehlein A, Offre P, Zumbrägel S, Haider S, Rychlik N, Nowka B, Schmeisser C, Lebedeva EV, Rattei T, Böhm C. 2012. The genome of the ammonia-oxidizing *Candidatus* Nitrososphaera gargensis: insights into metabolic versatility and environmental adaptations. *Environ Microbiol* **14**:3122-3145.

Spasov E, Tsuji JM Hug LA, Doxey AC, Sauder LA, Parker WJ, Neufeld JD. 2020. High functional diversity among *Nitrospira* populations that dominate rotating biological contactor microbial communities in a municipal wastewater treatment plant. *ISME J* **14**:1857-1872.

Stahl DA, de la Torre JR. 2012. Physiology and diversity of ammonia-oxidizing archaea. *Ann Rev Microbiol* **66**:83-101.

Stanley SH, Prior SD, Leak DJ, Dalton H. 1983. Copper stress underlies the fundamental change in intracellular location of methane monooxygenase in methane-oxidizing organisms: studies in batch and continuous cultures. *Biotechnol Lett* **5**:487-492.

Stieglmeier, M., Mooshammer, M., Kitzler, B., Wanek, W., Zechmeister-Boltenstern, S., Richter, A. and Schleper, C., 2014. Aerobic nitrous oxide production through N-nitrosating hybrid formation in ammonia-oxidizing archaea. *The ISME journal*, *8*(5), pp.1135-1146.

Stieglmeier M, Klingl A, Alves RJ, Rittmann SKM, Melcher M, Leisch N, Schleper C. 2014. *Nitrososphaera viennensis* gen. nov., sp. nov., an aerobic and mesophilic, ammonia-oxidizing archaeon from soil and a member of the archaeal phylum Thaumarchaeota. *Int J Syst Evol Microbiol* **64**:2738.

Stein LY, Klotz MG. 2011. Nitrifying and denitrifying pathways of methanotrophic bacteria. *Biochem Soc Trans* **39**:1826-1831.

Stein LY, Roy R, Dunfield PF. 2012. Aerobic methanotrophy and nitrification: processes and connections. *eLS*.

Stein LY, Klotz MG. 2016. The nitrogen cycle. *Curr Biol* **26**:94-98.

Stein LY. 2019. Insights into the physiology of ammonia-oxidizing microorganisms. *Curr Opin Chem Biol* **49**:9-15.

Su YC, Sathyamoorthy S, Chandran K. 2019. Bioaugmented methanol production using ammonia oxidizing bacteria in a continuous flow process. *Bioresour Technol* **279**:101-107.

Suzuki I, Dular U, Kwok S. 1974. Ammonia or ammonium ion as substrate for oxidation by *Nitrosomonas europaea* cells and extracts. *J Bacteriol* **120**:556-558.

Taher E, Chandran K. 2013. High-rate, high-yield production of methanol by ammonia-oxidizing bacteria. *Environ Sci Technol* **47**:3167-3173.

Taylor AE, Zeglin LH, Dooley S, Myrold DD, Bottomley PJ. 2010. Evidence for different contributions of archaea and bacteria to the ammonia-oxidizing potential of diverse Oregon soils. *Appl Environ Microbiol* **76**:7691-7698.

Taylor AE, Vajrala N, Giguere AT, Gitelman AI, Arp DJ, Myrold DD, Sayavedra-Soto L, Bottomley PJ. 2013. Use of aliphatic n-alkynes to discriminate soil nitrification activities of ammonia-oxidizing thaumarchaea and bacteria. *Appl Environ Microbiol* **79**:6544-6551.

Taylor AE, Taylor K, Tennigkeit B, Palatinszky M, Stieglmeier M, Myrold DD, Schleper C, Wagner M, Bottomley PJ. 2015. Inhibitory effects of C_2 to C_{10} 1-alkynes on ammonia oxidation in two *Nitrososphaera* species. *Appl Environ Microbiol* **81**:1942-1948.

Taylor AE, Giguere AT, Zoebelein CM, Myrold DD, Bottomley PJ. 2017. Modeling of soil nitrification responses to temperature reveals thermodynamic differences between ammonia-oxidizing activity of archaea and bacteria. *ISME J* **11**:896-908.

Tolar BB, Herrmann J, Bargar JR, van den Bedem H, Wakatsuki S, Francis CA. 2017. Integrated structural biology and molecular ecology of N-cycling enzymes from ammonia-oxidizing archaea. *Environ Microbiol Rep* **9**:484-491.

De la Torre JR, Walker CB, Ingalls AE, Könneke M, Stahl DA. 2008. Cultivation of a thermophilic ammonia oxidizing archaeon synthesizing crenarchaeol. *Environ Microbiol* **10**:810-818.

Tourna M, Stieglmeier M, Spang A, Könneke M, Schintlmeister A, Urich T, Engel M, Schloter M, Wagner M, Richter A, Schleper C. 2011. *Nitrososphaera viennensis*, an ammonia oxidizing archaeon from soil. *Proc Natl Acad Sci* **108**:8420-8425.

Thion C, Prosser JI. 2014. Differential response of nonadapted ammonia-oxidising archaea and bacteria to drying–rewetting stress. *FEMS Microbiol Ecol* **90**:380-389.

Thion, C.E., Poirel, J.D., Cornulier, T., De Vries, F.T., Bardgett, R.D. and Prosser, J.I., 2016. Plant nitrogen-use strategy as a driver of rhizosphere archaeal and bacterial ammonia oxidiser abundance. *FEMS microbiology ecology*, *92*(7).

Treusch AH, Leininger S, Kletzin A, Schuster SC, Klenk HP, Schleper C. 2005. Novel genes for nitrite reductase and Amo-related proteins indicate a role of uncultivated mesophilic crenarchaeota in nitrogen cycling. *Environ Microbiol* **7**:1985-1995.

Vajrala N, Sayavedra-Soto LA, Bottomley PJ, Arp DJ. 2012. Global analysis of the *Nitrosomonas europaea* iron starvation stimulon. *Arch Microbiol* **194**:305-313.

Vajrala N, Martens-Habbena W, Sayavedra-Soto LA, Schauer A, Bottomley PJ, Stahl DA, Arp DJ. 2013. Hydroxylamine as an intermediate in ammonia oxidation by globally abundant marine archaea. *Proc Natl Acad Sci* **110**:1006-1011.

Vannelli T, Hooper AB. 1995. NIH shift in the hydroxylation of aromatic compounds by the ammonia-oxidizing bacterium *Nitrosomonas europaea*. Evidence against an arene oxide intermediate. *Biochem* **34**:11743-11749.

Venter JC, Remington K, Heidelberg JF, Halpern AL, Rusch D, Eisen JA, Wu D, Paulsen I, Nelson KE, Nelson W, Fouts DE. 2004. Environmental genome shotgun sequencing of the Sargasso Sea. *Science* **304**:66-74.

Verhamme DT, Prosser JI, Nicol GW. 2011. Ammonia concentration determines differential growth of ammonia-oxidising archaea and bacteria in soil microcosms. *ISME J* **5**:1067-1071.

Versantvoort W, Pol A, Jetten MS, van Niftrik L, Reimann J, Kartal B, den Camp HJO. 2020. Multiheme hydroxylamine oxidoreductases produce NO during ammonia oxidation in methanotrophs. *Proc Natl Acad Sci* **117**:24459-24463.

Voysey PA, Wood PM. 1987. Methanol and formaldehyde oxidation by an autotrophic nitrifying bacterium. *Microbiol* **133**:283-290.

Vuillemin A, Wankel SD, Coskun ÖK, Magritsch T, Vargas S, Estes ER, Spivack AJ, Smith DC, Pockalny R, Murray RW, D'Hondt S. 2019. Archaea dominate oxic subseafloor communities over multimillion-year time scales. *Sci Adv* **5**:eaaw4108.

Wacker T, Garcia-Celma JJ, Lewe P, Andrade SL. 2014. Direct observation of electrogenic NH_4^+ transport in ammonium transport (Amt) proteins. *Proc Natl Acad Sci* **111**:9995-10000.

Walker CB, de la Torre JR, Klotz MG, Urakawa H, Pinel N, Arp DJ, Brochier-Armanet C, Chain PSG, Chan PP, Gollabgir A, Hemp J, Hugler M, Karr EA, Konneke M, Shin M, Lawton TJ, Lowe T, Martens-Habbena W, Sayavedra-Soto LA, Lang D, Sievert SM, Rosenzweig AC, Manning G, Stahl DA. 2010. *Nitrosopumilus maritimus* genome reveals unique mechanisms for nitrification and autotrophy in globally distributed marine crenarchaea. *Proc Natl Acad Sci* **107**:8818-882

Wang X, Wang C, Bao L, Xie S. 2014. Abundance and community structure of ammonia-oxidizing microorganisms in reservoir sediment and adjacent soils. *Appl Microbiol Biotechnol* **98**:1883-1892.

Ward BB. 1987. Kinetic studies on ammonia and methane oxidation by *Nitrosococcus oceanus*. *Arch Microbiol* **147**:126-133.

Ward BB. 1990. Kinetics of ammonia oxidation by a marine nitrifying bacterium: methane as a substrate analogue. *Microb Ecol* **19**:211-225.

Ward BB, Arp DJ, and Klotz MG. 2011 (ed), *Nitrification*. ASM Press, Washington, DC.

Ward LM, Johnston DT, Shih PM. 2021. Phanerozoic radiation of ammonia oxidizing bacteria. *Scientific Rep* **11**:1-9.

Weber EB, Lehtovirta-Morley LE, Prosser JI, Gubry-Rangin C. 2015. Ammonia oxidation is not required for growth of Group 1.1 c soil Thaumarchaeota. *FEMS Microbiol Ecol* **91**:fiv001.

Whittaker M, Bergmann D, Arciero D, Hooper AB. 2000. Electron transfer during the oxidation of ammonia by the chemolithotrophic bacterium *Nitrosomonas europaea*. *Biochim Biophys Acta Bioenerg* **1459**:346-355.

Whittenbury R, Phillips KC, Wilkinson JF. 1970. Enrichment, isolation and some properties of methane-utilizing bacteria. *Microbiol* **61**:205-218.

Wijma HJ, Canters GW, de Vries S, Verbeet MP. 2004. Bidirectional catalysis by copper-containing nitrite reductase. *Biochem* **43**:10467-10474.

Wilhelm E, Battino R, Wilcock RJ. 1977. Low-pressure solubility of gases in liquid water. *Chem Rev* **77**:219-262.

Williams TJ, Long E, Evans F, DeMaere MZ, Lauro FM, Raftery MJ, Ducklow H, Grzymski JJ, Murray AE, Cavicchioli R. 2012. A metaproteomic assessment of winter and summer bacterioplankton from Antarctic Peninsula coastal surface waters. *ISME J* **6**:1883-1900.

Winogradsky S. 1890. On the Organisms of the Nitrification. *CR L'Acad Des Sci* **110**:013.

Woese CR, Magrum LJ, Fox GE. 1978. Archaebacteria. *J Mol Evol* **11**:245-252.

Wright CL, Schatteman A, Crombie AT, Murrell JC, Lehtovirta-Morley LE. 2020. Inhibition of ammonia monooxygenase from ammonia-oxidizing archaea by linear and aromatic alkynes. *Appl Environ Microbiol* **86**:e02388-19.

Wuchter C, Abbas B, Coolen MJ, Herfort L, van Bleijswijk J, Timmers P, Strous M, Teira E, Herndl GJ, Middelburg JJ, Schouten S. 2006. Archaeal nitrification in the ocean. *Proc Natl Acad Sci* **103**:12317-12322.

Yan J, Haaijer SC, Op den Camp HJ, van Niftrik L, Stahl DA, Könneke M, Rush D, Sinninghe Damsté JS, Hu YY, Jetten MS. 2012. Mimicking the oxygen minimum zones: stimulating interaction of aerobic archaeal and anaerobic bacterial ammonia oxidizers in a laboratory-scale model system. *Environ Microbiol* **14**:3146-3158.

Zhang J, Hu Z, Liu T, Wang Z, Guo J, Yuan Z, Zheng M. 2021. Feasibility of methane bioconversion to methanol by acid-tolerant ammonia-oxidizing bacteria. *Water Res* **197**:117077.

Zhong H, Lehtovirta-Morley L, Liu J, Zheng Y, Lin H, Song D, Todd JD, Tian J, Zhang XH. 2020. Novel insights into the Thaumarchaeota in the deepest oceans: their metabolism and potential adaptation mechanisms. *Microbiome* **8**:1-16.

Zhu W, Wang C, Hill J, He Y, Tao B, Mao Z, Wu W. 2018. A missing link in the estuarine nitrogen cycle?: Coupled nitrification-denitrification mediated by suspended particulate matter. *Scientific Rep* **8**:1-10.

Zorz JK, Kozlowski JA, Stein LY, Strous M, Kleiner M. 2018. Comparative proteomics of three species of ammonia-oxidizing bacteria. *Front Microbiol* **9**:938.